Meridian School Bus Biodiesel Evaluation Study: Final Report

April 19, 2005

Prepared by:

Hampden Kuhns
Claudio Mazzoleni
M.-C. Oliver Chang
Judith C. Chow
Gayathri Parthasarathy
Vic Etyemezian
Hans Moosmüller
Peter Barber
Nicholas Nussbaum
Suresh Kumar K. Nathagoundenpalayam
Steve Kohl
Djordje Nikolic
John Watson

(hkuhns@dri.edu)
Desert Research Institute
2215 Raggio Pky
Reno, NV 89512
Ph: (775) 674 7111
Fax: (775) 674 7060

Report prepared for:

Community Planning Association of Southwest Idaho
Project Manager: Jay Witt
800 S. Industry Way, Suite 100
Meridian, ID 83642 USA
Ph: (208) 855-2558 x275

SYNOPSIS

This study evaluated the effects of B20 biodiesel fuel use on school bus emissions from the (Meridian) Joint School District #2 bus fleet in Meridian, ID. Measurements of bus exhaust indicated that switching to B20 biodiesel at best did not increase nitrogen oxide emissions, but did increase emissions of carbon monoxide by 34%, emissions of hydrocarbons by 24%, and particulate matter emissions by 88%. These results are contrary to many recent laboratory studies. Analysis of the fuels used in this study showed elevated levels of byproducts produced during the manufacture of biodiesel. Such byproducts in the fuel may result in higher emissions and fuel system failures as those observed in this study. The results of this study demonstrate need for diesel vehicle fleets using biodiesel fuel blends to implement best management practices that include fuel quality analyses. This study also demonstrates the need to regulate the production of biodiesel to conform to the newly published ASTM D6751 standard.

EXECUTIVE SUMMARY

Biodiesel is a fuel created by reacting oils and fats with alcohols. The reaction produces two products: ester and glycerin. Upon complete separation, the ester (biodiesel) can be used directly as fuel for diesel engines. Biodiesel is an attractive supplement or alternative to petroleum diesel because (1) it is a renewable energy source, (2) it is less toxic to humans than petroleum diesel, and (3) it has a low sulfur content and will not degrade catalytic or particle trap emission control systems.

Numerous controlled laboratory studies have been conducted to quantify differences in exhaust emissions attributable to switching to biodiesel fuel from petroleum diesel. A comprehensive EPA analysis of dynamometer emission tests on engines found that biodiesel emissions are lower for particulate matter (PM), hydrocarbons (HC), and carbon monoxide (CO). This same analysis also showed a slight increase in nitrogen oxide (NO) emissions when biodiesel is used. These emissions differences were found to increase with the relative quantity of biodiesel mixed with petroleum diesel.

The Community Planning Association (COMPASS) of Southwest Idaho contracted with the Desert Research Institute (DRI) to measure the change in exhaust emission factors associated with switching the (Meridian) Joint School District #2 (MJSD) bus fleet from 100% petroleum diesel to 20% biodiesel/80% petroleum diesel (i.e. B20). The MJSD operates a fleet of 205 school buses with model years ranging from 1983 to 2004. The field study took place on Lanark Road in Meridian, ID outside of the MJSD bus yard. The study was conducted in two phases: the first between January 11 and January 15, 2004 and the second between March 1 and March 4, 2004. During the first phase, the buses were operating on 100% petroleum diesel. The refueling tank at the school bus yard was filled with B20 on January 16, and all buses refueled with B20 until April 1, 2004. The average school bus odometer increase between January 16, 2004 and March 1, 2004 was approximately 3,000 km corresponding to 3 or 4 refuelings during the period.

A commercial vehicle exhaust remote sensing system (VERSS) augmented with an ultraviolet LIDAR was used to measure the emissions from all vehicles traveling on Lanark Road during the study. Using optical beams oriented across the roadway, the system measured the column content of CO_2, CO, HC, NO, and PM. By calculating the ratio of each pollutant to the total

carbon content of the exhaust, the measurements were converted into fuel based emission factors with units of grams (g) pollutant per kilogram (kg) fuel burned. Since there was no outlet on the eastern end of Lanark Road (i.e., a dead end street), the vehicles traveling eastbound were operating under hot stabilized conditions, while the westbound vehicles were generally operating under cold-start conditions. Between 230 and 540 valid measurements of school bus emission factors were collected for each pollutant during each phase and each operating condition. Motor vehicle emissions (especially those from light duty gasoline vehicles) are usually skewed due to a small number of vehicles causing the majority of the emissions. The diesel bus emission factors tended to be less skewed than gasoline powered vehicles.

Analysis of emissions factors by model year showed that buses with the newer engines (model years 1998 to 2000) emitted less CO and PM than the older engines (model years 1995 to 1998). These differences are likely due to computer controlled fuel injection systems on the newer buses that optimize both power and combustion efficiency.

For the school buses, cold start emissions of CO were 34% +/- 7% higher after the switch to B20. Average hot-stabilized CO emissions factors were not significantly different after the switch to B20. Average hot-stabilized HC emission factors increased 23% +/- 11% after the switch to B20, but cold-start HC emission factors were indistinguishable based on fuel type. Emission factors of NO for buses running on both fuels were not significantly different <1%. The largest change in emission factors was observed for PM. Hot stabilized PM emission factors were 88% +/- 11% higher with B20 and cold start PM emission factors were 65% +/- 8% higher after the buses has switch to B20. All noted differences in emissions were deemed statistically significant via a t-test with alpha = 0.05. Emission factor measurements of CO, NO, and PM from both sampling phases were corroborated by a redundant set of measurements using a novel in-plume sampling system.

These results are in disagreement with the majority of dynamometer biodiesel studies that show a decrease in CO, HC, and PM emission factors with biodiesel use.

In addition to the higher PM emission factors observed after the switch to biodiesel, a number of mechanical problems forced 6 buses out of service. Each bus had failures of the lift pump or fuel pump that delivers the fuel to the injectors. One failure occurred prior to the fuel switch on one of the control buses that had been using biodiesel for ~1.5 years.

These conflicting results prompted the analysis of the fuels used in the buses during the study. Samples of B100, B20, and petroleum diesel were collected directly from a manufacturer and at several distribution points in the Treasure Valley. The samples were sent to Caleb Brett Laboratories in Deer Park, Texas for testing. Analyses of these fuels indicated that the biodiesel used in the Treasure Valley was not in compliance with the newly published ASTM standard for B100 (D6751). All of the biodiesel samples collected in the Treasure Valley had elevated levels of glycerin (a byproduct of the biodiesel trans-esterification process). In addition, one of the B100 samples had a low flash point that is usually associated with residual methanol in the biodiesel. Based on the U.S. Department of Energy's (DOE's) "Biodiesel Handling and Use Guidelines", these deficiencies can cause fuel system failure and poor combustion characteristics. The findings of increased PM emission factors and fuel systems failures are consistent with B20 made from off-specification biodiesel fuel.

This study differed from many previous laboratory studies in that the effects of a fuel switch under real world conditions were tested. The analysis identified that the use of off-spec fuel can reverse some of benefits of using biodiesel.

ACKNOWLEDGEMENTS

We would like to express our appreciation to the following individuals and organizations for their generous contributions of time and effort to this project. Thanks to:

- Sue Johnston, Randy Owens, and the entire staff of the *(Meridian) Joint School District No.2 Transportation Department*
- *The (Meridian) Joint School District No.2* Bus Drivers
- *Idaho Transportation Department*
- Ada County Highway District
- Angel Fontenot-Staley - Laboratory Development/Outsourcing Representative Intertek Caleb Brett
- Dale Johnston – *United Oil*
- Dick Larson – *Idaho Department of Water Resources (retired)*
- Dennis Stegenga
- Yancey Willis, Pam Elliott – *COMPASS*

We would also like to thank the Technical Review Committee Participants:

- Beth Baird - *City of Boise*
- David Brzezinski - *US EPA Office of Transportation and Air Quality, Assessment & Standards Division*
- Jon Van Gerpen, Ph.D. - *University of Idaho, Department of Biological & Agricultural Engineering*
- Rick Hardy, Natalie Del Rio – *Idaho Department of Environmental Quality, Division of Technical Services*
- Steve Howell - *National Biodiesel Board, Technical Director*
- Robert McCormick, Ph.D. - *National Renewable Energy Laboratory, Center for Transportation Technologies and Systems*
- Matthew Moore, M.A. – *Idaho Transportation Department, Transportation Planning Division*
- Judi Steciak, Ph.D., P.E. - *University of Idaho, Associate Professor of Mechanical Engineering*

TABLE OF CONTENTS

TABLE OF TABLES

TABLE OF FIGURES

1. Introduction

The Treasure Valley includes Ada and Canyon counties in Southwest Idaho. It is a rapidly growing urban area situated within a geographic valley. In previous years, wintertime stagnation events have prevented emissions from mixing out of the valley causing levels of particulate matter less than 10 microns in diameter (PM_{10}) and of carbon monoxide (CO) to exceed the National Ambient Air Quality Standards (NAAQS). Emissions reductions from vehicle fleet turnover and wood burning restrictions during stagnant winter conditions have decreased the severity of pollution buildup during strong inversions.

The competing factors of population growth and new regulations for particles less than 2.5 microns in diameter ($PM_{2.5}$) and for ozone (O_3) necessitate continued vigilance on behalf of urban planners and the community at large to prevent future non-attainment designations. Valley-wide emissions will continue to grow as population increases unless practices or controls can be adopted that decrease per-capita emissions.

Use of alternative fuels is one method that may reduce emissions from vehicles. Biodiesel is classified as an alternative fuel under the Federal Energy Policy Act (EPAct) requirements. Biodiesel is produced from vegetable and animal oils and fats by reaction with methanol or ethanol in the presence of a catalyst. The methyl ester produced by this reaction can be used directly in existing vehicles without any engine modification or can be blended with petroleum diesel as an additive.

To evaluate the impact of this potential emissions control strategy, the Community Planning Association of Southwest Idaho (COMPASS) sponsored DRI to determine the emission changes that would occur if the (Meridian) Joint School District #2 bus fleet converted from petroleum diesel to a blend of 20% biodiesel with 80% petroleum diesel (B20). This report describes the measurements performed on the in-use school bus fleet and the data analyses applied. Figure 1-1 shows the location of the Treasure Valley in Idaho as well as the relative locations of the data collection sites in the area.

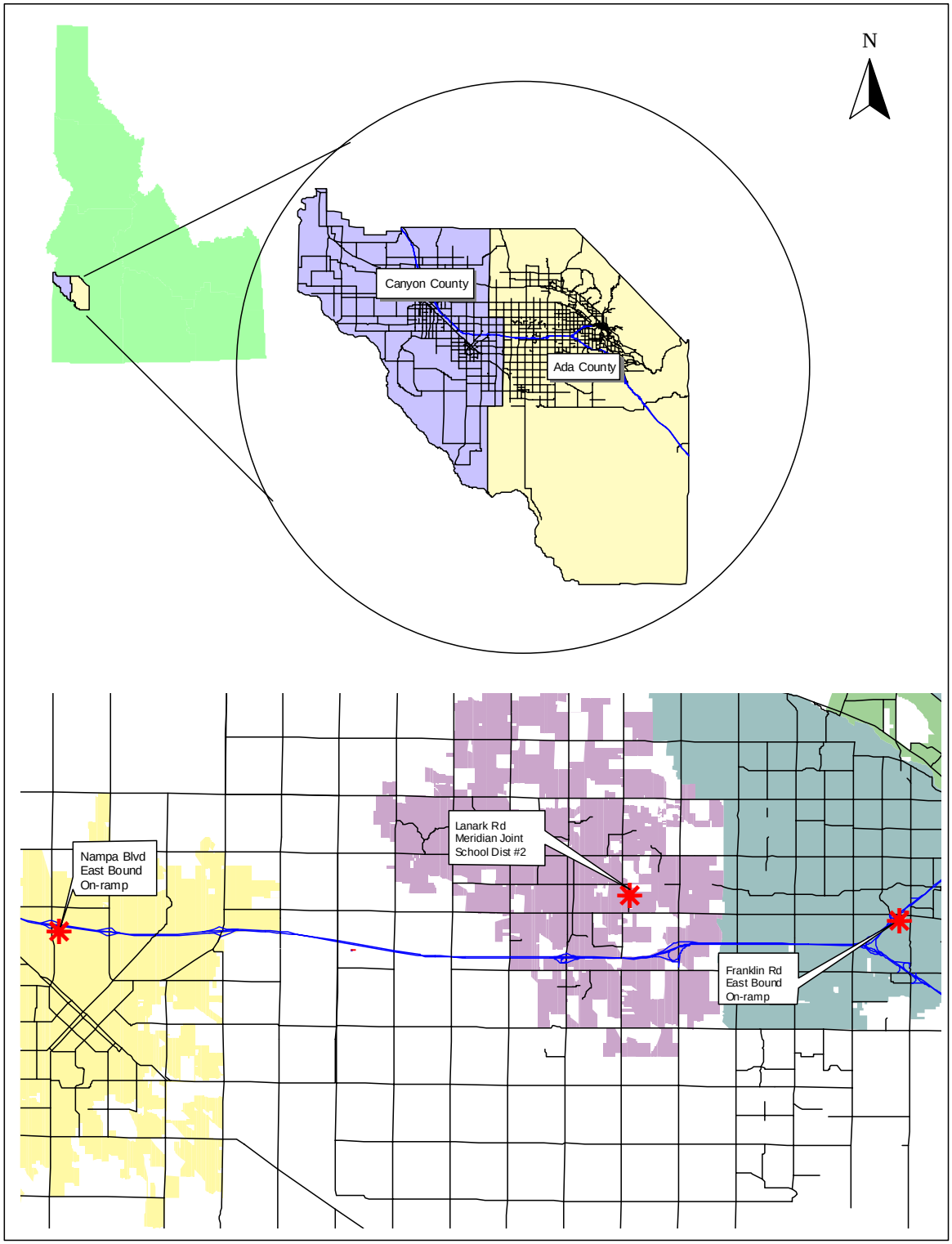

Figure 1-1. Location of the Treasure Valley, Idaho and Data Collection Sites.

1.1. Objectives

The primary objectives of this project were:

- To determine the effect on emission factors of PM, VOC, NO_x, and CO by switching the (Meridian) Joint School District #2 bus fleet from petroleum diesel to B20.
- To determine how school bus age and accumulated mileage affect emission factors from buses when using B20 and petroleum diesel.

A secondary objective of the project was:

- To measure emission factors from in-use fleet of on-road vehicles (i.e. both gasoline and diesel vehicles) operating in the Treasure Valley during winter sampling periods.

1.2. Guide to Report

This report is organized in eight sections and three appendixes:

- Section 1 describes the overall project and is an introduction to the report.
- Section 2 is the background section that describes emissions test methods and the results of previous studies that have investigated emission changes attributable to biodiesel.
- Section 3 describes the measurement methods used.
- Section 4 discusses the data processing step and validation checks performed to evaluate the quality of the data.
- Section 5 presents the results of the emission factor measurements when the buses were running on petroleum diesel and biodiesel.
- Section 6 describes the analysis of petroleum diesel and biodiesel fuel samples collected during this project.
- Section 7 presents the conclusions of the study and recommends additional studies.
- Section 8 lists all references cited in this report.
- Appendix A of this report is a stand-alone document that describes the freeway on-ramp sampling and analysis pertaining to the secondary objective of the study.
- Appendix B acknowledges the reviewers of the draft report and responds to some specific comments.
- Appendix C is a listing of acronyms used throughout the document.

2. Background

Diesel engines use compression ignition (CI), rather than the spark ignition (SI) of gasoline-fueled engines, to ignite fuel. In modern CI engines, fuel sprayed into the hot compressed air in the engine cylinder auto-ignites. The timing of the injection controls the timing of the ignition. This process is optimized for maximum combustion efficiency. The lean fuel-air mixture results in more complete combustion and reduced emissions of VOC and CO, while NO_x emissions increase due to the high combustion temperature. Diesel engines also emit large amounts of primary PM, mostly during transient operating conditions such as high load (acceleration) and cold start. Specifically, heavy fuel spray droplet combustion characteristics contribute to the higher PM emissions. PM emission rates and particle size are also influenced by the fuel sulfur content, which also causes diesel SO_2 emissions. Some of the SO_2 and NO_x transform into $PM_{2.5}$ (mass of particles with aerodynamic diameter <2.5 μm) which is regulated by National Ambient Air Quality Standards (U.S.EPA [1997]) and the regional haze rule (U.S.EPA [1999]). VOC and NO_x emissions are precursors to ozone (O_3) that are also regulated by NAAQS.

The following subsections describe current emission laboratory and field-testing methods that are available for evaluating emissions changes associated with different fuels.

2.1. Engine and Chassis Dynamometer Testing

Engine emissions tests are typically performed in a test cell for engines by using an engine dynamometer or on vehicles by using a chassis dynamometer. In either case, emissions are quantified for different engine loads. For an engine dynamometer, the engine is mounted on a test stand and its energy output is absorbed by a water brake dynamometer. In this configuration the engine can be tested at various speeds and loads in steady-state modes only. For a chassis dynamometer, the engine remains in the vehicle with its energy output measured at the wheels by a roller to which different resistances are applied by a water brake. Steady state resistances are defined for certification of non-road, marine, and locomotive engines. Engine and the chassis dynamometer approaches direct the whole exhaust to a full-scale dilution tunnel and employ the use of a constant volume system (CVS), laboratory-grade emissions measurement instrumentation, an environment control system, and associated data acquisition and control systems. Different dilution ratios yield different particle size distributions because small particles form and combine with each other depending on their concentrations and mixing characteristics (Abdul-Khalek et al. [2003]).

2.2. Mobile Laboratories

Mobile laboratories can sample exhaust emissions under real-world operating conditions by continuously extracting a portion or all of the exhaust into an analysis system while the vehicle is operating. Brown et al. [2000] and Brown et al. [2002] showed the importance of load and grade on the emissions of nitric oxides using a mobile system. The University of Minnesota has constructed a large mobile laboratory to measure the particle size properties that occur using natural dilution and has compared Brown's results to those found under controlled dilution conditions in a laboratory. Aerodyne, Inc., has built a van-sized vehicle that can follow vehicles throughout their normal operating cycle, but the van is really a "chase vehicle" that samples the diluted plume after it has been released into the atmosphere. A mobile laboratory that can

duplicate the EPA's emissions testing procedures would provide a bridge between certification and real-world tests.

2.3. On-Board Measurements

On-board measurements are those that are carried by the test engine throughout its real-world operating cycle. Because space and power are limited on a typical vehicle, on-board instrumentation must be portable, small, and low in power consumption. This imposes severe limitations on the accuracy and precision of the measurements.

Until recently, compact and sturdy instruments for the time-resolved measurement of diesel particulate mass emissions, and their organic carbon (OC) and elemental carbon (EC) components, have not been available. However, due to the importance of these measurements for obtaining modal emission factors and for minimizing such emissions, such instruments have recently been developed and characterized. Six different methods show potential for on-board PM monitoring. These include two inertial mass measurement methods (Tapered Element Oscillating Microbalance [TEOM] and Quartz Crystal Microbalance [QCM]), and four optical methods: a light scattering method (nephelometer); two light absorption methods, one which measures light absorption of aerosol deposited on a filter (aethalometer) and one which measures light absorption *in situ* (photoacoustic instrument); and a light extinction method (smoke meter). All of these methods, with the exception of QCM, were evaluated by Moosmüller et al. (2001a, 2001b) for the measurement of both particle mass and the mass of its elemental and organic carbon components.

2.4. In-Plume Measurements

Because of limitations associated with the number of vehicles available for dynamometer and onboard testing, the need exists to sample emissions from large numbers of vehicles to verify that modal testing is representative of the fleet at large. Fleet testing that collects data on individual vehicles provides additional information about the distribution of emissions for different vehicle types (i.e., age, fuel type, duty rating, etc). Methods to test large numbers of individual vehicles include in-plume and cross-plume measurements. In-plume techniques extract exhaust from a source-dominated environment and may employ a broader array of analyses to characterize the exhaust composition.

In the roadside environment, vehicle exhaust dilutes quickly as it leaves the exhaust pipe. Remote sensing techniques indicate that cross-plume gaseous carbon dioxide (CO_2) becomes indistinguishable from background measurements within 0.5 seconds after a vehicle has passed by. Consequently, in-plume measurements must be sensitive and have a fast time response to distinguish vehicle exhaust emissions from background. The technique of using a stationary measurement to quantify emissions from individual vehicles was originally used by Hansen and Rosen [1990]. They deployed a CO_2 monitor and an aethalometer downwind of a steeply graded road. The ratio of aerosol black carbon (BC) to CO_2 was calculated for each vehicle passing their instrumentation. The results found that fuel-based BC emission factors ranged over a factor of 100 for the measured on-road vehicles.

2.5. Cross-Plume Measurements

Vehicle Exhaust Remote Sensing Systems (VERSSs) measure emission factors by cross-plume measurements of the vehicle exhaust plume after the vehicle passes by the VERSS. These

systems measure the mass column content of several pollutants and consequently obtain fuel-based emission factors by adjusting the measurements of individual pollutants to the total carbon content of the column measurement (for details, Section 2.6). With this method, emission factors can be obtained without a prior knowledge of the changing plume dilution as the exhaust plume enters the ambient atmosphere.

VERSSs can measure gaseous emission factors for large numbers of individual vehicles (>1,000 per hour), albeit under a limited variety of operating conditions largely determined by monitoring location (Guenther et al. [1994]). Remote sensing studies have shown that comparatively few vehicles cause a majority of the emissions; that is, gaseous emission factors do not follow a symmetric frequency distribution (Zhang et al. [1994]). This further emphasizes the importance of measuring emissions from many vehicles to obtain meaningful emission distributions (Lawson et al. [1990]; Calvert et al. [1993]).

While measurements of gaseous emissions both on dynamometers and on-road with remote sensors have become routine, technology to measure time-resolved PM emissions during dynamometer testing is just starting to become available (Moosmuller et al. [2001a]; Moosmuller et al. [2001b]). VERSS technology to measure on-road PM emission factors was not available until the development of the Desert Research Institute (DRI) VERSS (Moosmuller et al. [2003]). In addition, emissions of gaseous pollutants are measured during inspection and maintenance programs while PM emissions are only addressed with language such as “no visible emissions” and/or opacity regulations for heavy-duty diesel vehicles (HDDVs) (Society of Automotive Engineers [1996]).

2.6. Fuel Based Emission Factors

Gaseous VERSSs (Stephens et al. [1996]; Guenther et al. [1995]; Zhang et al. [1996]; Nelson et al. [1998]; Popp et al. [1999]; Baum et al. [2000]; Jimenez et al. [2000]; Baum et al. [2001]) use infrared ([IR], used mostly for CO_2, CO, hydrocarbons [HC]) and ultraviolet ([UV], used mostly for NO) extinction across the road to measure the mass column content (a two-dimensional density with dimension of mass/area) of the emitted gases. This is done simultaneously using carbon mass content (carbon mass in vehicle exhaust is mostly in the form of CO_2 and some CO and HC) measurements of the same column. These measurements have a high temporal resolution (~10 ms) in order to yield multiple measurements (typically 20 to 50) before and after the vehicle passes the sensor. Since the carbon mass fraction of automotive fuel is known, the ratio of the two mass column contents can be used to calculate the mass emission of the pollutant of interest per mass of fuel consumed. This emission factor EF_P for pollutant P is defined as the ratio of the mass M_P of pollutant P emitted per mass M_{fuel} of fuel consumed

$$EF_P = \frac{M_P}{M_{fuel}} \ . \tag{2-1}$$

Defining CMF_{fuel} as the carbon mass fraction of the fuel (that is, the carbon mass CM_{fuel} of the fuel divided by its mass M_{fuel}), the fuel mass M_{fuel} can be replaced, yielding

$$EF_P = CMF_{fuel} \frac{M_P}{CM_{fuel}} \ . \tag{2-2}$$

The carbon mass emitted by the vehicle equals the carbon mass of the fuel consumed (carbon balance). Thereby, the fuel carbon mass CM_{fuel} can be replaced by the carbon mass of the exhaust, which is the sum of the mass of its main carbon containing components, weighted by their respective carbon mass fraction.

$$EF_P = CMF_{fuel}\frac{M_P}{CM_{exhaust}} = CMF_{fuel}\frac{M_P}{\sum_i CM_i} = CMF_{fuel}\frac{M_P}{\sum_i CMF_i\ M_i} = CMF_{fuel}\frac{\rho_{c\_P}}{\sum_i CMF_i\ \rho_{c\_i}}\ , \quad (2\text{-}3)$$

where the mass ratios have been replaced by the ratios of the respective exhaust mass column contents ρ_{c_P} and ρ_{c_i} as measured by a VERSS. Expanding the sum over the main carbon containing components of gaseous emissions (i.e., CO_2, CO, and HC) and dividing the numerator and denominator by the CO_2 mass (M_{CO2}) yields

$$EF_P = CMF_{fuel}\frac{\dfrac{\rho_{c\_P}}{\rho_{c\_CO2}}}{CMF_{CO2} + \left(CMF_{CO}\dfrac{\rho_{c\_CO}}{\rho_{c\_CO2}} + CMF_{HC}\dfrac{\rho_{c\_HC}}{\rho_{c\_CO2}}\right)}\ , \quad (2\text{-}4)$$

where the terms in the bracket can be neglected for most vehicles with the exception of gross CO or HC emitters. The contribution of particulate OC and BC emissions is even less significant and has been neglected in Eq. 1d. The fuel-based emission factor EF_P for pollutant P can be determined from a VERSS measurement of the mass column contents ρ_c using Eq. 1d if the carbon mass fractions (CMF) are known. For CO and CO_2, CMFs can be calculated directly from the respective atomic masses, yielding CMF_{CO} = 42.9% and CMF_{CO2} = 27.3%. For fuels, one may assume empirical formulas of $C_nH_{1.825n}$ for gasoline and C_nH_{2n} for diesel (Pierson et al. [1996]), resulting in $CMF_{gasoline}$ = 86.7% and CMF_{diesel} = 85.6%, in close agreement with values reported elsewhere (McCormick et al. [1997]). These values vary over time and by location by a few percent due to differences in refinery technology and emission regulations. In particular, $CMF_{gasoline}$ increased through 1994, partly as a result of the leaded gasoline phase-out, during which the fraction of aromatic hydrocarbons in gasoline increased. This trend was reversed beginning in 1996 with the development of fuel additives that raise oxygen content and have a low CMF. For example, the Bay Area of California introduced Phase 2 reformulated gasoline with 2% oxygen content by weight, which lowered the CMF from $CMF_{gasoline}$ = 87% in summers 1994–1995 to $CMF_{gasoline}$ = 85% in summers 1996–1997 (Kirchstetter et al. [1999]).

For exhaust HC, the situation is quite complex because HC is not a single component, but consists of hundreds of individual components. A VERSS measures each of these components with an individual weighting factor that depends upon the convolution of the IR absorption spectrum of the individual HC component and the transmission spectrum of the HC filter used in the VERSS (Singer et al. [1998]). In most cases, the correction of non-HC emission factors due to carbon emissions contained in HC is negligible. Exceptions include two-stroke engines, which can emit a substantial fraction of their fuel unburned (Bishop et al. [2001]).

While on-road remote sensing has previously not been used to measure PM emission factors, the exhaust optical opacity (opacity = 1 – transmission) of HDDVs has been characterized using the 3.9 µm reference channel of the University of Denver's VERSS (Morris et al. [1998]; Morris et al. [1999]). At the 3.9 µm wavelength, gaseous absorption is minimal and opacity is caused

almost exclusively by light absorption of the sub-micrometer diameter BC PM emitted mostly by diesel vehicles and potentially by the light scattering of coarse, freshly entrained road dust. This is illustrated in Figure 2-1, which shows a Mie theory (Mie [1908]) calculation of the mass extinction efficiency E_{ext} for black (e.g., BC; m = 1.5 - i 0.5 = (1.5, 0.5), where i = $(-1)^{0.5}$) and white (e.g., road dust or OC; m = (1.5, 0.0)) spherical particles at 3.9 μm wavelength as a function of diameter, where m is the complex index of refraction.

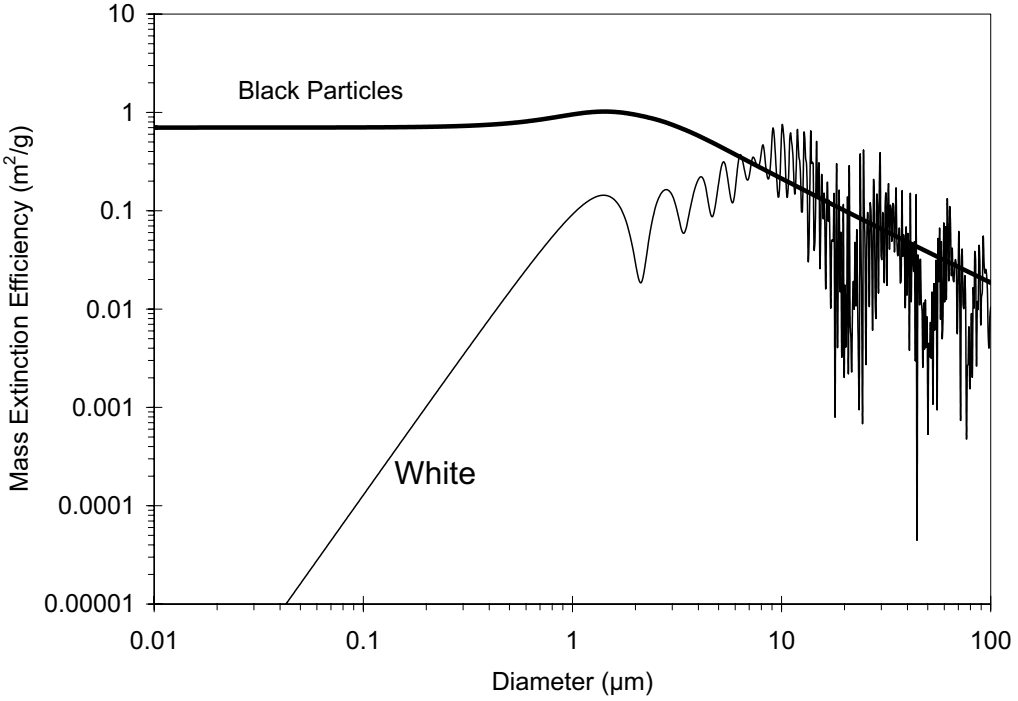

Figure 2-1. Mass extinction efficiency for black (e.g., BC; *m* = (1.5, 0.5)) and white (e.g., road dust or organic carbon (OC); *m* = (1.5, 0.0)) particles at 3.9-μm wavelength as function of diameter.

At 0.1 μm diameter (typical size for tailpipe PM), the optical interaction is in the Rayleigh regime, where the mass absorption efficiency is independent of particle diameter, while the mass scattering efficiency is proportional to the third power of the diameter. The mass extinction efficiency for black particles ($E_{ext} \approx 0.7$ m^2/g at 0.1 μm particle diameter) is dominated by absorption and is therefore nearly independent of diameter. The mass extinction efficiency for white particles ($E_{ext} \approx 1.3\times10^{-4}$ m^2/g at 0.1 μm particle diameter) is purely due to scattering and nearly four orders of magnitude smaller than that of black particles of the same size. For coarse particles, such as freshly entrained road dust, the mass extinction efficiency for white particles peaks around 10 μm diameter at about 0.7 m^2/g, decaying approximately proportional to their inverse diameter for larger sizes.

In the case of high stack HDDVs, road dust opacity can possibly be neglected and the opacity can be used as a measure of a strongly absorbing BC fraction of PM emissions. Total PM mass emissions consist nearly exclusively of BC and OC with their ratio (BC/OC) varying strongly between vehicles (Watson et al. [1994]). Variations of up to 2 orders of magnitude for individual diesel vehicles and 4 orders of magnitude for individual spark ignition vehicles have been reported for the BC/OC ratio (Gillies and Gertler [2000]). Because an opacity measurement at 3.9 μm is sensitive only to the highly variable BC mass component of tailpipe PM mass emissions, it is not adequate for quantifying tailpipe PM mass emissions. In addition, opacity measurements have limited sensitivity as they measure small changes in optical power. To minimize some of these limitations, the University of Denver group recently added two more wavelengths (633 nm and 240 nm) to their PM opacity measurement (Cadle et al. [2003]).

2.7. Effects of Biodiesel Fuel on Emissions

Numerous studies have been conducted comparing the emissions from diesel engines running on biodiesel to those from petroleum diesel. The majority of these studies are conducted under controlled laboratory conditions using a limited number of engines. Table 2-1 summarizes the results of these experiments as well as the results of this study. The type of measurement technique applied, the number of engines, and age of engines are used classify the studies. The engine dynamometer tests shows that emissions of CO, HC, and PM are consistently lower with biodiesel fuel than with petroleum diesel fuel. Emissions of NO tend to be equivalent or slightly higher with biodiesel than with petroleum diesel.

An EPA draft report (EPA, 2002) summarizes numerous engine dynamometer emissions studies investigating the effects of biodiesel on exhaust emissions. Emissions from heavy-duty diesel engines running on 100% biodiesel had ~50% lower emissions of CO and PM, ~65% lower emission of hydrocarbons (HC), and ~10% higher emissions of NO_x when compared with petroleum diesel. These estimates are based on tests conducted on 43 heavy duty engines varying in model year from 1980 to 2001. Emission changes in using a blend of petroleum diesel and biodiesel may be approximated by multiplying the emission changes from 100% biodiesel by the fraction of biodiesel in the blend.

As shown by the National Renewable Energy Laboratory (NREL) in 1998 and Canakci and Van Gerpen [2003]), emissions changes appear to be a function of the biodiesel fraction of the fule mixture. Chassis dynamometer studies involve placing a vehicle on a dynamometer where the vehicles wheels turn a drum connected to the dynamometer. These studies may be more representative of real world conditions since the test fuels travel through the vehicles entire fuel handling system. The results of chassis dynamometer tests conducted by Zou and Atkinson [2003] and Wang et al. [2000] are consistent with the engine dynamometer tests in that CO, HC, and PM emission decreased with biodiesel usage. In contrast the studies by Durbin et al. [2000] and Durbin and Norbeck [2002] show a variable increase in PM emissions after test vehicles were refueled with biodiesel. Significant increases in PM emission factors were also observed in this study from in-use buses fueled with B20. Differences in the testing configurations of engine dynamometer, chassis dynamometer, and remote sensing studies may be responsible for the variation in emissions factors.

Table 2-1. Summary of biodiesel studies and comparison with results from current study.

						Ratio of Biodiesel EF/Petrodiesel EF				
Citation	**Year**	**Test Type**	**Biodiesel Mix (%)**	**Number of Engines**	**Engine Year**	**R_{CO}**	**R_{PM}**	**R_{NO}**	**R_{HC}**	**Comments**
McCormick et al. [2001]	2001	Engine Dynamometer	100	1	1991	NA	0.3	1.1	NA	Multiple feedstocks tested. NO decreases with cetane and increases with density. PM relatively flat except for density >0.89 g/cm3 and cetane number < 45.
Cardone et al. [2002]	2002	Engine Dynamometer	100	1	Unknown	0.9	0.8*	1.4	NA	European passenger diesel engine. Rapeseed biodiesel. PM as Bosch Smoke Number.
Lindhjem and Pollack [2003]	2003	Dynamometer	20	20	1985-2002	0.87	0.91	1.0	0.82	Summary of multiple studies between 1998 and 2003
Lindhjem and Pollack [2003]	2003	Dynamometer	100	8	1985-2002	0.58	0.49	1.1	0.30	Summary of multiple studies between 1998 and 2003
Canakci and Van Gerpen [2003]	2003	Engine Dynamometer	20	1	Unknown	0.93	0.84	1.01	0.98	Tests with both soybean and yellow grease biodiesel.
Canakci and Van Gerpen [2003]	2003	Engine Dynamometer	100	1	Unknown	0.82	0.37	1.12	0.57	Tests with both soybean and yellow grease biodiesel. PM as Bosch Smoke Number.
Chen and Wu [2002]	2002	Engine Dynamometer	100	1	Unknown	NA	0.55	NA	NA	
Lue et al. [2001]	2001	Engine Dynamometer	20 - 30	1	Unknown	<1	>1	<1	<1	PM2 mass increases with biodiesel but smoke number decreases with biodiesel
Zou and Atkinson [2003]	2003	Chassis Dynamometer	100	2	Unknown	0.9	0.66	0.9	0.9	
Wang et al. [2000]	2000	Chassis Dynamometer	35	9	1987 - 1994	0.88	0.75	1.05	0.9	Soyate methyl ester biodiesel.
Durbin et al. [2000]	2000	Chassis Dynamometer	20	2	1988 - 1990	1.0	1.6	1.0	1.1	Vehicles w/o oxidative catalysts
Durbin et al. [2000]	2000	Chassis Dynamometer	100	2	1988 - 1990	1.0	2.3	1.1	0.84	Vehicles w/o oxidative catalysts
Durbin et al. [2000]	2000	Chassis Dynamometer	20	2	1995 - 1996	0.90	1	0.95	0.81	Vehicles w/ oxidative catalysts
Durbin et al. [2000]	2000	Chassis Dynamometer	100	2	1995 - 1996	0.85	1.1	0.98	0.46	Vehicles w/ oxidative catalysts
Durbin and Norbeck [2002]	2002	Chassis Dynamometer	20	7	1983- 1993	1.0	1.1	1.0	1.0	World Energy B20.
This Study	2004	Cross Plume	20	205	1983 - 2004	0.91	1.9	0.99	1.23	Hot Stabilized w/o oxidative catalyst
This Study	2004	Cross Plume	20	205	1983 - 2004	1.34	1.7	0.99	0.91	Cold Start w/o oxidative catalyst

3. Measurement Technologies

This section describes the instrumental setups used for this project. The Vehicle Exhaust Remote Sensing System (VERSS) was used to optically measure fuel based emission factors from in-use vehicles passing the sensor. The In-Plume Sampling System was used to develop emission factors for motor vehicle exhaust sampled at the road surface.

3.1. RSD

In 1987, University of Denver developed an infra-red remote sensing device (RSD) for automobile carbon monoxide (CO) exhaust emissions. An additional channel was soon added to measure hydrocarbon (HC) emission factors. Significant improvements in fuel economy result if rich-burning (high CO emissions) or misfiring (high HC emissions) vehicles are tuned or repaired to combust all of the fuel passing through the engine. The University of Denver remote sensor was named Fuel Efficiency Automobile Test (FEAT). In 1991, Sun Electric was licensed to develop the FEAT patent into an off-the-shelf commercial product. In 1993, EnviroTest bought Sun Electric, and the patent was licensed to Remote Sensing Technologies, Inc., a subsidiary of EnviroTest. Finally, in 1998, Environmental Systems Products, Inc. (ESPi) bought EnviroTest. The ESPi VERSS used in this study, the RSD3000, measures CO, HC, CO_2, and NO.

The highly skewed frequency distribution of vehicle emission factors is better quantified as a result of VERSS measurements (Zhang et al. 1994). Relatively few vehicles, called high-emitters, account for a disproportionately large amount of the fleet emissions. Remote sensing has been used in numerous studies to identify these high emitters (e.g., Lawson et al. 1990; Stephens 1994; Lawson 1995; McClintock 1999). In a report prepared by the California Inspection and Maintenance Review Committee (Schwartz 1998), remote sensing errors of omission (false pass) and errors of commission (false fail) are reported to be on the order of a few percent. This is an acceptable level since most of these cars are found to be marginal emitters anyway, i.e., cars with emissions near (just above or just below) the pass/fail cut-points for HC and CO. For example, remote sensing readings were used in California to immediately pull over apparently gross polluting vehicles. A team of Smog-Check (California's emissions testing program) engineers tested these cars and performed EPA IM240 dynamometer tests (Knapp 1992). Of 79 vehicles tested on IM240, 76 failed and the three which passed had all failed the previous Smog-Check. In a comprehensive high-emitter study in Orange County California, repair costs and emissions reductions were tracked from initial RSD identification through pre- and post-repair dynamometer tests. Lawson (1995) found that remote sensing is the most cost effective method of reducing automotive emissions. The fact that a remote sensor can be used to directly measure the on-road tailpipe emissions is also a considerable advantage over other tests, particularly if there are ways that individuals or manufacturers can circumvent other tests, thus rendering those results unrepresentative of the on-road fleet.

3.1.1. Gas Measurement

Automobile exhaust remote sensors (e.g., the RSD3000) emulate the results one would obtain using a conventional non-dispersive infra-red exhaust gas analyzer, such as those used by private emission testing stations in Ada County. Non-dispersive ultra-violet light is used for the NO channel on the remote sensor. An interference filter is placed in front of a detector to only

transmit light of a known wavelength absorbed by the molecule of interest. Gaseous molecules in the optical path across the roadway absorb the transmitted light and reduce the voltage output by the detector. Because the amount of plume seen by the detector is affected by the position of the vehicles exhaust pipe and the turbulence behind the vehicle, it is not possible to measure the rate of emissions for each species. Instead, fuel based emission factors are measured by the ratios of CO, HC, and NO to CO_2. The ratios of CO/CO_2, HC/CO_2, and NO/CO_2 are approximately constant during the 0.5 seconds that the plume from a passing vehicle is measured by the remote sensor.

These ratios are useful parameters for describing the combustion system. With the aid of a fundamental knowledge of combustion chemistry, many parameters of the vehicle's operating characteristics can be determined including: the instantaneous air/fuel ratio, the %CO, %HC, or %NO which would be read by a tailpipe probe, and the grams CO, HC, or NO emitted per gallon of gasoline (Bishop et al. 1996). Most new gasoline powered vehicles operating with a hot catalytic converter emit very little CO or HC with respect to older and higher emitting vehicles. For these vehicles, the values of CO/CO_2 and HC/CO_2 are frequently below the detection limits of the remote sensor. Elevated CO/CO_2 ratios are associated with fuel-rich air/fuel ratios and a defective emission control system. A lean air/fuel ratio, while impairing driveability, produces very little CO in the engine. A high HC/CO_2 ratio can be associated with either fuel-rich or fuel-lean air/fuel ratios. If the air/fuel ratio is lean enough to induce misfire then a large amount of unburned fuel (HC) is present in the exhaust manifold. If a catalyst is absent or non-functional, then high HC can be observed in the exhaust without the presence of high CO. To the extent that the exhaust system of this misfiring vehicle contains some residual catalytic activity, the HC may be partially or totally converted to a CO/CO_2 mixture.

The height of the sensing beam is typically set at 20-30 cm above the road surface to observe exhaust plumes from nearly all light duty vehicles. For this study, special platforms were constructed to elevate the middle height of the remote sensing beams to ~75 cm above the road at the average height of the school bus exhaust pipe. The RSD3000 is equipped with a video system to capture images of the back end of the vehicle as it passes through the test section. The video camera is coupled directly into the data analysis computer so that the image of each passing vehicle is displayed on the video screen and stored with the exhaust plume measurement.

3.1.2. Speed and Acceleration

Speed and acceleration strips provided with the RSD3000 consist of two aluminum bars approximately 2 meters in length, placed parallel to the flow of traffic on either side of the lane. One bar is equipped with diode lasers at the ends, and the other bar is equipped with two corresponding photo detectors. These are aligned such that each diode laser hits the photo detector across the lane of traffic. As the front and back tires sequentially break the upstream and downstream beams, the speed and acceleration can be computed for each vehicle.

3.1.3. License Plate Images

License plate and school bus numbers from each legible image were transcribed by DRI personnel for all vehicles at the Lanark Road site and by COMPASS staff for the freeway on-ramp sites. Using the software supplied with the RSD3000, the license plate data were linked to the corresponding emission measurement within the project database. Each complete remote sensing record in the RSD3000 data files contains the information for:

- Unit Code (i.e. serial number of RSD3000)
- Site Code
- Date and Time
- Vehicle Sequence Number
- Calculated CO, CO_2, HC, and NO Concentrations in the pure exhaust
- License Plate Information (Plate Flag and Plate Description)
- Speed and Acceleration.

3.2. VERSS LIDAR

This section describes the DRI's VERSS LIDAR. The system was deployed previously in a large field study in Las Vegas, NV and is the topic of several peer reviewed journal articles (Moosmuller et al. 2003; Kuhns et al. 2004 ; Mazzoleni et al. 2004a; Mazzoleni et al. 2004b; Barber et al. 2004).

3.2.1. Theory

The light detection and ranging system (LIDAR) developed by DRI is designed to measure the light scattering in a column defined by a laser beam through an exhaust plume of a passing vehicle. Simultaneously, the infrared source on the RSD3000 is used to detect the CO_2 through the exhaust plume. The ratio of integrated PM light scatter to CO_2 gives a relative measure of the pollution being generated by the vehicle in grams of PM per unit of fuel carbon consumed.

When laser light illuminates a pollution particle in an exhaust plume, the light is both scattered in all directions and absorbed by the particle. For a particular incident light beam, the nature of the scattering and absorption interaction is determined by the physical characteristics of the particle (i.e. its size, shape, and material composition). If the characteristics of the incident light are known, specifically its direction of propagation, polarization, wavelength, and intensity, then this knowledge, coupled with the nature of the scattered light and a laboratory calibration, can be used to determine the concentration of an assumed size distribution of particles.

Analysis of "backscattered" light to determine particle characteristics is analogous to what is done with radar, whereby microwave radiation is "bounced" back from an unknown airborne target to determine its location. The sensitivity of detection of the backscattered light can be maximized by choosing a light source at a wavelength that is comparable to the size of the particles being measured. Soot in vehicle exhaust generally falls in the size range of 0.05 to 0.5 μm.

In the DRI VERSS LIDAR, a narrow pulse of laser light (nominally 1 ns in duration) at an ultraviolet wavelength of 0.266 μm leaves the transmitting laser at one side of the road and is partially reflected back toward the transmitter by particles in the exhaust plume. The received signal is the output voltage of a photo-multiplier tube (PMT) versus time. The dimensions of the typical roadside configuration are such that a 1 ns pulse of light (traveling at the speed of light) interacts with the exhaust plume and is returned in less than 100 ns. For the given laser pulse repetition frequency of 6.8 KHz, a pulse is transmitted approximately every 150 μs, ensuring that only a single 1 ns transmitted pulse interacts with the exhaust plume at a time. The remote sensing configuration is shown in Figure 3-1.

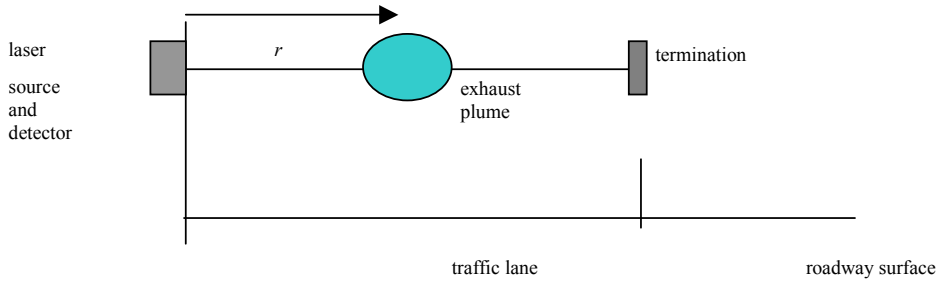

Figure 3-1. LIDAR configuration.

The calculated single-particle differential scattering cross section in the backscatter direction and the single-particle extinction cross section are the particle information required to predict the received power measured by a LIDAR system.

The basic operation of the system is defined by the LIDAR equation,

$$P(r) = P_L O(r) \frac{c\tau}{2} \frac{A}{r^2} \sum_i [N_i(r)\sigma_{d,i}(r,\pi)] e^{(-2\sum_i \int_o^r N_i(r')\sigma_{e,i}(r')dr')} \qquad (3\text{-}1)$$

where

$P(r)$ = Scattered laser power (Watts) received at the detector at a time corresponding to the leading edge of the laser pulse propagating to a range r, meters.

$O(r)$= Characterizes the overlap of the receiving telescope field of view with the UV-laser illuminated particulate path.

P_L = Average power (Watts) of the incident laser beam.

c = Speed of light, 3 x 10^8 m/s.

τ = Incident pulse width, s.

A = Area of receiver telescope aperture, m^2.

$N_i(r)$ = Number density of scatterer species i, #/m^3, at range r.

$\sigma_{d,i}(r,\pi)$ = Differential scattering cross section of species i in the backscatter (π) direction, m^2/steradian, at range r.

$\sigma_{e,i}(r)$ = Extinction cross section of species i, m^2, at range r.

i = An index denoting a particle that has a specific size, shape, and composition.

Equation 3-1 includes a summation over all of the different particles that may be present. The term $N_i(r)\ \sigma_{d,i}\ (r,\pi)$ quantifies the backscattering from particles of species i. The term $N_i\ (r')$ $\sigma_{e,i}(r')$ in the exponent quantifies the extinction from particles of species i, where the factor of 2 accounts for the roundtrip, two-way extinction experienced by the LIDAR pulse. Therefore, the initial amplitude of the backscattered pulse diminishes at later times during the two-way attenuation of the pulse by the scattering and absorption (the sum is the extinction) of the intervening particles.

In general, there are three sources of backscattered 266 nm light in the roadside environment: (1) the PM in the exhaust plume of the vehicle being measured, (2) the background molecular gases in the atmosphere, and (3) the ambient PM. This latter quantity may include multiple components, such as the background PM from regional sources, PM from vehicles that immediately preceded the vehicle currently being measured, and dust particles raised from the

road surface by vehicle motion and roadway tire contact. For purposes of the present analysis, species (2) and (3) will be incorporated in a single ambient term related to non-exhaust PM.

This form of the LIDAR equation incorporates a number of assumptions that simplify the analysis. Some of the assumptions include that the incident laser signal pulse is rectangular (in time), monochromatic (single wavelength), and the spatial distribution of PM in the exhaust plume is homogeneous.

The LIDAR equation is analyzed by first considering the combined effect of the scattering from two species of particulates – PM in an exhaust plume and an ambient background consisting of only atmospheric molecular scattering. Once this situation is illustrated, then it is straightforward to incrementally add additional ambient terms, including background regional PM, PM from preceding vehicles, and dust.

For a homogeneous particulate distribution within the plume, the exponential term in (3-1) can be simplified, since $N(r')$ and $\sigma_e(r')$ are constant with r. For a system consisting of two species of particles, background molecular gases and PM in the exhaust plume, the term in the exponent in (3-1) becomes:

$$-2(N_a\,\sigma_{e,a}\,r + N_{PM}\,\sigma_{e,PM}\,[r\text{-}r_o]) \qquad (3\text{-}2)$$

where the quantities with the subscript a are associated with molecular gases and variables with the subscript PM are associated with the exhaust plume. Then (3-1) becomes:

$$P(r) = P_L O(r)\frac{c\tau}{2}\frac{A}{r^2}\sum_i [N_i\sigma_{d,i}(\pi)]e^{-2(N_a\sigma_{e,a}r + N_{PM}\sigma_{e,PM}[r-r_o])} \qquad (3\text{-}3)$$

Here it is important to remember that $\sigma_d(\pi)$ and σ_e associated with the exhaust plume only have value within the plume and are zero when the range variable r is not within the plume.

It is useful to consider the special case when the term in (3-2) can be approximated as zero. This assumes that the extinction by both the ambient particles and the PM in the exhaust plume are negligible. The extinction by molecular gases (the first term) over the limited range of the system will be quite small. In the case of the exhaust plume (the second term), this would be small when the product $N_{PM}\,\sigma_{e,PM}$ is small, either because the particle density N_{PM} in the plume is low or the particles in the plume have low extinction coefficients, or the thickness of the plume is small, or some combination of all three factors. When the quantity in (3-2) is negligibly small, $e^o = 1$ and (3-3) becomes:

$$P(r) = P_L O(r)\frac{c\tau}{2}\frac{A}{r^2}\sum_i [N_i(r)\sigma_{d,i}(\pi)] \qquad (3\text{-}4)$$

Except for the $O(r)$ and $1/r^2$ terms, the term preceding the summation is a system constant that can be represented by C_o. Making this substitution and expanding the summation in (4) gives:

$$P(r) = \frac{C_o O(r)}{r^2}[N_a \sigma_{d,a}(\pi) + N_{PM} \sigma_{d,PM}(\pi)] \qquad (3\text{-}5)$$

The first term in brackets, the backscatter from molecular gases includes no range dependence – it exists across the entire range. The second term, as mentioned earlier, is zero outside the plume and has value only when the range variable r is within the plume. Both terms decrease as $1/r^2$ with range r.

Equation 3-5 also describes the temporal behavior since $r = ct/2$. If the leading edge of the laser pulse leaves the source at time $t = 0$, then the scattered power is received at the detector as some later time $t = 2\ r/c$, where the factor of 2 accounts for the round trip transit time. Scattered power from the exhaust plume is only received when the pulse overlaps the plume. There are three distinct regions of overlap: 1) when the pulse is entering the plume, 2) when the pulse is entirely within the plume, and 3) when the pulse is exiting the plume.

As an example, consider an arrangement where the total path length is 11 m with a 1 m thick exhaust plume located at the center. The first signal to arrive back at the receiver is from the leading edge of the incident pulse entering the exhaust plume at a distance of 5 m. This occurs when $t = (2)(5\text{ m})/3 \times 10^8$ m/s = 33.3 ns. Scattered power from the pulse interaction with the leading edge of the plume will continue to be received until the trailing edge of the pulse is at 5 m, which occurs 1 ns later, so the last signal from the leading edge of the exhaust plume arrives at 34.3 ns. The last signal from the exhaust plume arrives at the receiver when the trailing edge of the pulse is leaving the trailing edge of the plume at a distance of 6 m. The leading edge of the pulse is at 6 m when $t = (2)(6\text{ m})/3 \times 10^8 = 40$ ns. Signal will continue to be received until the trailing edge of the pulse is at 6 m, which occurs 1 ns later, so the last signal from the trailing edge of the exhaust plume arrives at 41 ns. The reflected signal from the beam termination is received when $t = (2)(11\text{ m})/3 \times 10^8 = 73.3$ ns. The duration of the beam termination signal is 1 ns.

The received LIDAR power for the two-species system defined by (3-5), background molecular gases and exhaust PM, is qualitatively described, for this example, by Figure 3-2.

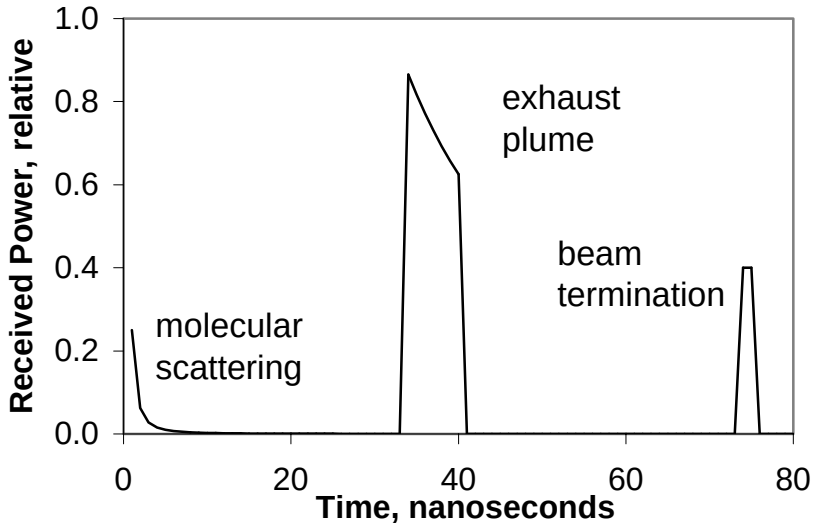

Figure 3-2. LIDAR signal for a 1 ns pulse transmitted at $t = 0$.

Note that the received power from the exhaust plume increases between 33.3 and 34.3 ns as the incident 1 ns pulse enters the plume, decreases as the pulse transits the plume, and then decreases between 40 and 41 ns as the incident 1 ns pulse exits the plume. The received power from the background molecular scattering is only observable at early times, when the transmitted pulse is close to the source. At later times the molecular scattering is significantly reduced by the $1/r^2$ term in (3-5). The returned power from the beam termination has been given an arbitrary amplitude for purposes of this example.

This has been a qualitative example. A quantitative simulation of the LIDAR process defined by (3-5) requires specific knowledge of the exhaust PM and its scattering and extinction characteristics.

For gasoline and diesel vehicle exhaust, it is necessary to determine the physical characteristics of the particles contained within the plumes, i.e., their size, shape and index of refraction (related to composition). This is so the quantities $\sigma_d(\pi)$ and σ_e may be approximated or calculated, thereby enabling backscattering and extinction calculations. Obtaining this information requires some knowledge of the form in which elemental carbon and organic carbon are present in the particulate distributions as separate particles, homogeneous spherical mixtures, agglomerations, or in layered configurations. In addition to the characteristics of individual particles, we need to know the particle size and shape distributions that may be expected for vehicle exhaust. A number of studies have considered the above factors.

3.2.1.1. Vehicle Exhaust Characteristics

Horvath (1993) focuses on the properties of black carbon and its role in light absorption in the atmosphere. He indicates that for atmospheric particles, only elemental carbon, the main constituent of black carbon, is highly light absorbing. His report summarizes 15 refractive indices that have been used for elemental carbon. Real parts of the refractive index vary from 1.5 to 2.0 and imaginary parts vary from 0.1 to 1.0. He indicates that combustion processes,

which are most often anthropogenic, form light-absorbing particles. Incomplete oxidation of the carbon-containing fuel causes the formation of black carbon. Major sources of elemental carbon in the atmosphere are diesel motors, small furnaces, and biomass burning. For vehicles, black carbon emissions from pre-1992 diesel engines are about 100 times those of a hot stabilized pre-1992 gasoline engine for an equivalent driving distance. A specific example for a particular pre-1992 diesel engine shows that the emitted particulates can contain both elemental and organic carbon, with the fraction of each varying from 10% to 90% depending upon the quality and the operating conditions of the engine.

Völger et al. (1996) give a table of refractive indices of aerosol components at different wavelengths. Specifically, the refractive index of soot at wavelengths of 250 nm and 300 nm, is given as 1.62- i0.45 and 1.74-i0.47, respectively.

Kittelson (1998) indicates that particulate mass emissions from pre-1992 heavy-duty diesel engines typically are 10-100 times higher than those from spark ignition engines. The structure of unaged diesel exhaust particles is shown in his figure 1 of his report as agglomerated solid carbonaceous material, ash, and volatile organic and sulfur compounds. Figure 3 of his report shows a typical engine exhaust size distribution, for both mass and number weighting. Most of the particle mass exists in the 0.1-0.3 μm diameter range. This is where the carbonaceous agglomerates and associated adsorbed materials reside. The nuclei mode typically consists of particles in the 0.005-0.05 μm diameter range. Nuclei mode particles usually consist of volatile organic and sulfur compounds that form during exhaust dilution and cooling, and may also contain solid carbon and metal compounds.

Martins et al. (1998) use a layered-sphere configuration to model particles from biomass burning. The model consists of a highly-absorbing black-carbon core surrounded by a much lower absorbing shell. They indicate that this low-absorbing shell is likely formed by gas-to-particle conversion and condensation of volatile compounds. At a wavelength of 0.55 μm, the refractive index of the black carbon is assumed to be 2.0-i1.0 and that of the low-absorbing shell is assumed to be $1.5 - i10^{-6}$.

Shi et al. (2000) have determined the physical properties (size distribution, number, volume, mass concentrations, and density), chemical properties (organic and elemental carbon, PAH, sulfate, and nitrate), and morphology of particles of from a diesel engine. They found wide variations in particle size distributions and particle concentrations depending upon dilution conditions and humidity. They found that combustion particles are largely present in the form of clusters. Large particles were found to be clusters of small basic particles that ranged from 10 to 40 nm. Their measurements provide some confirmation that emitted particles consist of a nonvolatile core covered by a volatile liquid material.

Bessagnet and Rosset (2001) focus on the plume emitted by diesel vehicles. They indicate that recent studies have shown that particles exist as aggregates of carbon spherules displaying linear to quasi-spherical structures. Fresh combustion particles, presumably elemental carbon spheres, each about 20-30 nm in diameter, are emitted together with sulfuric acid, water vapor and a number of other species, including volatile organic species. These species nucleate, condense and are absorbed on the carbonaceous particles. Figure 1 of their report is a schematic drawing that depicts the evolutionary processes that occur immediately at the exit of the vehicle exhaust system. They indicate that emissions from vehicle exhaust that occur under different meteorological conditions can influence the composition of the plume. This pertains particularly

to humidity. Furthermore, the makeup of the emission depends strongly upon vehicle type and operating conditions. One example shows that the mass fraction of dry aerosol emitted in the exhaust of a diesel vehicle is 15.8% elemental carbon and 83.7% organic carbon, with much smaller percentages of other components. The size distribution of particles has been simulated in the immediate area of the exhaust pipe. A nucleation burst occurs at the exit of the exhaust pipe and intense coagulation follows, such that in only a few meters a bimodal particle spectra with peaks at 5 and 60 nm occurs (their Fig. 3a).

The selection of particulate models to use in the mathematical simulation of the LIDAR interaction with vehicle exhaust involves a tradeoff. The particulate systems are so complex and variable that it is unlikely that exact particle models can be formulated. Furthermore, even if an exact model could be formulated, the ability of available electromagnetic scattering and absorption computer programs to obtain numerical results is restricted to a small class of particle configurations. In the end, the goal is to obtain numerical results that will indicate the semi-quantitative behavior of the real-world light scattering and absorption interactions. For purposes of the present LIDAR simulation, the above considerations and information contained in the literature indicate that the use of a layered sphere model may be the best compromise between reality and our ability to obtain numerical results.

Furthermore, for purposes of this simulation, we will use an index of refraction of $1.5 + i0.5$ for elemental carbon and $1.5 + i0.0$ for organic carbon. Presumably these two components appear together in the same particle. The most commonly assumed particle configuration is a layer of organic carbon condensed upon an elemental carbon base particle.

The literature shows wide agreement that the number distribution of the particles in a vehicle's exhaust is a lognormal size distribution. The rough diameter of pollution particles in vehicle exhaust peaks around the 0.1 to 0.2 μm range. The paper by Bessagnet and Rosset (2001) for diesel engines probably is the most useful in defining number distributions for different cases.

3.2.1.2. Light Scattering Calculations

Clearly, the quantities of interest are the particle differential scattering cross section in the backscatter direction, $\sigma_d(\pi)$, and the particle extinction cross section, σ_e. These calculations have been made for particle diameters from 0.01μm to 10μm, encompassing the expected size range of vehicle exhaust particles. Results have been obtained for solid spheres with an index of refraction characteristic of organic carbon as well as for two-layer spheres consisting of an elemental carbon core and an organic carbon shell. The calculated quantities, $\sigma_d(\pi)$ and σ_e, have been normalized by particle volume. Calculations have been made for a wavelength of 0.266 μm, the ultraviolet wavelength of the LIDAR system.

Figure 3-3 shows the results of a calculation of $\sigma_d(\pi)$ and σ_e for a homogeneous spherical particle with an index of refraction of $m = 1.5 + i0.0$, representing a sphere of solid organic carbon. This particle is nonabsorbing (the imaginary part of the index of refraction is 0.0), so the extinction cross section (σ_e) is equal to the scattering cross section. Like the backscatter cross section, $\sigma_d(\pi)$ exhibits a straight-line log-log behavior in the range 0.01 to 0.1 μm, indicative of the scattering behavior of particles that are small relative to a wavelength.

A layered sphere program has been obtained and the program has been successfully tested for a variety of core and shell configurations representative of the particle distributions that we expect

to use. Figure 3-4 shows the result of a calculation for a layered spherical model consisting of an elemental carbon core surrounded by an organic carbon shell.

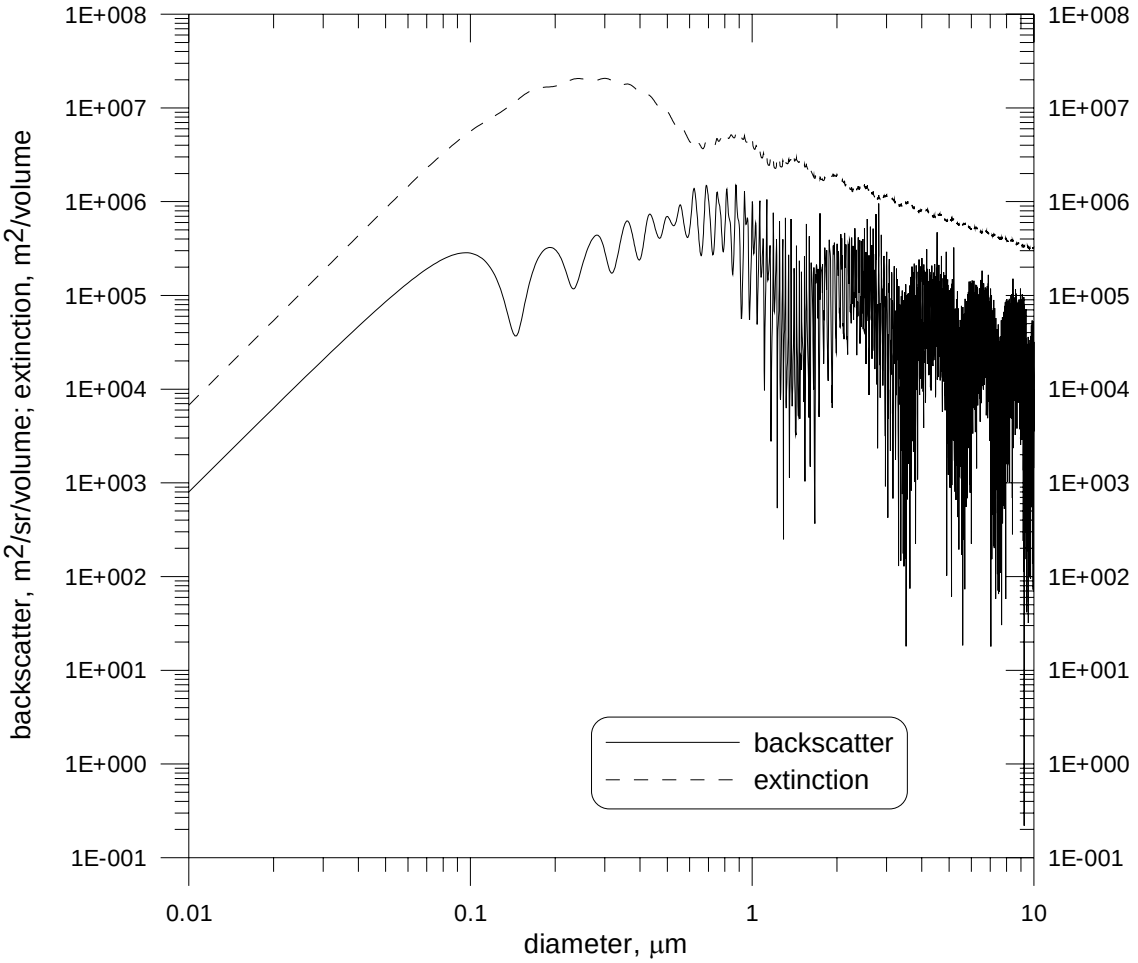

Figure 3-3. Backscatter and extinction (normalized by particle volume) for a homogeneous spherical particle with an index of refraction of m = 1.5 +i0.0 at λ = 0.266 μm.

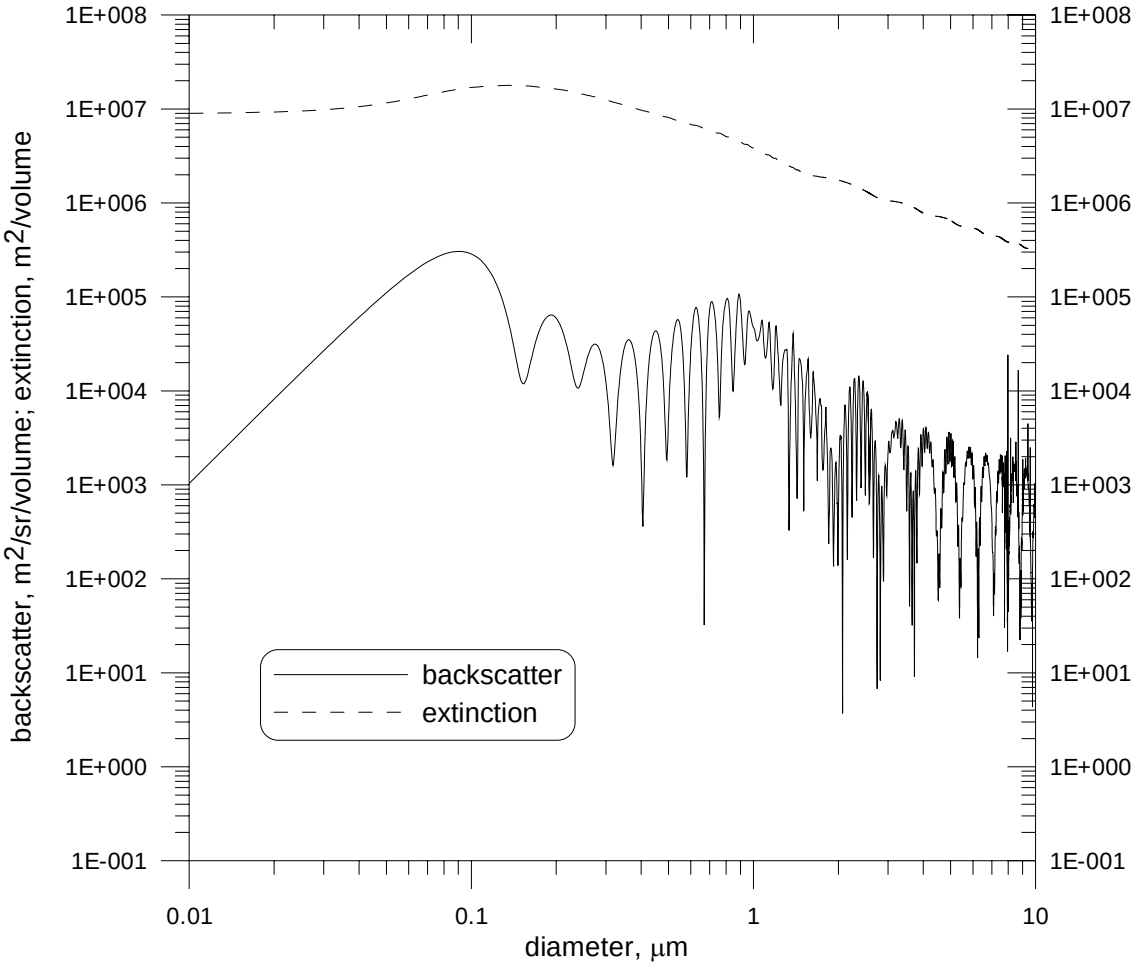

Figure 3-4. Backscatter and extinction (normalized by particle volume) for a layered spherical particle with an index of refraction of mcore = 1.5 +i0.5 and mshell = 1.5 +i0.0 at λ = 0.266 μm. Fractional core volume is 0.5.

3.2.2. LIDAR Experimental Set-up

PM light scattering is measured with an ultraviolet (UV) backscattering LIDAR (light detection and ranging) system using a pulsed Nd:YAG laser (Uniphase PowerChip NanoLaser PNU-001025-040) frequency quadrupled to a wavelength of 266 nm as a radiation source. A laser pulse, with a pulse width of ~1 nsec, and 10 μJ/pulse energy, is transmitted across the lane about every 1 millisecond (1000 Hz). The LIDAR receiver is located in a biaxial arrangement next to the ongoing beam. A 15-cm diameter spherical mirror collects the light backscattered by the particles suspended along the laser beam path, at ~180 degree and focuses it onto a fast, solar blind photomultiplier tube (PMT) (Hamamatsu R7400U-06). A band pass filter is mounted in front of the PMT (Corion G10-265-F) to reduce the contribution of background radiation. The PMT generates a negative current, which is a function of the incident optical power. A high bandwidth (i.e., 1.5 GHz with a 4 Gsa/s sampling rate) digital oscilloscope measures this current, yielding a time dependent waveform for each laser pulse. This time dependent waveform is converted to a distance dependent waveform by multiplication of the time since the firing of the laser pluse with one half the speed of light to account for the roundtrip of the UV radiation. A

computer-based data acquisition system collects ~60 waveforms before and ~100 waveforms just after the vehicle passes for a total collection time of ~0.3 and ~0.5 seconds, respectively.

Under routine operation, the laser beam is propagated through the exhaust and reflected back by a set of mirrors on the opposite side of the road. The transmitted beam is collected by a 5 cm UV transparent fused silica lens and focused onto a large area photodiode operated in photovoltaic mode (UDT Sensor, Inc. UV-100). The photodiode's signal is processed by an analog gated integrator and digitized for further processing into a transmission or opacity reading for 0.266 μm light. Figure 3-5 shows a diagram of the LIDAR system with the laser, telescope, PMT for light scattering, and photodiode for light absorption.

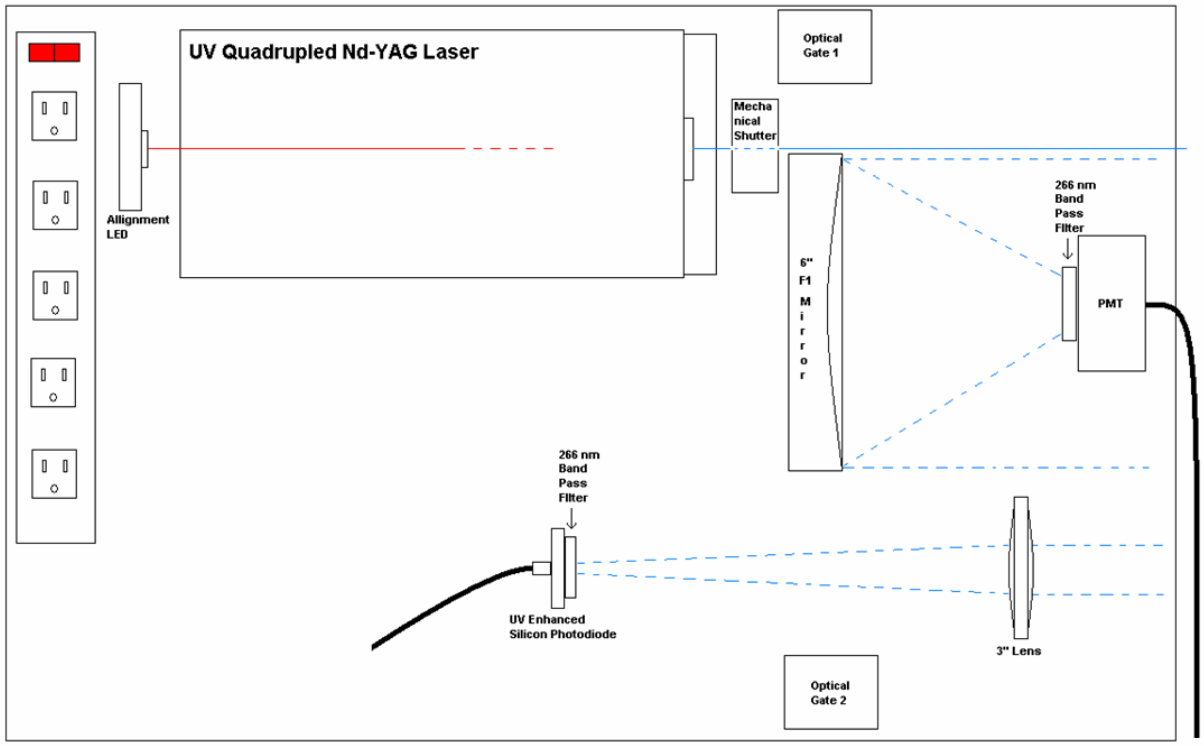

Figure 3-5: Schematic of UV LIDAR and Transmissometer Unit.

The backscattering waveform is range corrected, and calibrated using a non-linear sensitivity curve measured in the laboratory using CO_2 and HEPA filtered air as standards of known scattering efficiency (Figure 3-6). Neutral density filters of known opacity were inserted in front of the PMT to obtain addition calibration points for the system.

Figure 3-6. LIDAR calibration configuration showing HEPA filtered air inflating the calibration cell (lawn and leaf bag material).

Mass efficiency constants are used to convert the quantity of backscattered light to PM mass within the optical column based on published measurements of PM bulk density, composition, and size distribution (Barber et al. 2004). For spark-ignition vehicles, PM optical properties are modeled as homogeneous, spherical particles with a real index of refraction of 1.5 and negligible absorption at 266 nm. Particle diameters are assumed log-normally distributed with mass

median diameter of 0.15 μm and geometric standard deviation of 1.5. The bulk density of each individual particle was assumed to be equal to 1.25 g cm^{-3}. From these assumptions a backscattering mass efficiency of 0.16 ± 0.05 $m^2/(g \cdot sr)$ was calculated for gasoline vehicle exhaust PM. The error was estimated assuming reasonable uncertainties for the parameters used in the mass efficiency calculation. For diesel exhaust, the mass backscattering mass efficiency was calculated to be 0.08 ± 0.03 $m^2/(g \cdot sr)$ (Barber et al. 2004).

The calculated mass concentration is then integrated over the range spanning the roadway to obtain a PM column content (Moosmüller et al. 2003). The total carbon mass column content determined by the gaseous VERSS (RSD3000) was used to calculate the fuel-based PM emission factor (i.e., mass of PM emitted per mass of fuel consumed).

3.3. In-Plume Sampling System

DRI's In-Plume Sampling System was developed to measure concentrations of gaseous and PM emissions from combustion sources. Using a carbon mass balance approach, fuel-based emission factors (in grams of pollutant per kg fuel burned) can be calculated from the simultaneous measurements of gases and particles provided by the system (Pokharel et al. 2002; Moosmüller et al. 2003). A sampling inlet is placed near a source plume. Exhaust is passively cooled and diluted with ambient air prior to being drawn into the inlet. Since emissions of pollutants are referenced to the total carbon emitted (i.e., CO_2 + CO + HC), it is not necessary to capture the entire plume to obtain an emission factor. The In-Plume Sampling System permits the measurement of emission factors for sources in real world conditions. For example, emission factors for motor vehicle exhaust in the fleet can be estimated by deploying the system to sample exhaust at the road surface to collect partial plumes from passing vehicles, which vary by year, make, model, type, and speed.

Figure 3-7 shows a schematic of the In-Plume Sampling System and Table 3-1 describes the instrumentation used. Gaseous emissions are measured with a Fourier Transform Infrared (FTIR) spectrometer equipped with a ducted gas cell to permit fast response times (1.5 s) over a 10 m optical path. Particles are measured using a combination of real-time and integrated techniques including TSI DustTraks, an Electronic Low Pressure Impactor (ELPI), and filter-based methods. The sampling system is field transportable. Instruments are mounted on two handcarts for easy offloading and positioning near the plume. The In-Plume System uses a time-integrated filter-based PM sampling system for chemical sampling speciation. Teflon-coated Bendix 240 cyclones are used to remove particles greater than a specified aerodynamic diameter from the sample flow prior to PM sample collection. PM_{10} and $PM_{2.5}$ 50% cutpoints for the Bendix 240 cyclone were achieved by running the sample flows at 45 and 113 liters per minute (lpm), respectively. Airflow, temperature, and gauge pressure behind each filter pack are monitored by TSI Series 4102 mass flow meters. These data are logged on a field computer. The operator can adjust the flow control valves over the sampling period to maintain the appropriate particle size cut for each filter.

The real-time gas and particle sampling instruments using the FTIR and ELPI were deployed during initial tests on March 12, 2003 (2003/03/12) and March 31, 2003 (2003/03/31) along Highway 28 near Sand Harbor on the eastern shore of Lake Tahoe, Nevada. The initial setup used a 1-meter tall by 10 centimeters wide funnel oriented vertically next to the traffic lane. Emissions from passing vehicles entered the funnel and were drawn into the gas and particle sampling instruments. Vehicles passed the equipment at 60 to 90 km/hr. During the sampling,

winds were approximately 3–5 m/s. Initial tests found that the roadside plume was too dilute to resolve exhaust emissions. Increased particle concentrations in the fine and coarse size ranges, measured with DustTraks and the ELPI, were detected downwind.

The sampling system was reconfigured to collect gas and particle measurements closer to exhaust pipes. A cable protector designed to prevent vehicles from damaging extension cords across roads was fitted with a sampling line, and a 2.54 cm inlet hole was drilled in the middle of the cable protector to draw air into the sampling system from the center of the traffic lane. The inlet line was then connected to a plenum and redirected to numerous sampling instruments. Tests with this configuration indicated that CO_2 could be measured above background (>600 ppm) for vehicles traveling at speeds of less than 50 km/hr. Optimal sampling occurred when the plume was not dispersed over a long distance (i.e., slow vehicle speed). It was this configuration of the In-Plume System that was used to collect data for this biodiesel emissions factor study.

Figure 3-7. Schematic of In-Plume Sampling System.

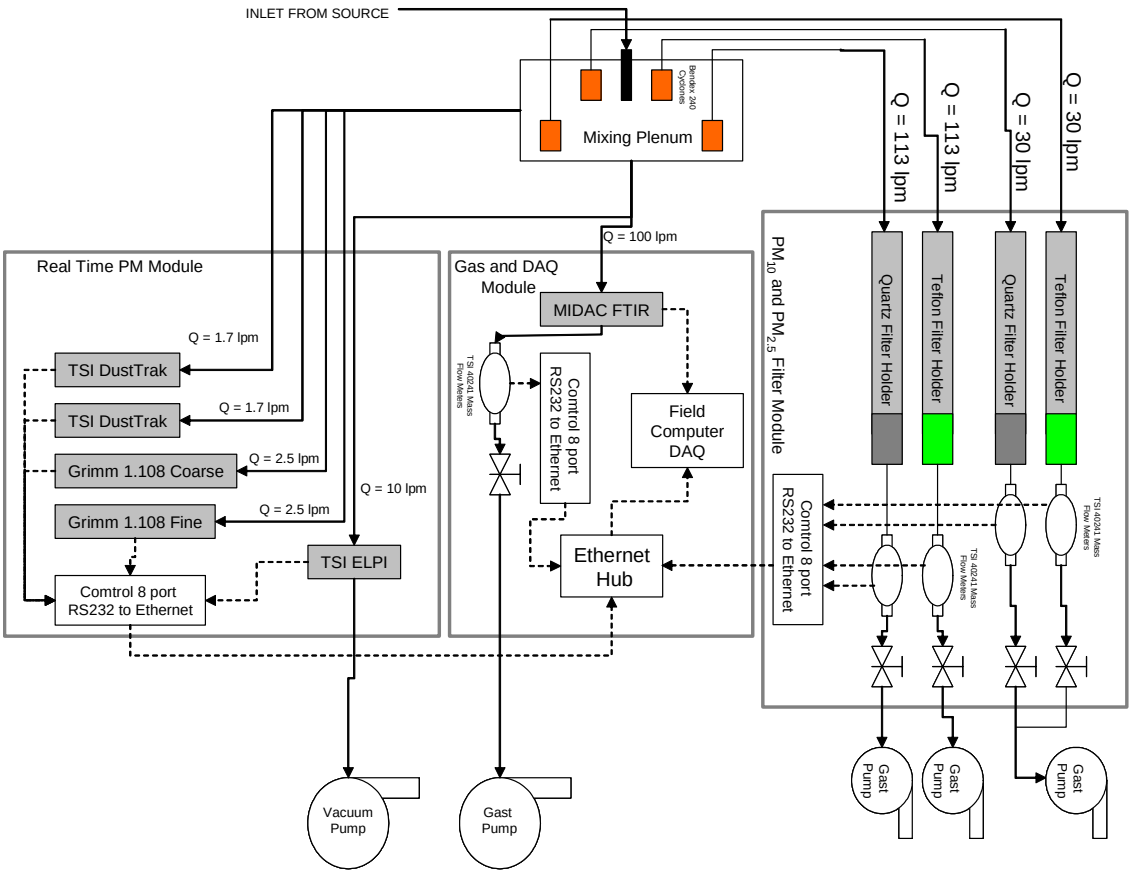

Table 3-1. Instrumentation of In-Plume Sampling System.

Instrument	Measurement	Method	Response Time (s)
Midac I-Series FTIR	Molecular gas species concentration	Dispersive IR	1.5
Dekati Electronic Low Pressure Impactor (10 lpm)	Aerodynamic number size distribution of particles	Current dissipation arising from deposition of charged particles to impactor substrates	5
TSI DustTrak	Particle mass	780 nm laser light scattering of particle stream at 90 degrees	1
Nuclepore filter sampler	Mass and chemical composition of particles and gases	Collection and analysis of exposed filters	>1000
TSI 4043 Mass Flow Meters	Mass flow through filter	Hot wire anemometer	<1
Timemark Delta III Traffic Counter	Vehicle speed, direction, axel spacing, acceleration, and classification	Timing intervals of wheel strikes on road tubes across lane	1
Video	Vehicle type	CCD	<1

3.3.1. Instrument Descriptions

3.3.1.1. FTIR

A Midac FTIR spectrometer was used to measure infrared exhaust absorption spectra at a frequency of one scan per 1.5 s. The instrument uses a Michelson interferometer with a mercury-cadmium-tellurium (MCT) liquid nitrogen cooled detector. Measured species, wave number regions, calibration ranges, and typical concentrations are listed for 10 gases in Table 3-2. Calibration spectra were created using EPA-certified gases diluted with ultra-pure nitrogen using an Environics gas dilution system. A custom ducted gas cell with a 10 m folded optical path length was designed to facilitate rapid air changes in a 2-liter analytical volume. Typical flow rates through the gas cell are 100 lpm. The FTIR is referenced with ambient air in the field. As a result, gas concentrations are measured as the difference from the ambient air. For example, when a typical vehicle passes over the road level inlet at 20 km/hr results in a 7 s CO_2 peak with an average concentration of 150 ppm above ambient air.

A typical absorbance spectra averaged over a 60 second period is shown in Figure 3-8. Water vapor has a very high ambient background with respect to the concentrations that would be measured in an exhaust plume. The absorbance bands for these regions appear as negative values. Since water vapor concentrations can change substantially over the coarse of a day, the negative values likely reflect a decrease in ambient water vapor concentrations from the time the reference background for the FTIR was collected.

Table 3-2. Gases analyzed using classical least squares analysis of infrared spectra from FTIR.

Species	Reference Region (cm^{-1})		Average In-Plume Concentration (ppm)	Uncertainty Standard Error (ppm)	Calibration Range (ppm)	
	Lower υ_1	Lower υ_2				
CO_2	723.00	750.00	150	17	100	4730
CO	2133.31	2142.20	1.93	0.05	1.0	1005
NH_3	955.55	976.14	0.04	0.01	1.0	110
NO	1873.00 1880.60 1898.60 1926.00 1934.60	1878.50 1883.80 1901.30 1932.00 1939.90	0.12	0.13	0.2	20
H_2O	1200.00	1300.00	93	27	5.0	5294
C_4H_{10}	3041.30	2825.64	0.04	0.05	1.0	100
C_6H_{14}	3029.79	2817.96	0.06	0.04	0.2	200
C_2H_4	957.97	936.57	0.00	0.08	0.5	20
NO_2	1584.00 1597.50 1604.30 1610.60	1588.70 1600.20 1605.90 1613.80	0.00	0.11	0.2	20
SO_2	1112.50 1123.40 1138.60 1153.60 1166.60 1176.60 1188.00 1199.90 1226.90	1120.30 1134.00 1148.10 1164.00 1172.50 1185.10 1197.20 1209.00 1235.70	0.00	0.14	1.0	100

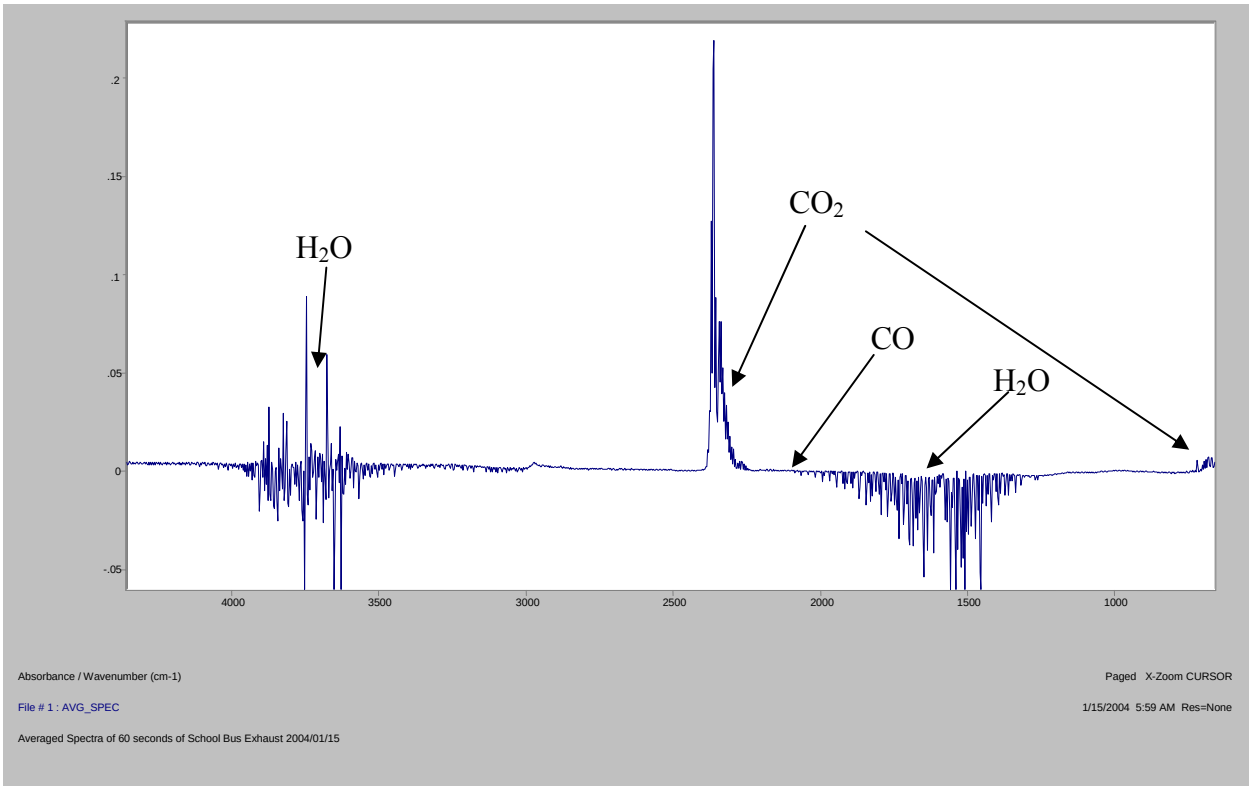

Figure 3-8. Infra-Red Spectra of school bus exhaust from Phase I (2004/01/15).

3.3.1.2. ELPI

The ELPI (Dekati Instruments, Finland) uses a unipolar corona charger to impart a positive charge on the measured aerosol. The particles then travel through a cascade impactor and are deposited on 1 of 12 substrates (0.030 µm to 9.6 µm) based on their aerodynamic diameter. The substrates are electrically isolated with Teflon supports and the accumulating charge on each of the substrates is measured by an array of electrometers. The measured current on each of the stages is proportional to the number of particles depositing on the stage. The ELPI measures the number concentration (i.e. particles per cubic meter) of particles based on their aerodynamic size at a frequency of 1 Hz.

Van Gulijk et al. (2001) investigated the performance of the ELPI through controlled tests on a diesel soot aerosol. Scanning electron microscopy (SEM) analysis of the impactor stages indicated that the fractal structure of the aerosol quickly formed mounds on the impactor substrates, resulting in a dynamic shift in the impactor cut sizes. Subsequent analyses (van Gulijk et al., 2003) found that the use of oiled sintered stages on the impactor extended the sampling capacity of the ELPI by more than a factor of 50 by wicking particles away from the impact area. For this study, the ELPI was operated using oiled sintered substrates followed by a filter stage.

The mass of particles collected on the filter stage is negligible (<0.01%) with respect to the larger stages. However, the abundance of these nanoparticles in the sample stream can cause a bias in the measurement of coarse particles. The corona charger imparts a positive charge on all particles passing through the impactor. While most particles deposit onto the substrates due to inertial forces, a fraction of the smallest particles diffuse to all impactor surfaces and deposit

their charge. The charge deposited to the upper stages of the impactor by nanoparticles is substantially larger than the charge deposited by coarse aerosol particles. Marjamäki et al. (2002) developed an algorithm to use the number concentration of particles collected on the filter stage to estimate the diffusion of particles to the upper stages of the impactor. This algorithm was applied to all ELPI measurements to reduce the coarse particle artifact in the dataset.

Measurements of diesel exhaust size distributions (assuming unit density particles) indicate that the coarse particle correction algorithm may not be entirely correct for nanoparticles that deposit a charge on the upper stages while passing through the filter stage. Experiments were performed by measuring a mixed fleet of vehicles passing over the cable protector inlet and by using the probe to sample exhaust from elevated diesel stacks. Chemical analysis of filters sampled using these two methods indicated that the soil (the sum of the oxide forms of aluminum [Al], silica [Si], calcium [Ca], iron [Fe], and titanium [Ti]) accounted, on average, for 41% of the $PM_{2.5}$ mass for samples collected at road level using the cable protector inlet and 8% of the $PM_{2.5}$ mass using the probe on elevated exhaust stacks.

Previous studies of tailpipe exhaust show that more than 90% of exhaust particles are less than 1 μm in size (Brown et al. 2000; Kleeman et al. 2000). In contrast, road dust emissions are predominantly associated with particles larger than 1 μm (Kuhns et al. 2001). Converting the number size distribution produced by the ELPI to a mass size distribution requires assumptions about the shape and density of particles depositing on each stage. Transmission electron microscopy (TEM) images of diesel exhaust aerosol show a fractal morphology of the particles (Park et al., 2003). The authors observed that diesel particles are chain agglomerates consisting of primary particles (20–40 nm) and connected by condensed material. Shi et al. (2000) divided the mass of particles collected on a filter by the volume (assuming spherical particles) deposited on ELPI stages 1–8 (0.030 to 1.090 μm) to obtain a density for particles emitted from a diesel engine. Repeated measurements under different engine speeds and loads indicated that particle density ranged from 0.25 to 0.75 g/cm^3. In an earlier study, Kittelson et al. (1978) measured particle densities from a diesel engine between 0.8 g/cm^3 and 2.0 g/cm^3.

3.3.1.3. DustTrak

The TSI DustTrak nephelometer measures particle scattering at a wavelength of 780 nm in a cone of scattering angles near 90 degrees. PM_{10} and $PM_{2.5}$ aerodynamic size cut inlets may be installed upstream of the analytical chamber to limit the size of measured aerosol particles. The DustTrak has a flow rate of 1.7 lpm and is calibrated using National Institute of Standards and Technology (NIST) Arizona Road Dust. The calibration material is lightly absorbing with a median diameter of approximately 2 μm. The instrument is most sensitive to non-absorbing particles with diameters on the same length scale as the light source (0.78 μm). The sensitivity is reduced for particles of other sizes. Exhaust particles have a DustTrak mass scattering efficiency similar to the calibration aerosol despite their difference in size and index of refraction. As a result, the DustTrak provides reasonable (within a factor of 2) measurements of aerosol mass for both exhaust and dust particles. In an evaluation of the DustTrak and other real-time instruments, Moosmüller et al. (2001) determined that the DustTrak provided a useful fast response measurement of particle concentration. Accurate real-time measurements of PM mass are possible if the DustTrak is calibrated with filter-based measurements.

3.3.1.4. Licor CO_2 Monitor

During the second phase of this project, a Licor Model 840 CO_2 monitor was used to provide a more precise measure of the CO_2 in the passing vehicle exhaust. The unit measures non-dispersive infra-red absorbance at several wavelengths to infer the CO_2 and H_2O concentrations. The analytical cell has a path length of 10 cm and is heated to 50 degrees C. The sample flow rate through the instrument is maintained at 1 liter per minute. The Licor instrument was installed in parallel with the ELPI. The detection limit of the Licor is less than 1 ppm CO_2 and data is recorded once per second.

3.3.1.5. Data Acquisition System

Data from the flow meters, FTIR, DustTraks, Licor, and ELPI were logged in real time through serial ports into Ethernet hubs on each cart. The hubs were each linked to an Ethernet switch and data was logged and displayed in real time using a portable computer. When operating multiple instruments, the use of real-time displays increases data recovery because the user can monitor the status of all instruments from a single location. The data acquisition system assigns a common time stamp to all measurements to ensure that 1 Hz data are synchronized.

4. Data Processing and Validation

4.1. Data Processing

4.1.1. VERSS Data Processing

Emission factors of CO, NO, and HC from the VERSS are calculated with proprietary software as they are collected in the field. The database produced presents emissions in terms of pure exhaust concentrations: CO_2 and CO in % and HC and NO in ppm. These values represent the concentration of these gases in the exhaust pipe prior to dilution with ambient air. Fuel-based emission factors were calculated from the background subtracted average plume concentrations. Using the carbon mass balance technique described by Moosmüller et al. (2003) and Fraser et al. (1998), the fuel-based emission factors were calculated as:

$$EF_P = CMF_{fuel} \frac{C_P}{C_{CO_2}\left(\frac{M_C}{M_{CO_2}}\right) + C_{CO}\left(\frac{M_C}{M_{CO}}\right)} \quad (4\text{-}1)$$

where EF_P is the emission factor of pollutant P in g pollutant per g fuel, CMF_{fuel} is the carbon mass fraction of the fuel (typically 85% to 88% for gasoline and diesel, and 45% to 50% for wood fuel), C_i is the mass concentration of species i in grams per cubic meter, and M_i is the molecular (or atomic) weight of species i in grams per mole.

4.1.2. LIDAR Data Processing

The data processing for the LIDAR signal is more complex than for the VERSS and took place in the laboratory after the end of the field sampling campaign. The PM column content was calculated from the backscatter measurements. The first step in the process was to acquire both the backscatter and transmission waveforms from the two photodetectors. Second, all backscatter signals are range corrected to account for range-dependencies of the instrument that are unrelated to the light scattered by particles in the optical beam. The range corrected data were also transformed into scattering units based on calibration measurements conducted with gases of known light scattering properties. Third, a LIDAR-inversion was performed on each backscatter waveform when the optical density of exhaust plumes exceeded some threshold. The inversion was used to account for the extinction of transmitted light across the road since the return signal from particles farther down range will be weaker if some of the incident light has already been extinguished by particles closer to light source. The inversion was calculated using both the backscatter waveforms and the transmission waveform. Fourth, the background signal (i.e. measurements collected prior to the passing of the vehicle) was subtracted from the exhaust LIDAR-inverted signal to obtain an excess signal related exclusively to the presence of the plume in the beam path. Fifth, a particle range-dependent concentration is calculated using backscattering efficiency coefficients for either gasoline exhaust or diesel exhaust. Sixth, the concentration is integrated over the LIDAR path to determine the PM column content. Finally, the column integrated concentrations were divided by the CO_2 column content from the VERSS to calculate a fuel based PM emission factor.

The LIDAR data processing was performed on a desktop computer using a customized LabView application written by DRI.

4.1.3. In-Plume Data Processing

Data from the In-Plume system were downloaded from the field computer to a data server. The ELPI, DustTrak, and flow meter data were imported into a relational database and constant time offsets were added to each dataset to synchronize the occurrence of concentration peaks.

The FTIR spectra were processed using the Autoquant Pro version 4 package. Concentrations were calculated using a classical least squares fit of the data. These data were then processed using linear interpolation to fit the 0.66 Hz dataset to coincide with the other 1 Hz datasets. The FTIR 1 Hz dataset was imported into the relational database and joined to the data from the ELPI based on time. The master table of all measurements was then exported to a separate custom software program and processed to identify peaks in the CO_2 signal.

The simplest form of peak finding algorithm compares a measurement with a threshold value to determine if the point is significantly above background. For road-surface measurements of CO_2, the background concentration can vary by 50 ppm or more over the course of a day. These variations may be associated with atmospheric mixing of combustion emissions close to the ground and vegetative respiration that consumes CO_2. To account for the low frequency changes in background concentration, the CO_2 data were initially filtered by subtracting the 15th percentile value from a moving 100 s window (i.e., 50 s ahead and 50 s behind) surrounding each data point. The choice of the percentile value and the size of the window are arbitrary and should be based on how frequently the inlet is sampling a plume. If no plumes are present, the background would be defined at the 50th percentile or median concentration. In dense traffic areas, this percentile is likely to reflect CO_2 concentrations impacted by vehicle exhaust and a lower percentile value should be used. The size of the moving window should be sufficiently larger than the duration of the individual peaks so that the 15th percentile value will be representative of a point that is not influenced by exhaust plumes.

Figure 4-1 shows the time series of example CO_2 measurements from the In-Plume system. The CO_2 gas concentrations are referenced to ambient concentrations at the beginning of the sampling period. For periods where there is no apparent exhaust peak (i.e., 14:37:25 to 14:37:45 and 14:38:40 to 14:39:00), the moving 15th percentile background appears to pass through the middle of these background data points.

The following example dataset was collected in Incline Village, NV on 2003/07/26. The sampling configuration at the Lanark Road site was identical to this deployment. The lower panel of Figure 4-1 shows the background (i.e., moving 15th percentile value of 100 s window) subtracted from the raw CO_2 signal. This signal is then compared with the analytical uncertainty (i.e., standard error) of the CO_2 measurement. If the background subtracted signal is more than three times the uncertainty, then the data point is defined as part of a peak. If the next data point is also greater than three times the uncertainty, then the one-second measurement is associated with the same peak. To ensure that the peak is sufficiently large to calculate a meaningful fuel-based emission factor, the time integrated CO_2 peak must be more than 1000 ppm s. In many instances, plumes from passing vehicles are insufficient to meet this criteria and these results are not included in average emission factor calculations.

The sensitivity of the CO_2 peak integral to the choice of the percentile background value can be assessed with the data in Figure 4-1. The peak that begins at 14:36:12 and ends at 14:36:19 is 7 s long and has an integral of 1366 ppm s using the 15th percentile 100 s window as background. If the 5th percentile or 25th percentile background had been used, the integrated values of the peak

would have been 1282 ppm s (-9%) or 1422 ppm s (+4%), respectively. Thus, the choice of background percentile may introduce <10% uncertainty into the emission factor calculations.

The start and stop points of the CO_2 peaks were used to integrate the pollutant concentrations. The peak finding software identifies a CO_2 peak when CO_2 is above the background by more than three standard errors of the CO_2 measurement. The background is defined as the 15th percentile value of the CO_2 over a 100 s window centered on the measurement.

The exhaust concentrations of each species were calculated as the instantaneous signal measured during each peak minus the average of the points in the 100 s window that are not associated with CO_2 peaks. This process provides an unambiguous peak definition while compensating for low frequency drift in the background CO_2 measurement observed throughout the day. Fuel-based emission factors were calculated from the background subtracted average peak concentrations using the same approach as the remote sensing system.

Figure 4-2 shows a time series of concentration data measured by the sampling system. With a traffic density of ~200 vehicles per hour per lane, many of the identified plumes represent the emissions of more than one vehicle traveling close together. The lower panel of Figure 4-2 is the CO_2 time series. The segments identified as single peaks using the algorithm described above are shaded black. The vehicles passing over the inlet that were identified by video are labeled in Table 4-1. The periods of the species time series affected by exhaust plumes are shaded black. The analytical uncertainties of the measurements are shown by the dotted line in each figure, with the exception of the particle data from the DustTraks and ELPI, since these instruments do not report an uncertainty.

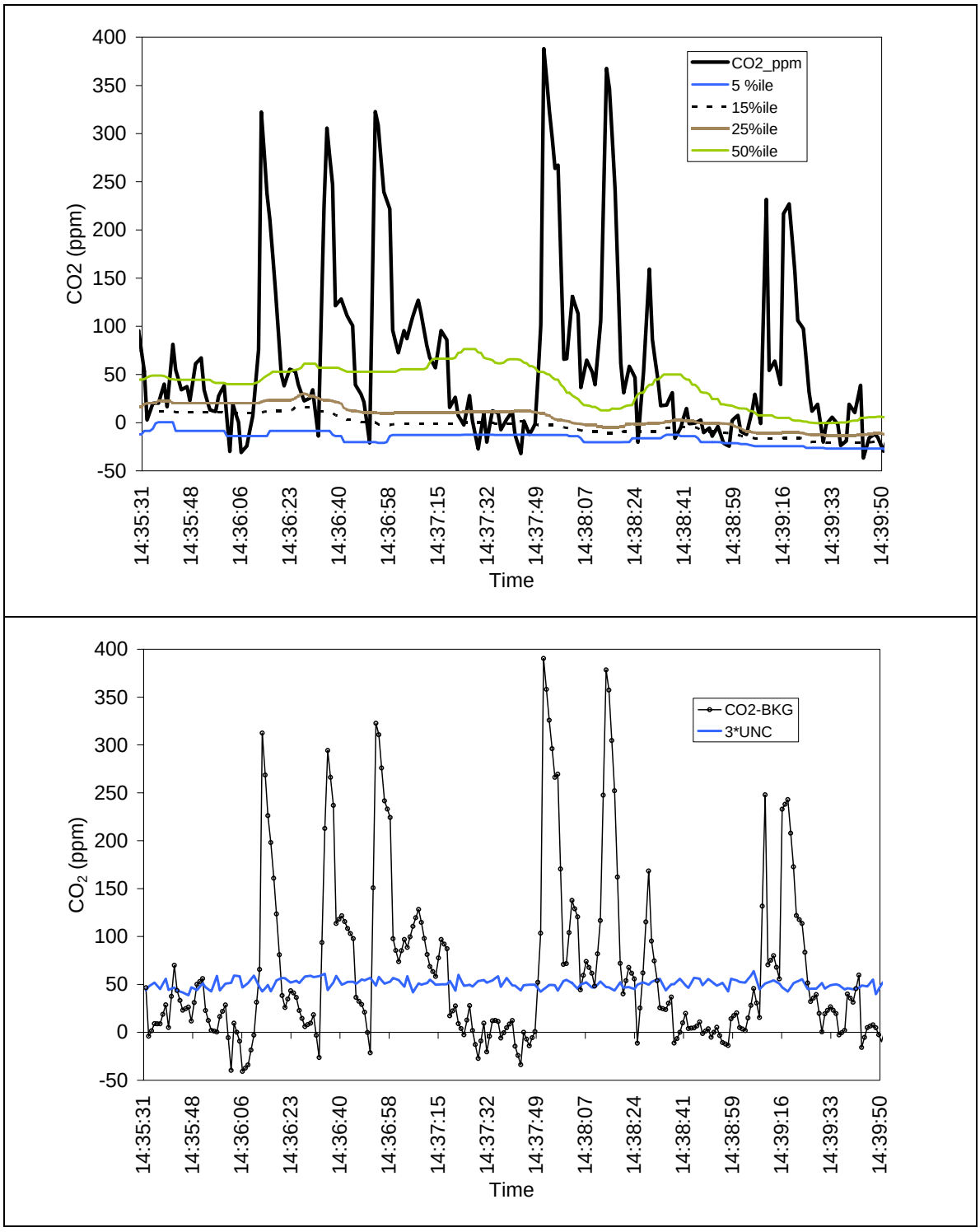

Figure 4-1. Upper panel shows the raw CO_2 concentration with the moving 100 s window percentile baselines. The time series shows that the CO_2 baseline decrease by ~20 ppm over the period and that the 15th percentile baseline best fits the non-plume points. The lower panel shows the CO_2 concentration with the 15th percentile value subtracted (line with marker points). The horizontal line at ~50 ppm is 3 times the analytical uncertainty of the CO_2 measurement.

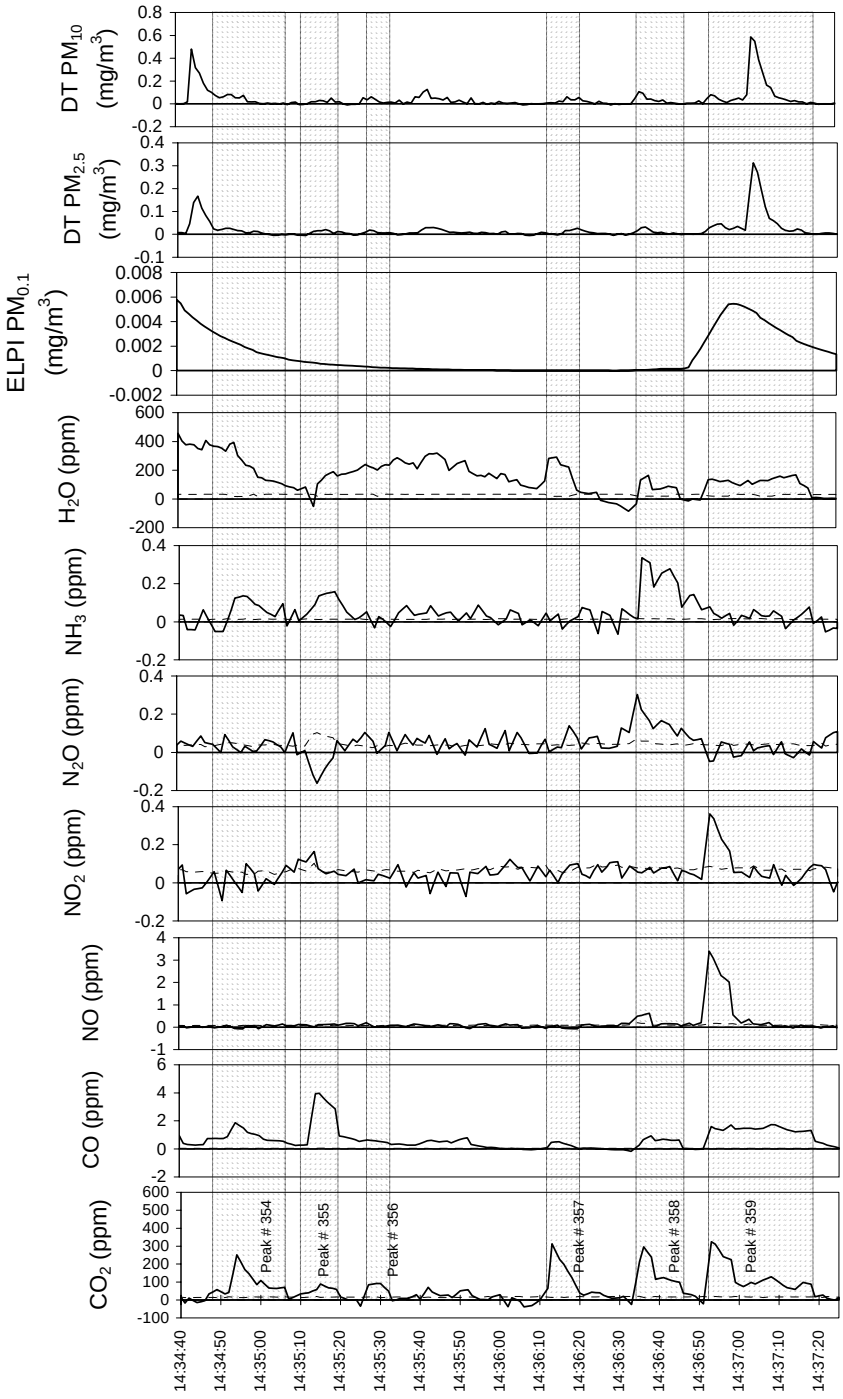

Figure 4-2. Concentration time series of CO_2, CO, NO, NO2, N_2O, NH_3, H_2O, and PM measured by ELPI and DustTraks collected at Incline Village, NV. The shaded areas are periods when the measured plume is linked to the passage of one or more vehicles. The dotted black line represents the analytical uncertainty of the gaseous measurements.

The times series given in Figure 4-2 show very different chemical profiles for each of the plumes. Plume 355 not only has the lowest integrated CO_2 concentration, but also has the highest CO concentration, indicating a higher fuel-based CO emission factor than the other plumes. Plume 359 shows features that indicate mixing of two or more exhaust plumes. The first 10 s of the plume show elevated levels of NO and NO_2, and these levels decrease in the latter 20 s of the plume, although CO_2 and CO remain above background. This composition of plume 359 is very different from plume 358, which shows elevated N_2O and NH_3 concentrations. These species likely represent the emissions from a vehicle with a three-way catalytic converter that is reducing thermal NO_x beyond N_2 and O_2 to create NH_3.

Particle emissions measurements show similar variability between vehicles. The mass of particles (assuming spheres) with aerodynamic diameters below 0.1 μm is shown in the upper panel of Figure 4-2. During this experiment in Incline Village, NV, the ELPI was operated with the electrometers set to their largest detectable range (400,000 fA). This resulted in a very sensitive measurement. However, the time scales of the measurements were on the order of 20 s. As a result, the ELPI was able to detect fresh ultrafine emissions from the vehicles, but the time response was too slow to link these concentrations to individual plumes. For the experiments at Lanark Road in Meridian, the ELPI was operated at a range of 10,000 fA, and data signal has a time scales of 1-3 seconds. The TSI DustTrak has a fast 1 Hz time response. The time series of the DustTraks operating with a 2.5 μm and 10 μm inlets are shown below the ELPI time series in Figure 4-2. A PM_{10} and $PM_{2.5}$ peak was observed during the middle of plume 359. This peak does not appear to be associated with the same vehicle that created the NO peak. The first peak in the DustTrak time series appears to precede the CO_2 peak. These elevated levels may be due to exhaust or road dust from a vehicle passing in the opposite direction.

Emission factors for all species measured and their propagated uncertainties are shown in Table 4-1. To ensure sufficient plume densities for each peak, valid CO_2 peaks were required to have integrated plume values of more than 1000 ppm s. Peaks 355 and 356 had integrated values of ~500 ppm s, resulting in larger emission factor uncertainties. The detection limit of the In-Plume Sampling System is affected by both the variability of the ambient background and the detection sensitivity of instruments used. The measurement of water appears to be influenced by the background concentrations. Figure 4-2 shows that variations in background water concentrations are generally larger than the variations introduced by vehicle exhaust. Although the FTIR can measure propane, hexane, ethylene, formaldehyde, sulfur dioxide (SO_2), and other species found in exhaust, the levels typically observed in the exhaust are lower then can be detected.

Table 4-1. Emission factor results for vehicles associated with individual plumes measured in Incline Village, NV.

Peak Number	354	357	358	359
Vehicles	Volkswagen Car Dodge Car	Lincoln Car	GMC PU Toyota Car	GMC PU Ford PU Ford SUV
CO_2 * Plume Duration (ppm s)	1645	1366	1771	3257
Species	**Emission Factors (g/kg fuel)**	**Emission Factors (g/kg fuel)**	**Emission Factors (g/kg fuel)**	**Emission Factors (g/kg fuel)**
CO	15.8 ± 3.0	0.3 ± 0.4	4.2 ± 0.8	19.0 ± 2.8
NO	-1.1 ± 1.9	-1.3 ± 2.1	3.0 ± 2.0	12.0 ± 2.7
NO_2	-1.1 ± 2.0	0.4 ± 1.5	0.5 ± 1.9	1.4 ± 2.0
N_2O	-0.7 ± 1.5	0.1 ± 0.8	2.6 ± 1.2	-1.2 ± 1.1
H_2O	2703 ± 925	917 ± 1217	-1493 ± 502	-542 ± 551
Formaldehyde	-1.5 ± 2.5	-0.3 ± 1.5	0.0 ± 1.6	0.2 ± 1.8
Hexane	-2.9 ± 2.4	-1.9 ± 3.0	-5.5 ± 2.9	-1.0 ± 2.3
Propane	-0.9 ± 2.2	-0.4 ± 1.5	-0.4 ± 1.7	0.0 ± 1.8
NH_3	0.4 ± 0.2	-0.1 ± 0.2	1.6 ± 0.3	0.0 ± 0.2
Ethylene	-0.5 ± 0.5	0.0 ± 0.3	-0.1 ± 0.4	0.3 ± 0.4
SO_2	-0.8 ± 8.0	4.3 ± 7.2	-4.5 ± 5.1	1.2 ± 5.7
$PM_{2.5}$ (DustTrak)	0.03	-0.02	-0.02	0.73
PM_{10} (DustTrak)	0.29	-0.07	0.06	1.13

Figure 4-3 shows the ELPI measured volume size distributions normalized to the total volume of particles collected on stages 1 through 10 (i.e., particles less than 2.3 μm aerodynamic diameter) for samples collected with the elevated and road-level inlets. The elevated sample set was collected in Las Vegas in August 2003, and the road level data set was collected at Incline Village in July 2003. Both size distributions show a large increase in particle volume on Stages 8 through 10 (0.7 μm to 2.3 μm) accounting for more than 50% of the total particle volume. For experiments using the road-level inlet, some enhancement in particle concentrations on the upper stages of the impactor was expected because road dust was sampled along with the exhaust. This was not the case with the elevated inlet, where vehicles (i.e. city buses) were stopped or traveling at speeds of less than 10 km/hr. Moreover, soil concentrations on collocated filter samples were less than 10% of the $PM_{2.5}$ mass at the city bus depot in Las Vegas, NV.

As confirmed by the ELPI manufacturer, a portion of the increase in particle concentrations on Stages 8 and higher is an artifact of sampling fresh exhaust with large number concentrations of nucleating particles. The small particles become charged in the ELPI's corona charger and diffuse to the impactor substrates of the higher stages. Since there are a very small number of larger particles impacting on these upper stages, the small particles add a significant bias to the ELPI's coarse particle measurement. For the purposes of evaluating vehicle exhaust emissions, measurements of particles greater than 0.6 μm (Stage 8 and higher) are ignored. This should not introduce a bias into the integrated ELPI particle volume measurements since exhaust particles have volume median diameters of ~0.1 μm.

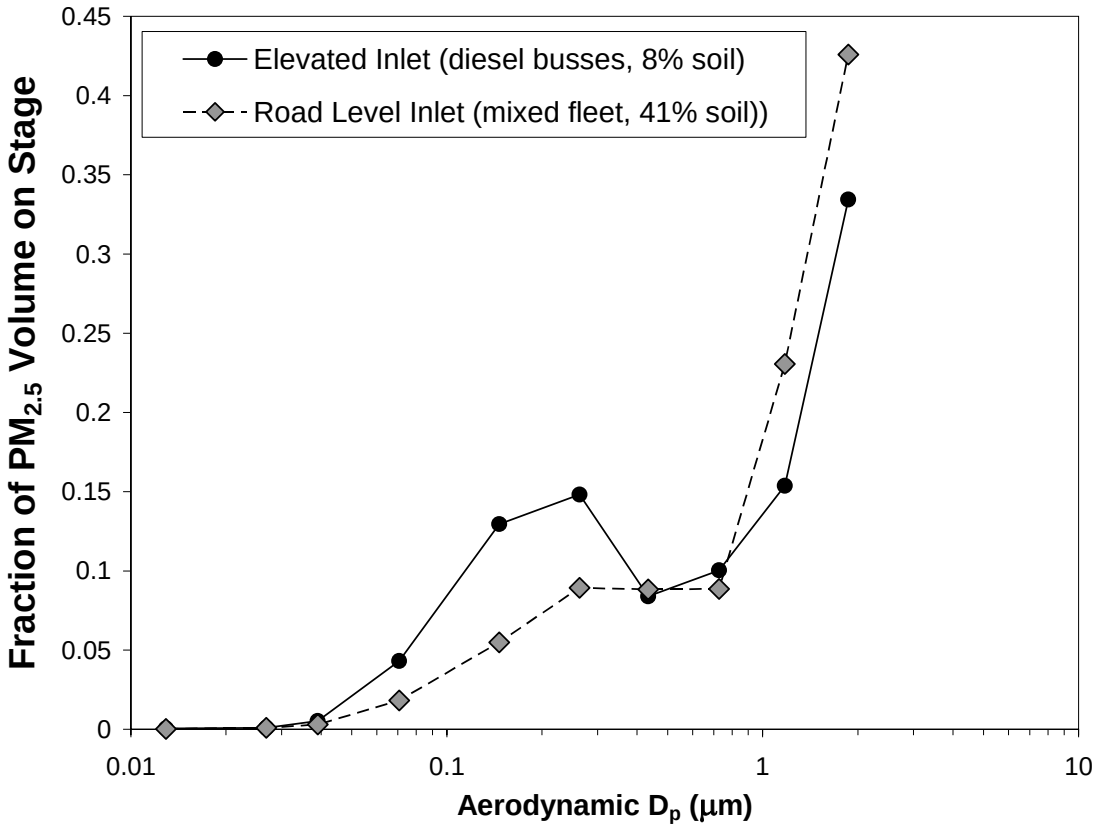

Figure 4-3. ELPI size distributions of exhaust samples measured using elevated and ground level inlets. Each data point represents the relative particle volume on a single impactor stage on the ELPI.

4.2. Validation

The In-Plume sampling system was designed to be an independent empirical tool to evaluate the Cross-Plume measurement system (VERSS with LIDAR). In the following section, the integrated PM emission factor results from the In-Plume system are compared with the emission factors from the VERSS.

Only a limited dataset of valid In-Plume results are available from the two study phases. The ELPI system was configured to sample in its most sensitive mode during Phase I. This had the consequence or increasing the response time of the instrument to nearly 1 minute. As a result, it was impossible to link a single PM peak with a vehicle since typically several vehicles per minute would pass by the instruments. During Phase II, the ELPI was configured to measure PM concentrations with a fast time response (~1 second). During Phase II, the inlet to the FTIR had a leak so that the air flow through the analytical cell was substantially reduced. No significant exhaust emissions could be detected above the ambient background using the FTIR during Phase II. The Licor CO_2 monitor was purchased between Phase I and Phase II, so Licor CO2 data are only available during Phase II.

4.2.1. Comparison of In-Plume with Cross-Plume PM Emission Factors

Both the VERSS and the In-Plume systems are relatively new, designed to measure exhaust emission factors in the field. Tests have recently been conducted to compare the In-Plume emission factors with the University of California Riverside's Mobile Emissions Test Lab. The results of this comparison have not been assembled at the time of finalizing this report.

An intercomparison of the results from the VERSS and the In-Plume systems may illuminate sources of bias or uncertainty not detectable with a single measurement system study. As noted above, the VERSS system measures the emissions from each passing vehicle. In contrast, the In-Plume system identifies peaks of CO_2 sampled from an inlet in the middle of the road. The CO_2 peaks may correspond to one or many passing vehicles or due to the position of the vehicle's exhaust pipe, no CO_2 peak may be observed by the instrumentation. This difference complicates the one-to-one comparison of individual measurements of the two systems. Individual vehicle comparison for PM is additionally complicated by the different time lags and time responses of gases and PM monitoring instruments (i.e. the ELPI operating in its most sensitive mode has a time constant of more than 20 seconds whereas the FTIR and Licor CO_2 measurements have a 1 second time constant. Selecting peaks associated with a single vehicle is not possible with a 20 second time constant in heavy traffic conditions such as those found during the experiment conducted in Idaho. Time averaging reduces errors associated with matching the appropriate peak to a single vehicle.

To simplify data processing, daily averages were calculated for days during which both measurement systems were operational. In this comparison, no peak identification was used for the In-Plume system. Instead, the integrated (i.e. daily average) CO_2 and the integrated PM were calculated after background subtraction. The overall average PM emission factor was calculated by dividing the PM daily average emissions factor by the CO_2 daily average emissions factor using equation 4-1. For this calculation, the CO concentration was assumed to be negligible with respect to CO_2. In most cases CO accounts for < 5% of the carbon emissions from gasoline vehicles and < 1% for diesel vehicles.

Upon analysis of the results, the background subtraction method described in section 4.1.3 was found to introduce positive biases in the integrated CO_2 concentrations. The running 15^{th} percentile value was lower than the true CO_2 background. When this background was subtracted from the CO_2 signal, the resulting background subtracted CO_2 was too high. This problem has been resolved in the current iteration of the In-Plume systems by using two high precision CO_2 monitors to simultaneously measure the vehicle exhaust in the middle of the road and the background CO_2 away from the road.

To correct the issue with the CO_2 measurements form this study, a more robust data analysis method of calculating the background was utilized. The CO_2 and PM medians were calculated over a moving 30 s window (i.e., 15 s ahead and 15 s behind) and therefore the minimum median over a moving 600 s window (i.e., 300 s ahead and 300 s behind) was computed and assumed to represent the background. The 600s and 30s windows are somewhat arbitrary; however a visual inspection of the resulting background determination provides confidence that little bias is introduced with this method. Effectively, the algorithm selects the 30 s median concentration of a period with the least number of CO_2 peaks over a 10-minute period.

The daily averaged PM emission factors calculated from the VERSS and In-Plume systems are shown in Figure 4-4. The fleet average PM emissions from phase I of this study on 2004/01/14

and 2004/01/15 are in excellent agreement with each other. In addition, there is very good agreement between the two independent measurement methods. The last set of columns on the right side of Figure 4-4 shows higher average PM emission factors than on other days. These values represent the daily average emission factors (of the mixed fleet, passenger vehicles and school buses) after the buses were switched to B20. Overall the two systems show excellent agreement for PM emission factors over both sampling periods.

This is a very significant result since the two sets of emission factors are calculated using very different techniques for particle measurement. The VERSS uses light scattering from particles as the fundamental PM measurement. Whereas the In-Plume system uses a count of particles of different aerodynamic sizes to infer PM mass concentrations.

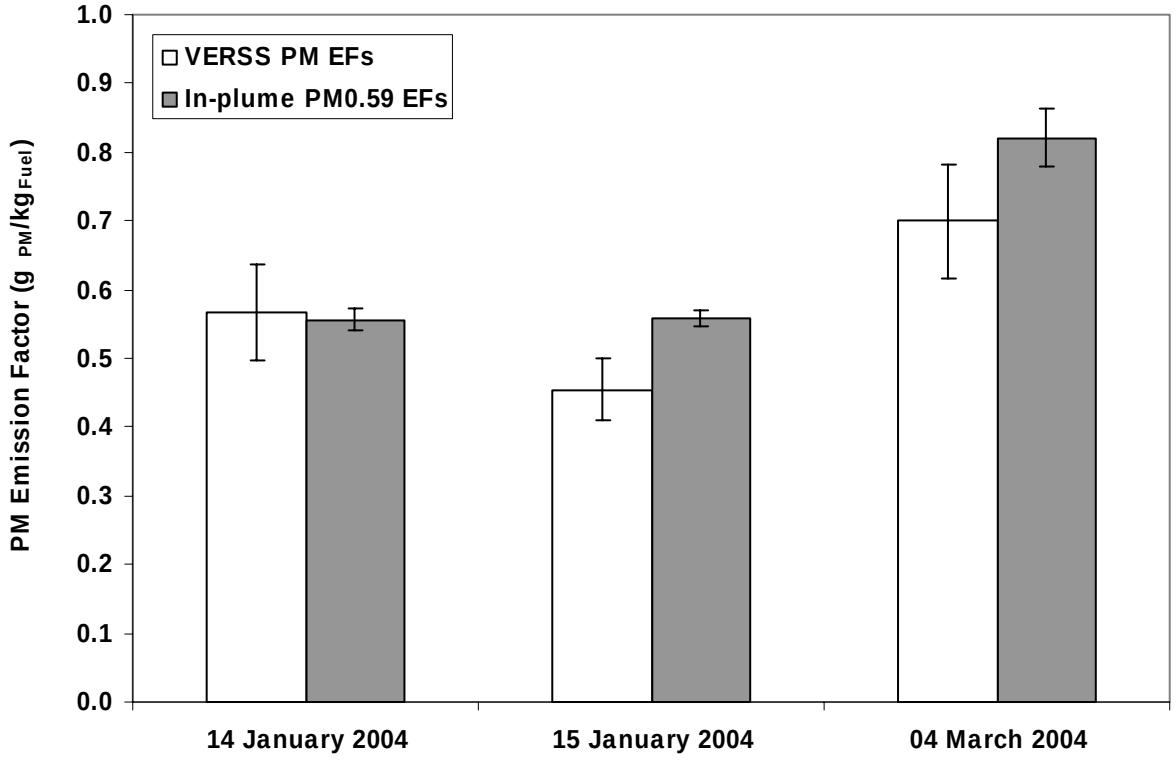

Figure 4-4. Comparison of PM emission factors measured by the LIDAR remote sensing system and the In-Plume system. Error bars are the standard error of the mean. All columns represent that average of samples collected between 6:00 and 18:00. $PM_{0.59}$ is the mass concentration of particulate matter less than 0.59 µm in aerodynamic diameter.

To further investigate the quality of the PM emission factors measurements, half-hour averages of In-Plume PM background subtracted concentrations were calculated and normalized to In-Plume CO_2 concentrations for March 4, 2004. Half-hour cross-plume PM emission factor averages were calculated over the same time periods and compared to In-Plume averages. Figure 4-5. Due to different validity rates between the two instruments and throughout the day, the two instruments did not record data for exactly the same set of vehicles. Nevertheless, the measured emission factors from the two systems track each other during most of the day. This is

true regardless of the composition of traffic passing both sensors (see second and third panels of Figure 4-5).

Figure 4-6 shows a scatter plot of the two measurements for the half-hour averages, with a linear regression slope of 0.71 and a correlation coefficient of 0.69. The average PM EFs measured by the two systems were 0.78±0.09 g_{PM}/kg_{Fuel} for the Cross-Plume and 0.80±0.006 g_{PM}/kg_{Fuel} for the In-Plume system. The average agreement is good with no apparent bias.

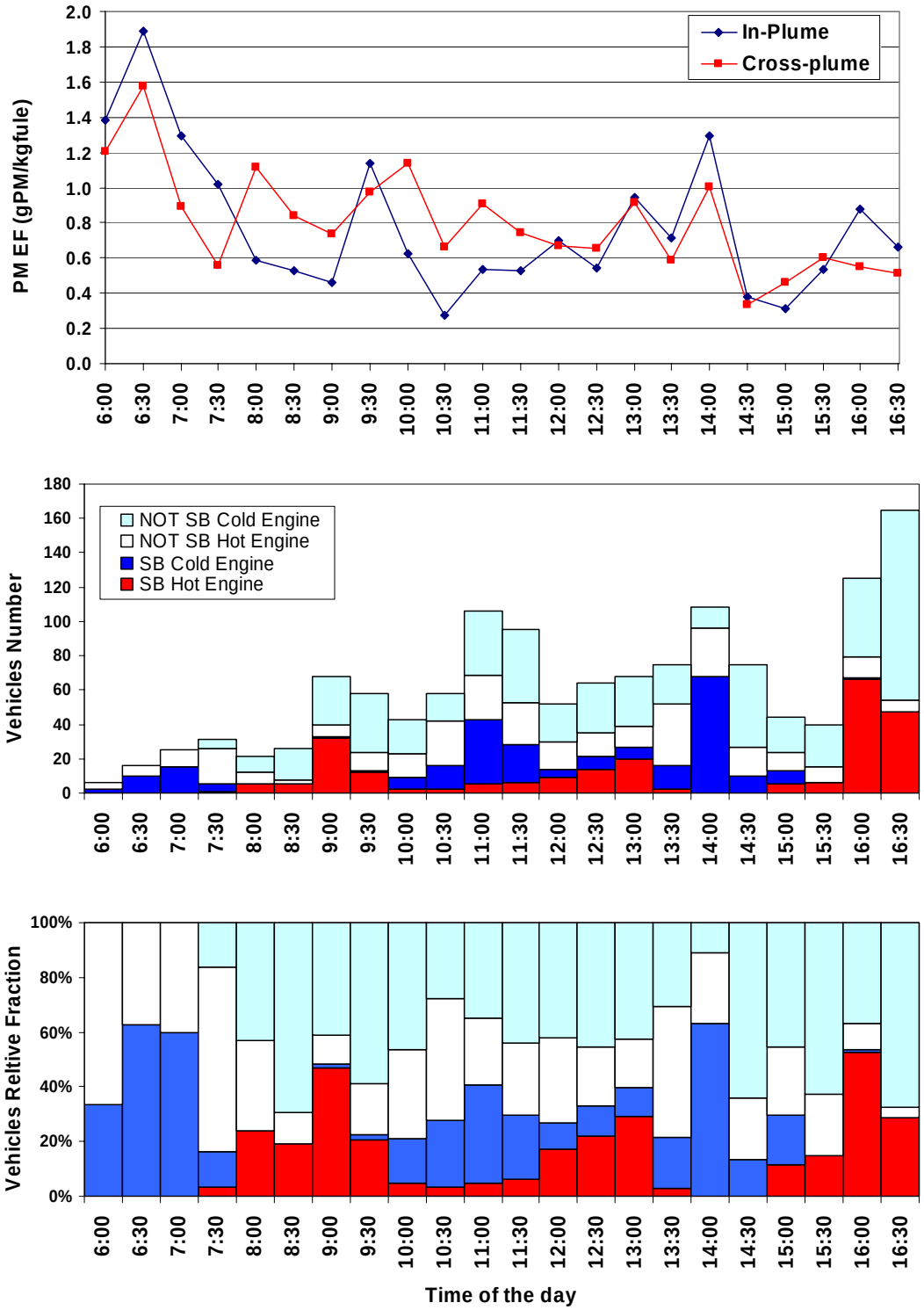

Figure 4-5. Comparison of PM measurements from In-Plume and Cross-Plume monitors. Top graph: half hour averaged PM emissions factors as a function of time. Middle graph: half hour traffic composition. Lower graph: fraction of vehicles in each class. These data were collected in Boise, ID during March 4, 2004.

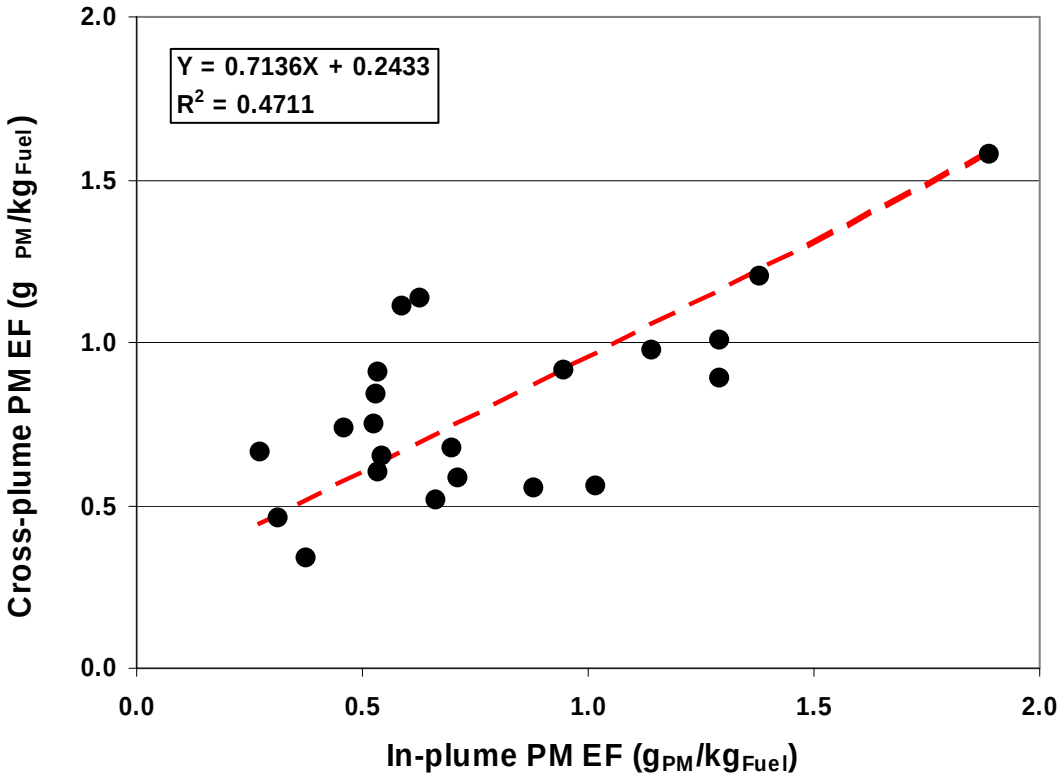

Figure 4-6. Scatterplot of PM EFs for In-Plume and Cross-Plume measurements.

4.2.2. Comparison of In-Plume and Cross-Plume CO and NO Emission Factors

A comparison between In-Plume and Cross-Plume gaseous measurements was performed on individual vehicles. Since the CO and NO as measured by the FTIR has the same temporal resolution as the CO_2, matching peaks with individual vehicles was feasible. Figure 4-7 compares CO emission factors (EF) for the In-Plume and Cross-Plume systems applied to the same set of gasoline and diesel vehicles (selected by matching individual CO_2 and CO peaks to Cross-Plume records). The linear regression slope is 0.86 with a correlation coefficient of 0.75. Average CO EFs measured by the two systems on this dataset are: CO EF = 60 ± 8 g_{CO}/kg_{Fuel} from the Cross-Plume (VERSS) and CO EF = 69 ± 7 g_{CO}/kg_{Fuel} from the In-Plume system. This indicates good agreement between the two systems.

Figure 4-8 shows a similar comparison for NO, for which the regression slope is 1.0 and the correlation coefficient is 0.68. Average NO was 17±1 g_{CO}/kg_{Fuel} for the In-Plume system and 18±1 g_{CO}/kg_{Fuel} for the Cross-Plume system. As with CO, the average emissions measurements are nearly identical.

As discussed above, a sharp peak in the CO2 signal generally identifies individual vehicles measured by the In-Plume system. It is not always possible to match without ambiguity vehicles measured by the Cross-Plume system with vehicles measured by In-Plume system. This may explain the presence of many outlying data points on the figures. The ambiguity may introduce a random error in the regression, but should not bias the results. The average emission factors are in good agreement for CO, NO, and PM between the two independent measurement systems.

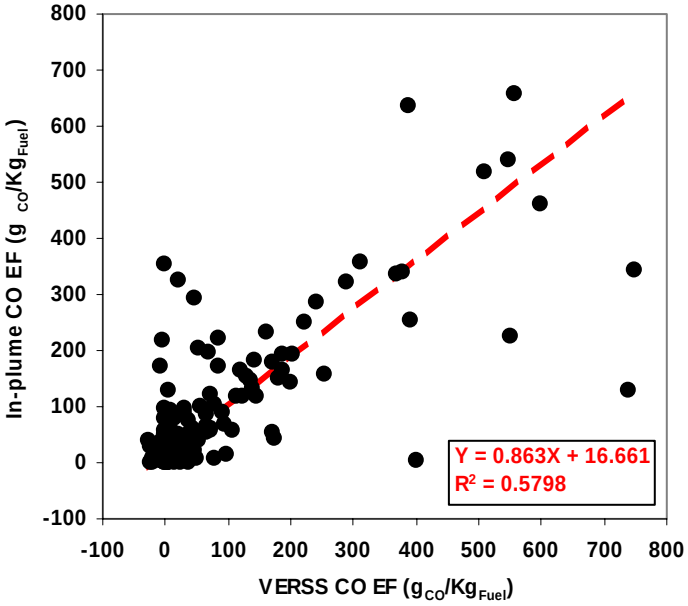

Figure 4-7. Comparison of In-Plume and Cross-Plume Vehicle Exhaust Remote Sensing System (VERSS) emission factors (EF) for CO for individual vehicles.

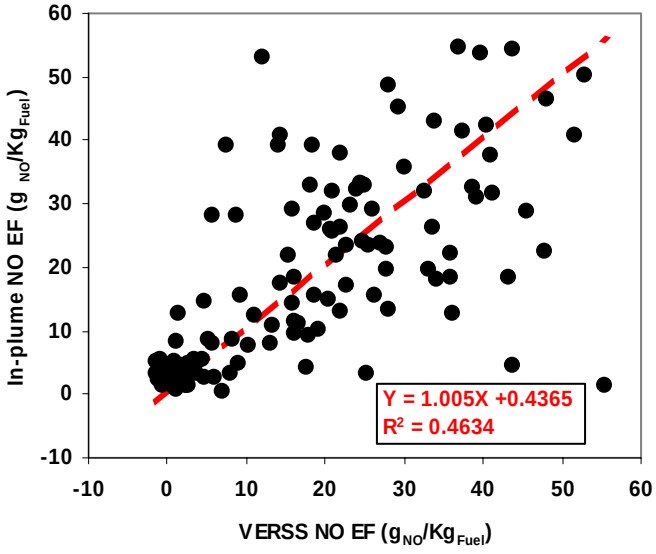

Figure 4-8. Comparison of In-Plume and Cross-Plume Vehicle Exhaust Remote Sensing System (VERSS) emission factors (EF) for NO for individual vehicles.

4.2.3. Effects of Temperature and Humidity on Emission Factors

A concern with the design of this study is that other factors besides the fuel may change from one sampling period to another. These differences may result in changes in emission factors that are not related to, but attributed to, the differences in fuel. To assess these potential biases associated with ambient temperature and relative humidity, measured emission factors for school buses heading westbound on Lanark Road (cold start) were compared with met data collected at a nearby weather station. For each phase of data collection, average measured emission factors were calculated from temperature intervals of ~1 degree C (2.0 degrees F) and relative humidity intervals of 5%. Average emissions and standard errors of the mean were calculated for intervals with more than 10 valid emission measurements. These data are shown in Figure 4-9 through Figure 4-12. Temperatures during phase I were consistently colder than phase II. Despite mutually exclusive differences in temperature intervals between phase I and phase II, there appears to be no consistent effect of temperature on the emission factor measurements. Relative humidities were generally higher in phase I than phase II with the exception of a rain event on 2004/03/04. This period offers a controlled overlap of measurement phases with RH between 90% and 95%. No consistent trends were observed during either data collection phase that suggests differences in temperature or relative humidity are responsible for changes in measured emission factors.

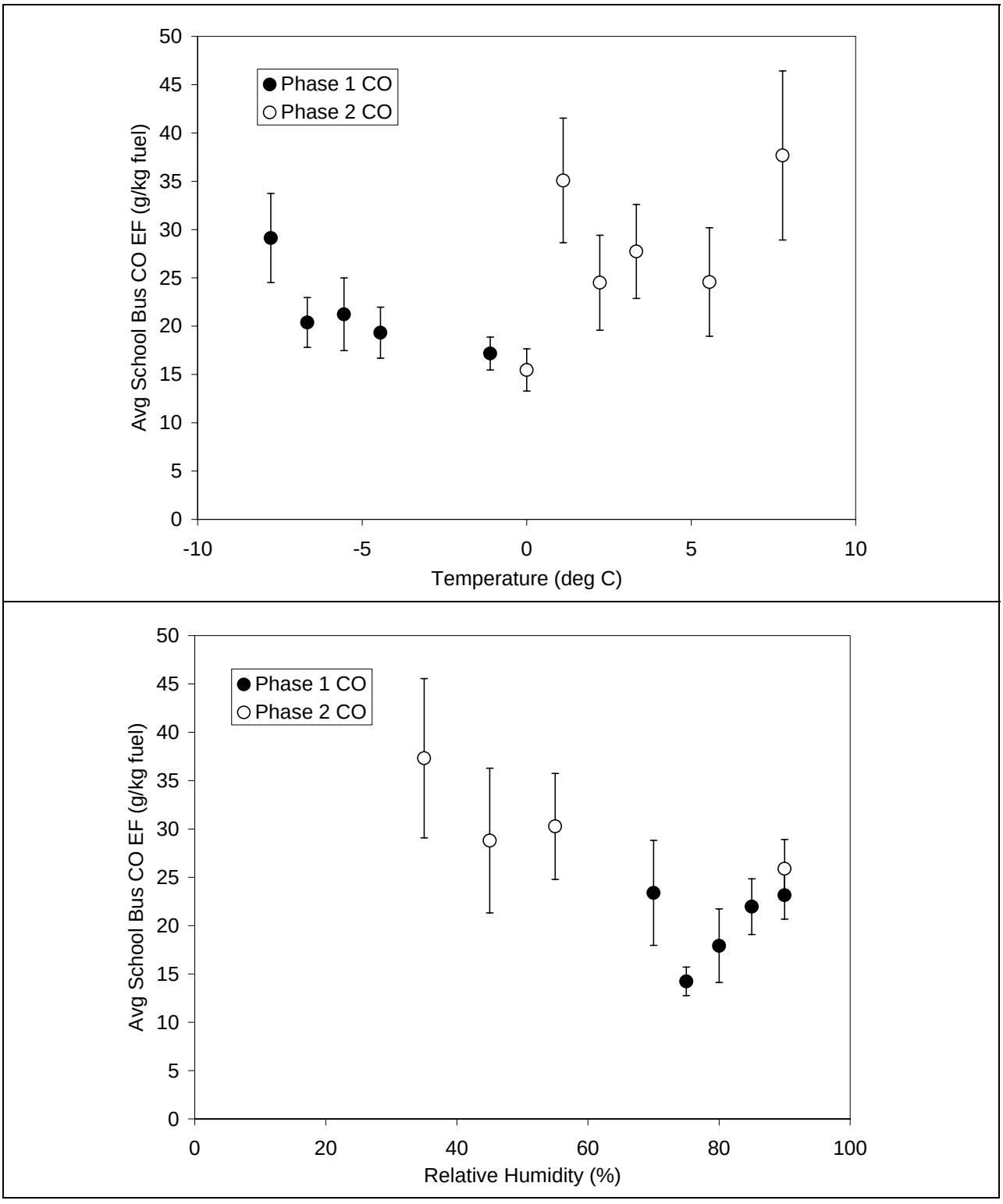

Figure 4-9. Comparison of temperature and relative humidity with CO emission factors for phase I (petroleum diesel) and phase II (biodiesel). Points represent the average of at least 10 measured emission factors for school buses heading westbound on Lanark Road.

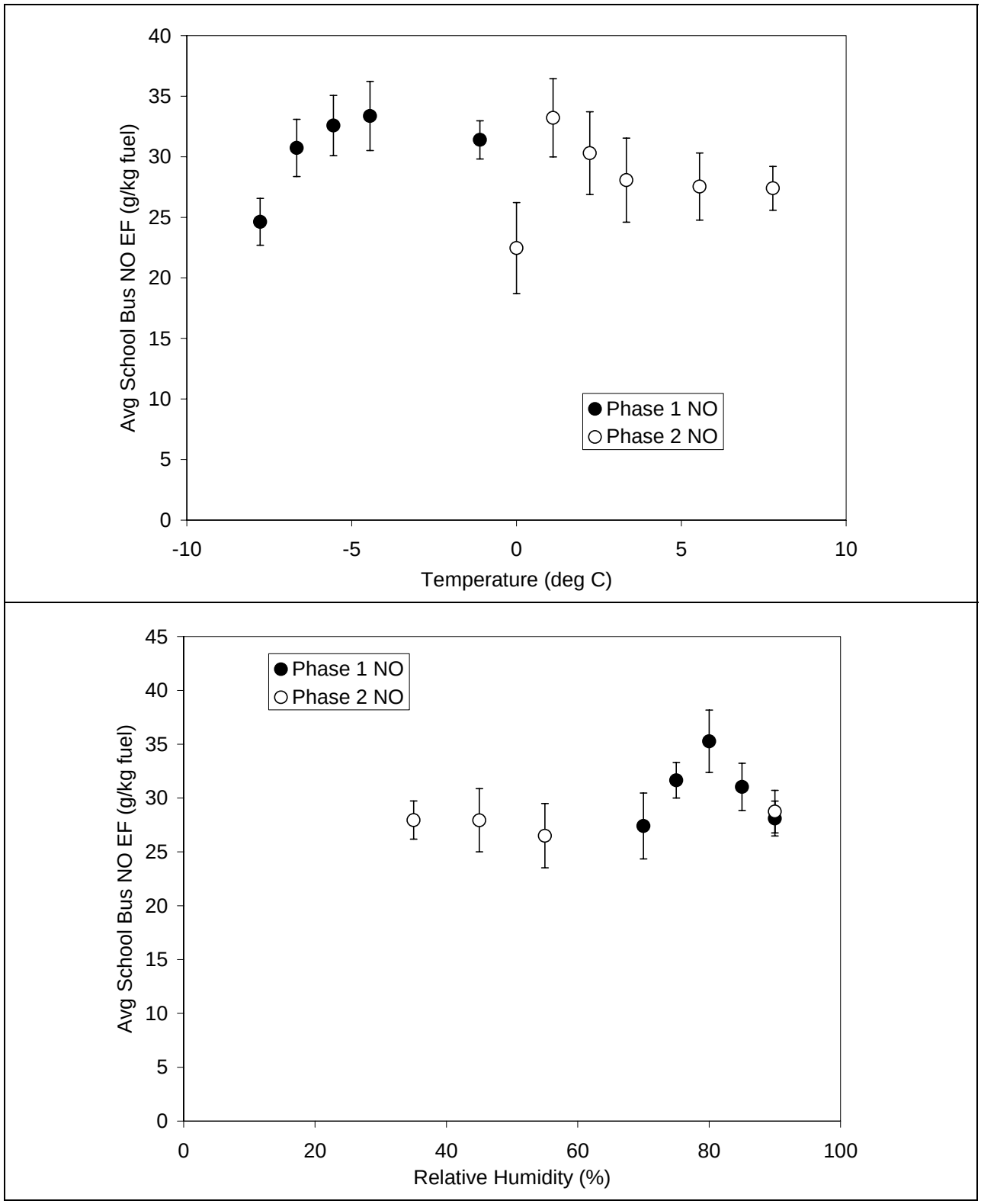

Figure 4-10. Comparison of temperature and relative humidity with NO emission factors for phase I (petroleum diesel) and phase II (biodiesel). Points represent the average of at least 10 measured emission factors for school buses heading westbound on Lanark Road.

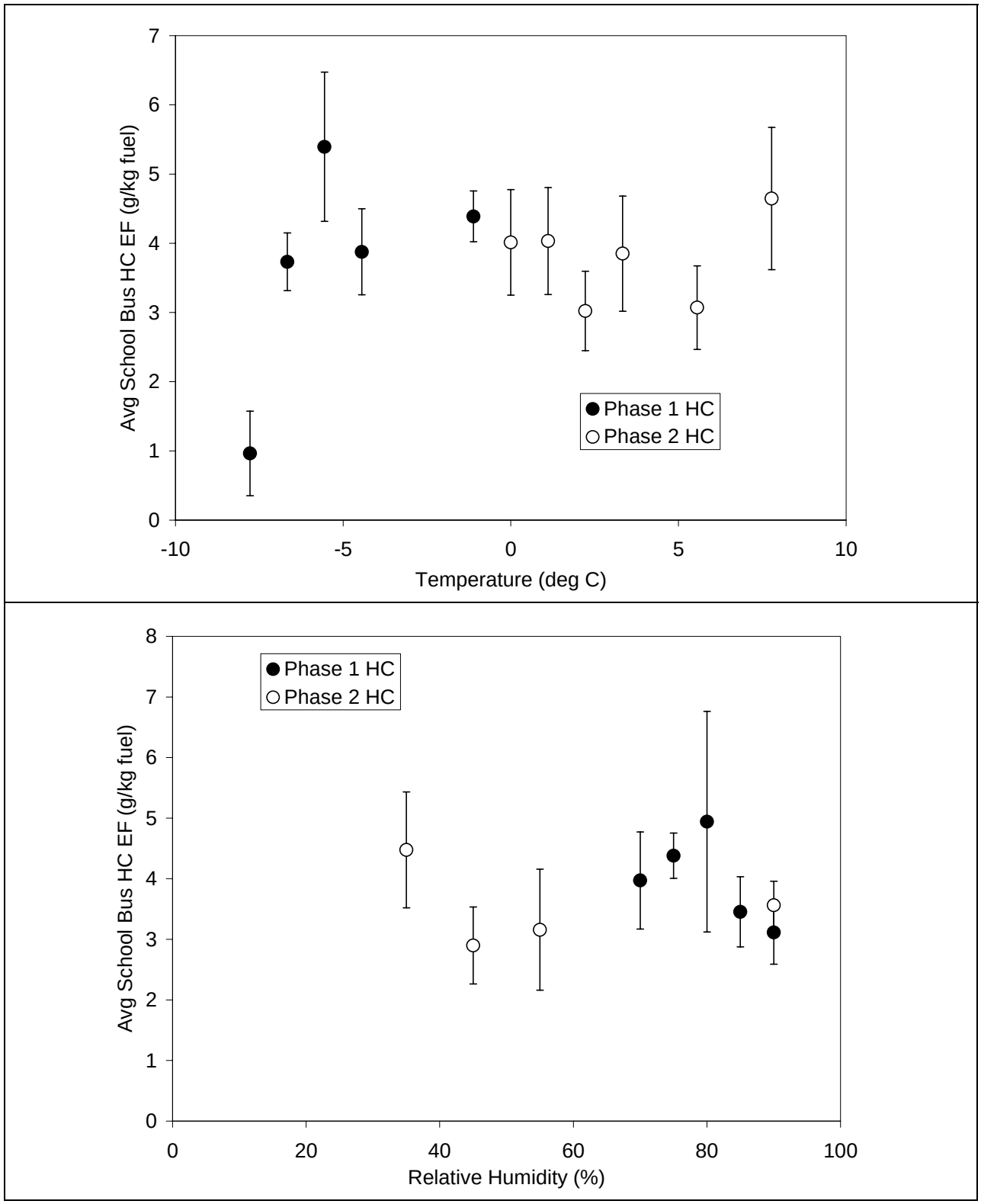

Figure 4-11. Comparison of temperature and relative humidity with HC emission factors for phase I (petroleum diesel) and phase II (biodiesel). Points represent the average of at least 10 measured emission factors for school buses heading westbound on Lanark Road.

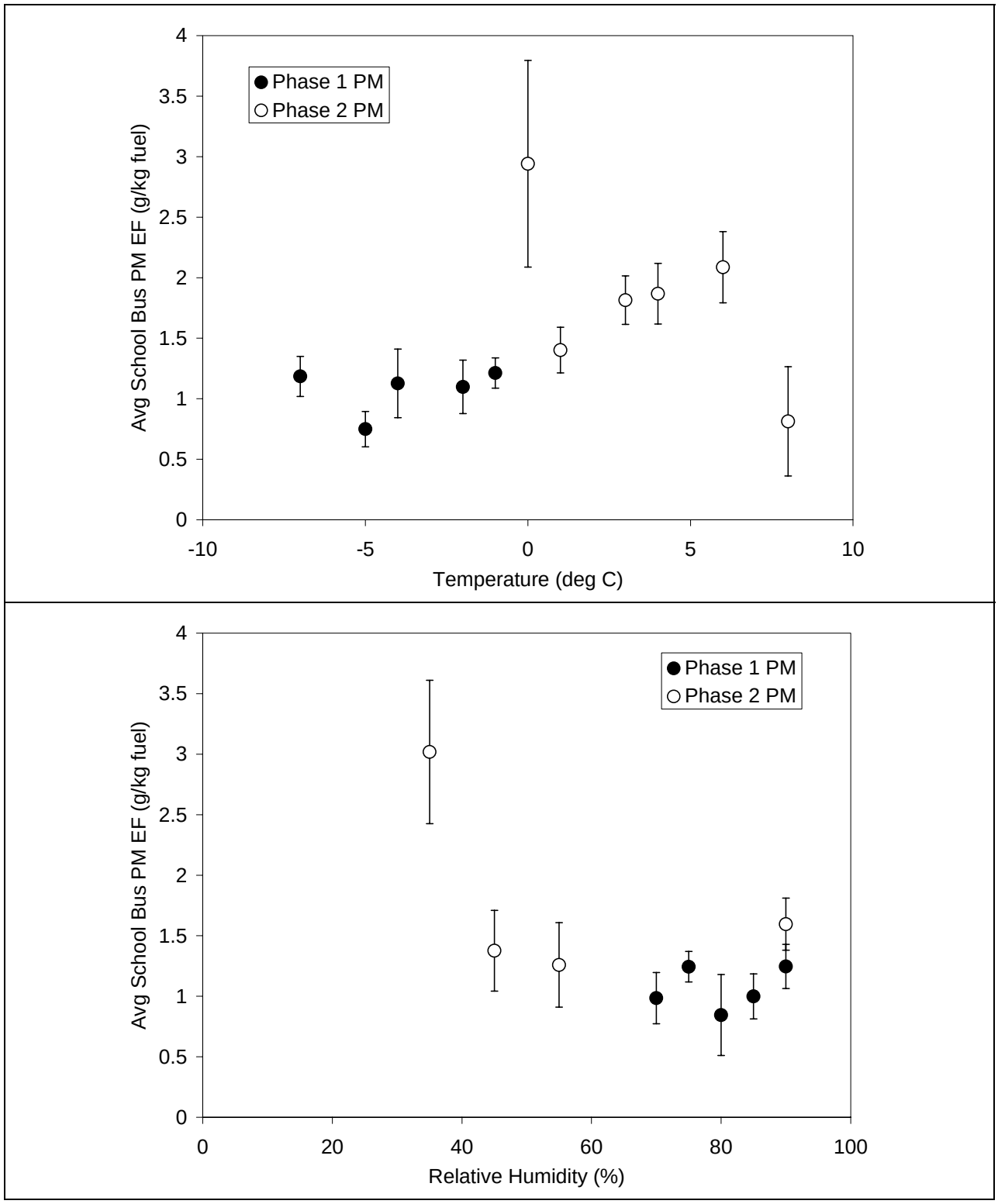

Figure 4-12. Comparison of temperature and relative humidity with PM emission factors for phase I (petroleum diesel) and phase II (biodiesel). Points represent the average of at least 10 measured emission factors for school buses heading westbound on Lanark Road.

5. Results

5.1. Experimental Setup

The experiment to measure the emission changes associated with switching buses from petroleum diesel to a 20% biodiesel fuel mixture (B20) was conducted in two phases:

Phase I: Emissions from school buses were measured between January 12, 2004 and January 15, 2004 outside the (Meridian) Joint School District #2 bus depot while the buses were using a winter blendpetroleum diesel. Five buses had been running on B20 fuel since April 2003. During this period, other vehicles (mainly passenger cars, vans and pick-ups owned by the school district employees and students of a high school at the end of Lanark) were measured. On January 16, 2004 vehicles were measured on the Nampa Road I-84 eastbound freeway on-ramp in Canyon County.

Phase II: Buses were measured again between March 1, 2004 and March 4, 2004 while running on a B20 fuel. The fuel in the holding tank at the Meridian School Bus District was filled with B20 on January 16, 2004. The 15,000-gallon fuel tank was nearly empty at the time of the fuel switch. On March 5, 2004 vehicles were measured on the Franklin Road I-184 eastbound cloverleaf on-ramp lane.

Figure 5-1 through Figure 5-3 are pictures of the measurement site on Lanark Road showing the remote sensing units and the In-Plume collection system.

The remote sensing trailer, the VERSS and LIDAR main units, the truck with the In-Plume system, and a power generator were located on the south side of the road. The retro-reflectors for the gases and the PM remote sensing units were aligned facing the main units on the north side of the road.

A 4 cm tall cable protector enclosing the inlet sampling line for the In-Plume system was installed across the lane. The road was restricted to a single lane with traffic cones and the appropriate road signs. Eastbound vehicles were instructed to yield to on-coming traffic. At the beginning of each sampling day on Lanark Road, MJSD Transportation Department employees would travel eastbound through the test section (inbound) with vehicles that were presumably warm from the commute to work. The vehicles were parked and left in the bus depot parking lot for most of the day. Both buses and vehicles leaving the bus depot (outbound) were generally inactive for several hours and were representative of cold engines within the first 3 minutes of start-up. For both sampling phases, the buses were plugged into engine block heaters overnight to facilitate starting the engine in the morning.

The vehicle driving direction at this location is an excellent surrogate for either cold start conditions (outbound/westbound) or hot stabilized conditions (inbound/eastbound). It is likely that some vehicles heading westbound may have stopped temporarily and been operating in hot stabilized condition, the majority of the traffic at the site were school bus drivers and high school students that would be starting there vehicles after a 4+ hour cool down period.

Images were captured of all vehicles passing through the test section. License plates and bus numbers were generally legible for outbound vehicle, but not for in-bound vehicles. The images of both inbound and outbound vehicles were generally sufficient to classify each vehicle as a car, van, pick-up truck, SUV, heavy-duty truck, or school bus.

Figure 5-1. Image of school bus passing through on-road experimental set-up. The picture is facing west. The outbound vehicles had the right of way. The car on the left side of the image is yielding to the westbound bus. This bus would be categorized as have a steam plume.

Figure 5-2: Bus depot set-up. Out-going school bus. Image is facing south.

Figure 5-3. Remote sensing and In-Plume system configuration. Image is facing southwest.

Since the non-school bus vehicles did not undergo a fuel switch from phase I to phase II, emissions data from these vehicles were used to evaluate the consistency of the measurement system.

5.2. Statistical Terminology

At this point it is helpful to review some basic statistical terminology that will be used in the following analyses. It is widely known that a small number of light duty gasoline vehicles (LDGV) are responsible for the majority of the fleet's emissions. This is because vehicle emissions are not *normally distributed* about the average. Rather, the majority of vehicles are low emitting and a generally small number of poorly tuned vehicles can emit 1000 times more pollution than a clean vehicle. This type of distribution is called *skewed* and has the property that the median (i.e., the emission factor that is at the midpoint of a sorted list) is lower than the mean (or average). That is because the small number of high emitting vehicles has a large effect on increasing the mean. When developing emission inventories, the mean emission factor is the appropriate term to use even though the mean emission factor is higher than the emissions from most vehicles. In contrast, the median is less representative of the overall emission factor of a population of vehicles. Outliers in the data do not generally influence the median.

Another useful concept is the *standard error of the mean*. The mean and standard deviation can be calculated for any set of real numbers. The standard deviation is an indicator of the amount of spread in the data. For a normally distributed population, 68% of all values lie within one standard deviation of the mean. The standard error of the mean is a measure of how well one knows the mean and is defined as the standard deviation divided by the square root of the number of samples. Although the standard deviation is primarily meaningful only for normally distributed data, the standard error of the mean is relevant to all types of distributions including skewed distributions. The standard error of the mean has the property of decreasing with an increasing number of samples. Therefore, a data set may have a large amount of spread but the mean can be very well known if there are a sufficient number of samples.

For each group of emission factors, the standard error of the mean and median standard errors were calculated. The median standard errors were calculated using a bootstrap technique by resampling with replacement from the raw data. The spread of each median value was determined by constructing a frequency distribution of 50,000 bootstrap estimates. Confidence intervals do not account for accuracy of any of the constants used in the calculation of the emission factors.

5.3. Meteorological Conditions during Study

The weather conditions were similar during the two phases with cold temperatures (-7 deg C to 0 deg C for phase I and -4 deg C to 8 deg C for phase II) and generally humid conditions (Figure 5-4 and Figure 5-5). A wintertime stagnation event was occurring throughout phase I. Relative humidity (inferred from the difference between the temperature and the due point) was consistently higher in phase I than in phase II. However, a rain shower fell beginning on the evening of Wednesday of phase II and continued intermittently through Thursday. The precipitation did not affect the sampling system, however elevated humidity did influence some of the measurements as described in Section 5.5.

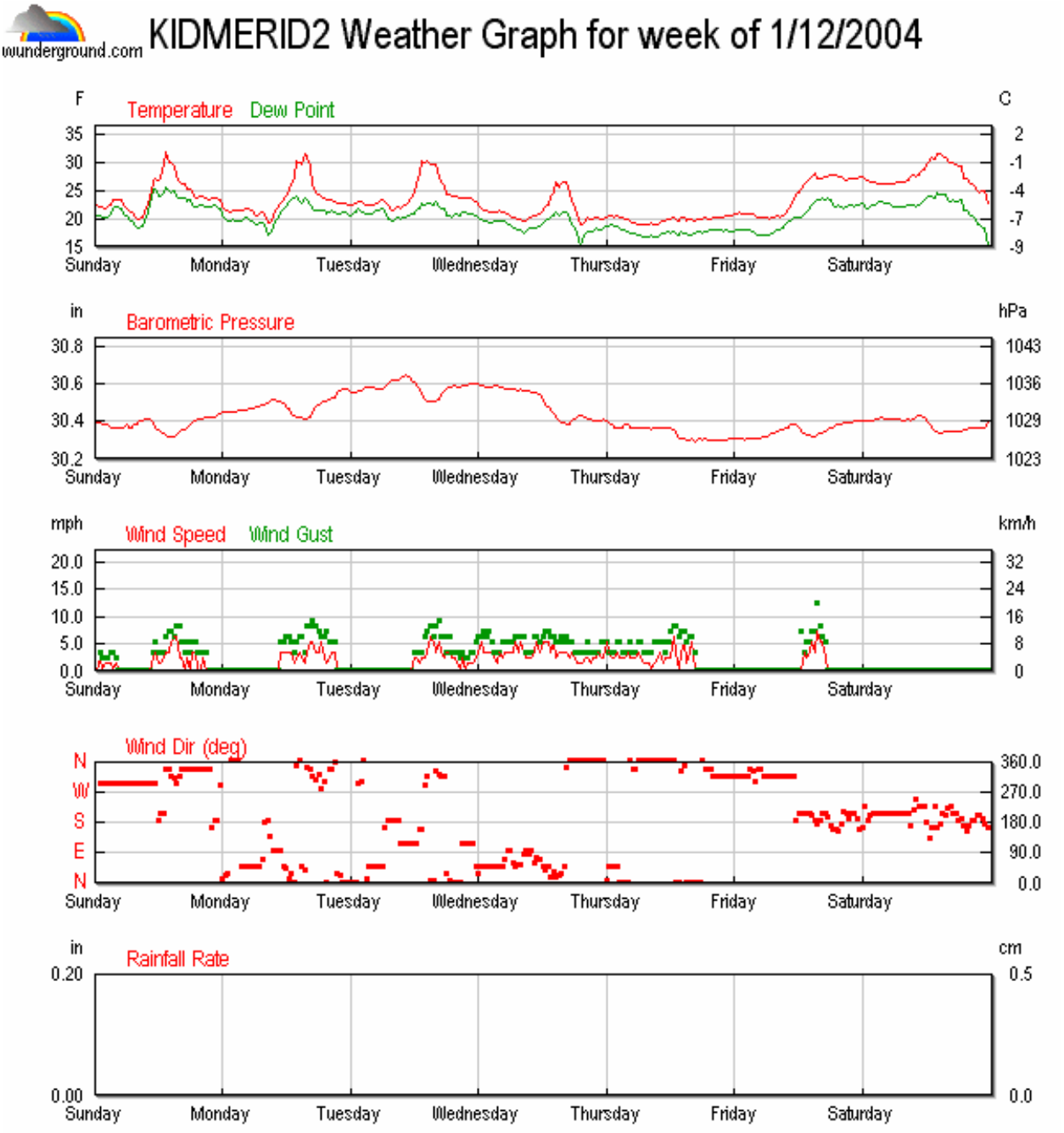

Figure 5-4. Weather summary of conditions near the Lanark sampling site during phase I.

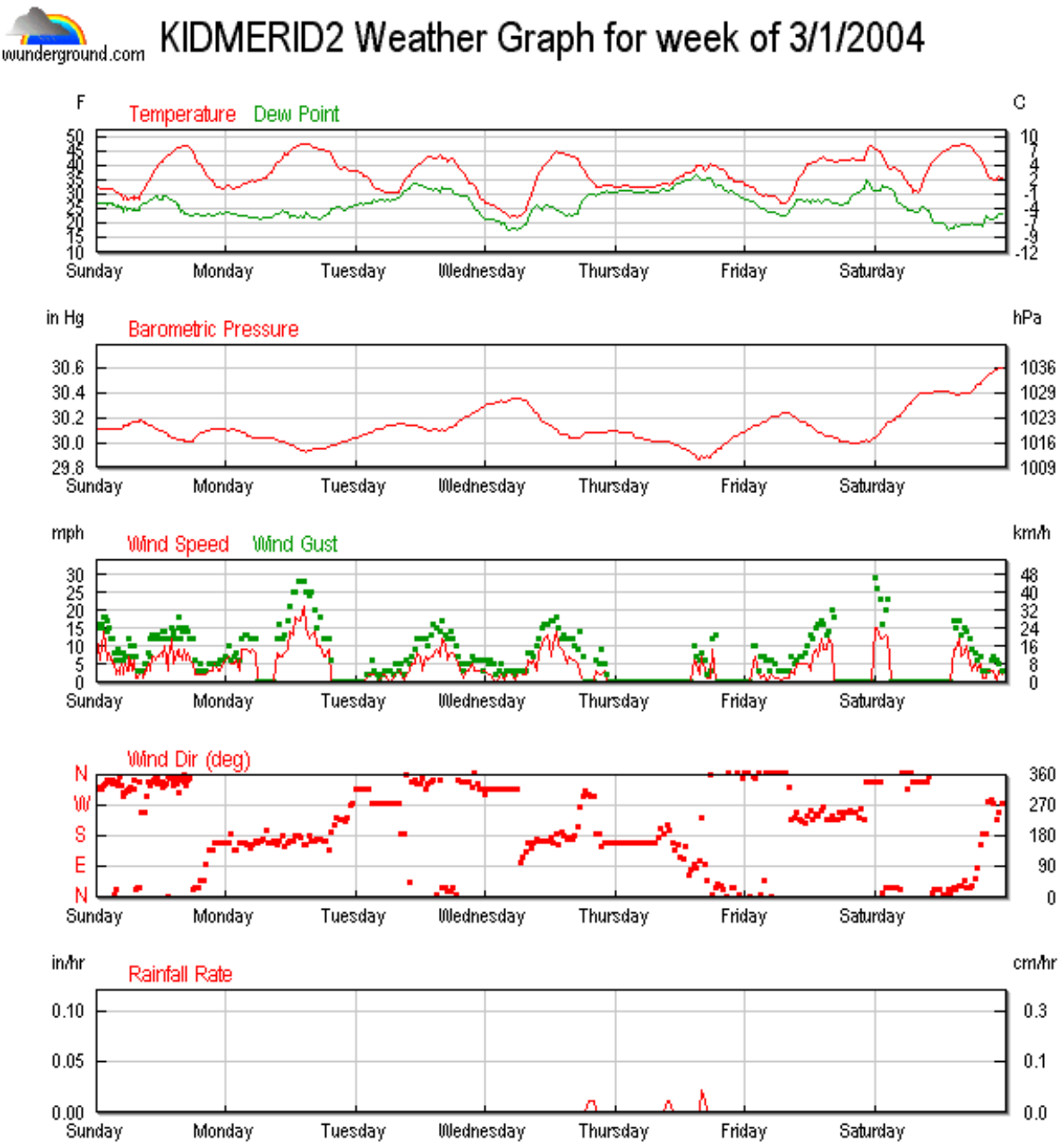

Figure 5-5. Weather summary of conditions near the Lanark sampling site during phase II.

5.4. Non-bus Vehicles

The emission factors of non-bus vehicles (i.e. light duty cars and trucks) were calculated assuming that the vehicles were gasoline powered. The data are analyzed here to evaluate the performance of the measurement systems, to determine the effect of cold and hot stabilized engine conditions on emissions, and to verify the consistency of the results between phases I and II. The vehicle fleet at Lanark Road was presumably very consistent since most of the drivers using this road were school bus drivers or high school students.

Table 5-1 reports the averages (or means) and the medians of the emission factors in g pollutant/kg fuel for the passenger vehicles (assuming gasoline engines) driving through the sensors at the Lanark Road site. The uncertainties represent the 68% confidence limits (i.e. standard error of mean and median). When there is overlap of the error bars for two quantities, the difference between them is not considered to be significant at a 95% or larger confidence level, or equivalently, the populations would not pass a Student t-test with alpha = 0.05.

Table 5-1. Averages and medians of gases and PM emission factors for passenger cars (gasoline) at the Lanark Road site.

POLLUTANT	STATISTIC	PHASE I		PHASE II	
		IN	*OUT*	*IN*	*OUT*
CO (g_{CO}/Kg_{Fuel})	*Average*	25 ± 6	192 ± 15	49 ± 7	175 ± 10
	Median	4.0 ± 0.7	77 ± 7	4.0 ± 0.7	71.2 ± 7
	Number	216	312	394	552
HC (g_{HC}/Kg_{Fuel})	*Average*	3.8 ± 0.6	15.5 ± 1.2	3.2 ± 0.5	10.7 ± 0.6
	Median	1.34 ± 0.16	10.2 ± 0.6	0.75 ± 0.13	7.9 ± 0.4
	Number	189	273	371	525
NO (g_{NO}/Kg_{Fuel})	*Average*	1.5 ± 0.3	8.5 ± 0.6	1.47 ± 0.15	8.1 ± 0.4
	Median	0.82 ± 0.2	5.4 ± 0.46	0.71 ± 0.1	4.3 ± 0.5
	Number	152	219	347	502
PM (g_{PM}/Kg_{Fuel})	*Average*	0.22 ± 0.03	0.34 ± 0.04	0.18 ± 0.04	0.43 ± 0.04
	Median	0.16 ± 0.02	0.16 ± 0.02	0.055 ± 0.014	0.19 ± 0.02
	Number	124	264	354	483

The effect of engine operating temperature on emissions is evident when comparing cold engine (outbound) with hot stabilized engine (inbound) emission factors. This is especially true for CO and HC since a cold catalytic converter is unable to reduce emissions. The difference between average and median is indication of the skewness of the emission distribution across the fleet, implying a disproportionate contribution of higher emissions when the difference is large. For gasoline vehicles, it is well known that the emission distribution is highly skewed especially for CO. These results are consistent with this observation for the hot stabilized engine case.

In the case of cold start, all vehicles have a cold catalytic converter and are likely to have elevated emissions. The distributions of emissions from all non-bus vehicles are less skewed (i.e. the median is closer to the mean) in the cold start case.

The data reported in Table 5-1 are displayed using bar graphs in the following figures. Each graph compares the average emission factors for phase I (left) and phase II (right) and for hot stabilized engine (top) and cold start (bottom). The medians are reported (without uncertainties for clarity) as a horizontal line across each average column plot.

Figure 5-6 shows the mean (or average) and the median CO emission factors from the non-bus vehicles on Lanark Road. As indicated by the labels of the y-axis, the hot stabilized emission factors are approximately 1/5 of the cold start emission factors. The mean of CO for the hot engine case is significantly larger in phase I than in phase II. However, the strong skewness of the data set suggests that the average could be easily influenced by a small number of high emitters. A comparison of the medians from the two phases indicates good data consistency.

Figure 5-7 shows the mean and the median HC emission factors. As with CO, the hot stabilized HC emission factors also are lower (~1/4 of the cold start emission factors). The mean of the HC emission factors for the hot engine case is insignificantly larger in phase I than in phase II. Both the mean and the median cold start and the median hot stabilized HC emission factors are significantly (alpha = 0.05) larger in phase I than in phase II. This may represent a potential bias in the HC dataset with higher measured emission factors in phase I than in phase II.

Figure 5-8 shows the mean and the median NO emission factors. Once again, the hot stabilized emissions are much lower (1/6) than the cold start. The NO emissions are less skewed than the CO emissions. This may be due to the formation mechanism of the pollutants. CO and HC are generally emitted from incomplete combustion of fuel. Whereas NO is emitted from the thermal combination of oxygen and nitrogen that are readily present in the air. NO emission factors from both cold and hot engine cases compare very well between the two phases.

Figure 5-9 reports the mean and the median PM emission factors as measured with the LIDAR system. The hot stabilized emissions are lower than the cold start emissions. The skewness of the emission factor distribution is higher in cold conditions for phase I and lower for phase II measurements. Previous measurements of PM emission factors in Las Vegas with the remote sensing system also found a skewed distribution (Mazzoleni et al., 2004). For both cold and hot engine operating conditions, the PM average readings compare well between the two phases, being the differences statistically insignificant (hot engine) or just marginally significant (cold engine).

Analysis of the data indicates that the remote sensing emissions measurement system were consistent between phases I and II for NO and PM. Average CO emission factors were higher in phase I than in phase II for hot stabilized conditions. Average HC emission factors were higher in phase I than in phase II for the cold stabilized conditions. Average PM emission factors were slightly lower in phase I than in phase II for hot stabilized conditions. These variations may be due to a small number of high emitting gasoline vehicles that have a large impact on the average emission factors.

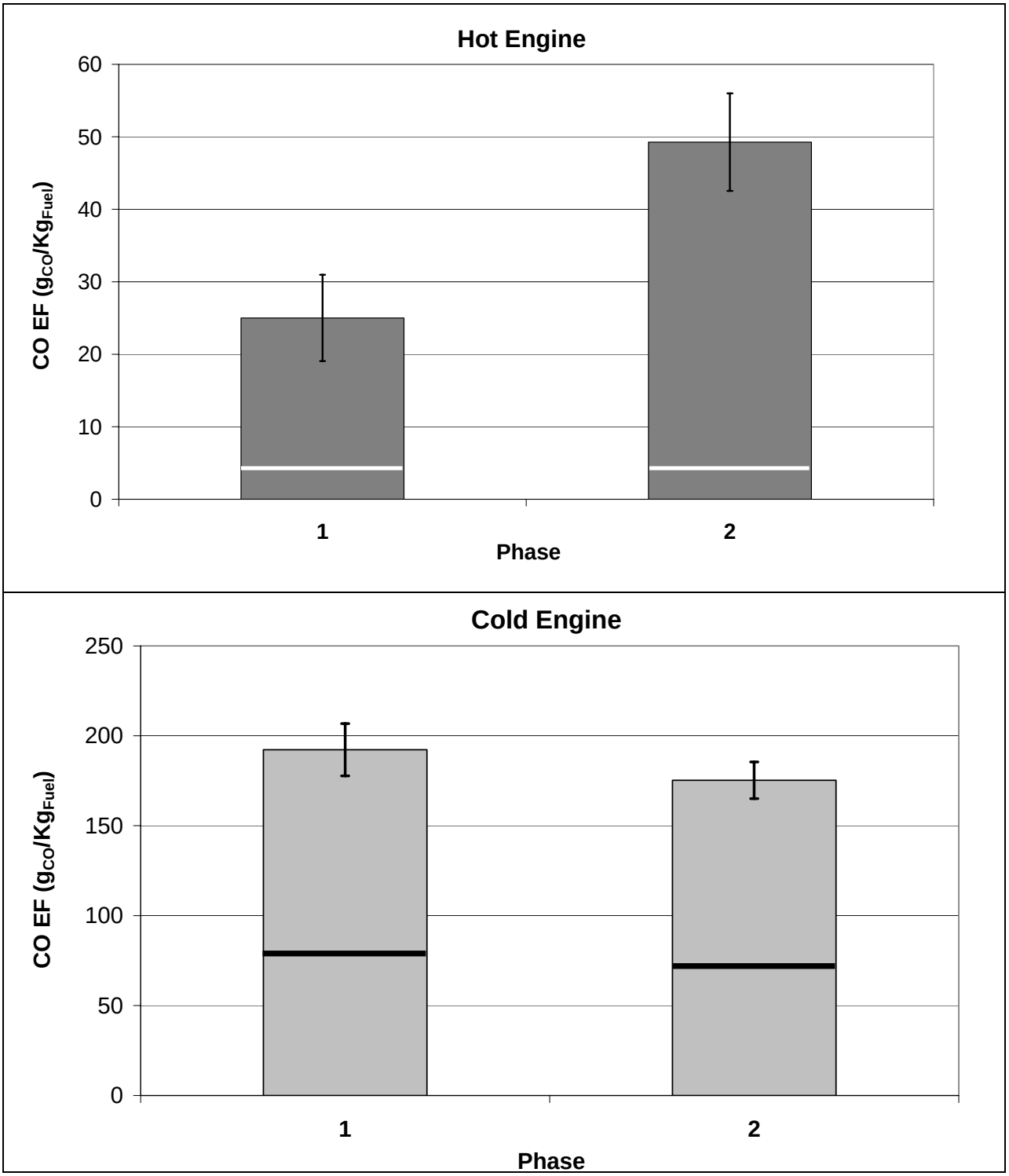

Figure 5-6. Average and median CO emission factors for non-buses at the Lanark Road site. The columns represent the average emission factors, while the error bars are the standard error of the mean. The horizontal lines represent the median emission factors. Hot stabilized emission factors are significantly higher during phase II than phase I at the 95% confidence level, while the difference is not significant for the cold start case.

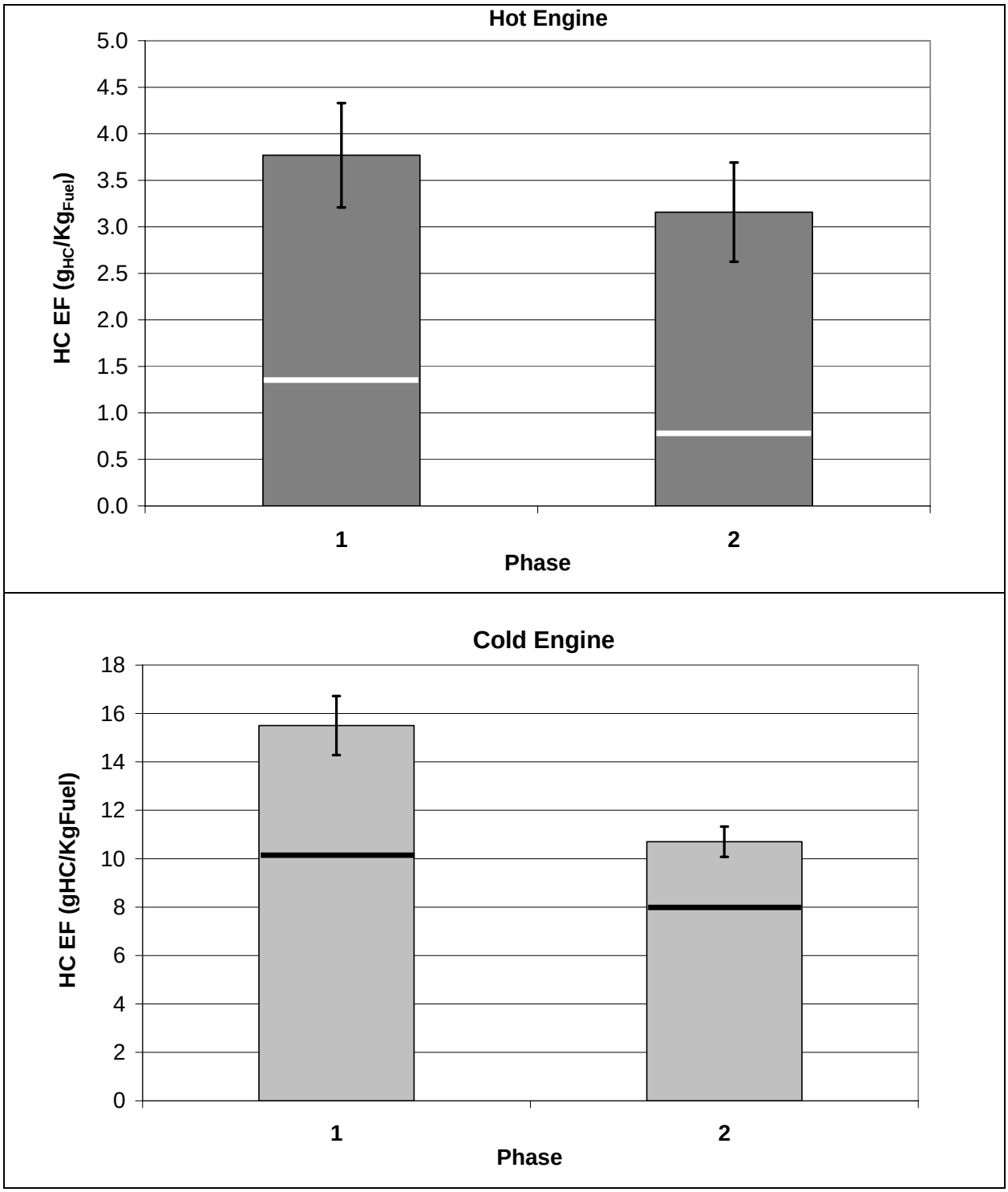

Figure 5-7. Average and median HC emission factors for cars at the bus depot. The columns represent the average emission factors, while the error bars are the standard error of the mean. The horizontal lines represent the median emission factors. For the hot stabilized case, the difference between average emission factors for phase I and phase II is not significant at the 95% confidence level, while the difference is significant for the cold start case.

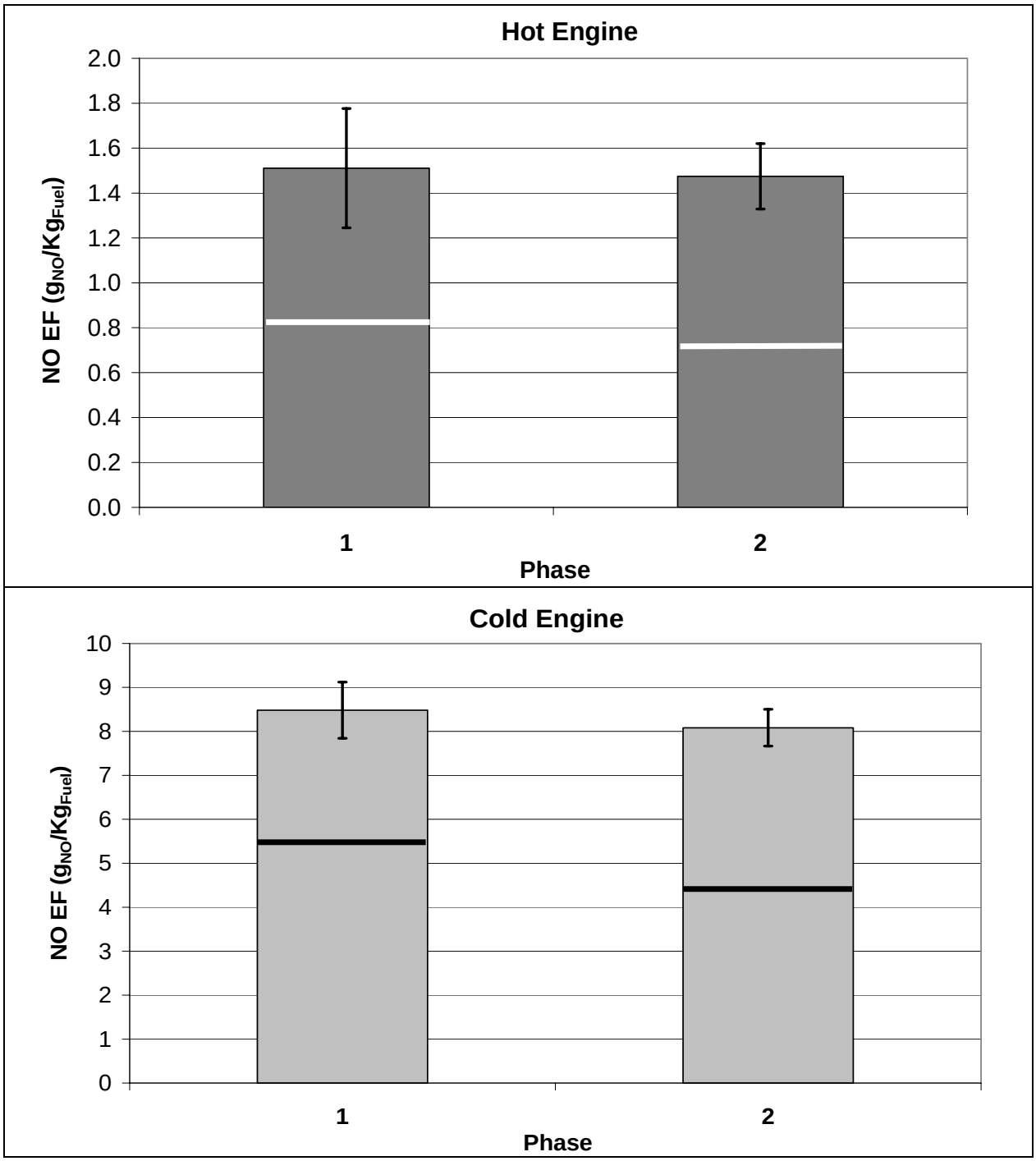

Figure 5-8. Average and median NO emission factors for cars at the Lanark Road site. The columns represent the average emission factors, while the error bars are the standard error of the mean. The horizontal lines represent the median emission factors. For both the hot and the cold engine cases the differences between average emission factors for phase I and phase II are not significant at the 95% confidence level.

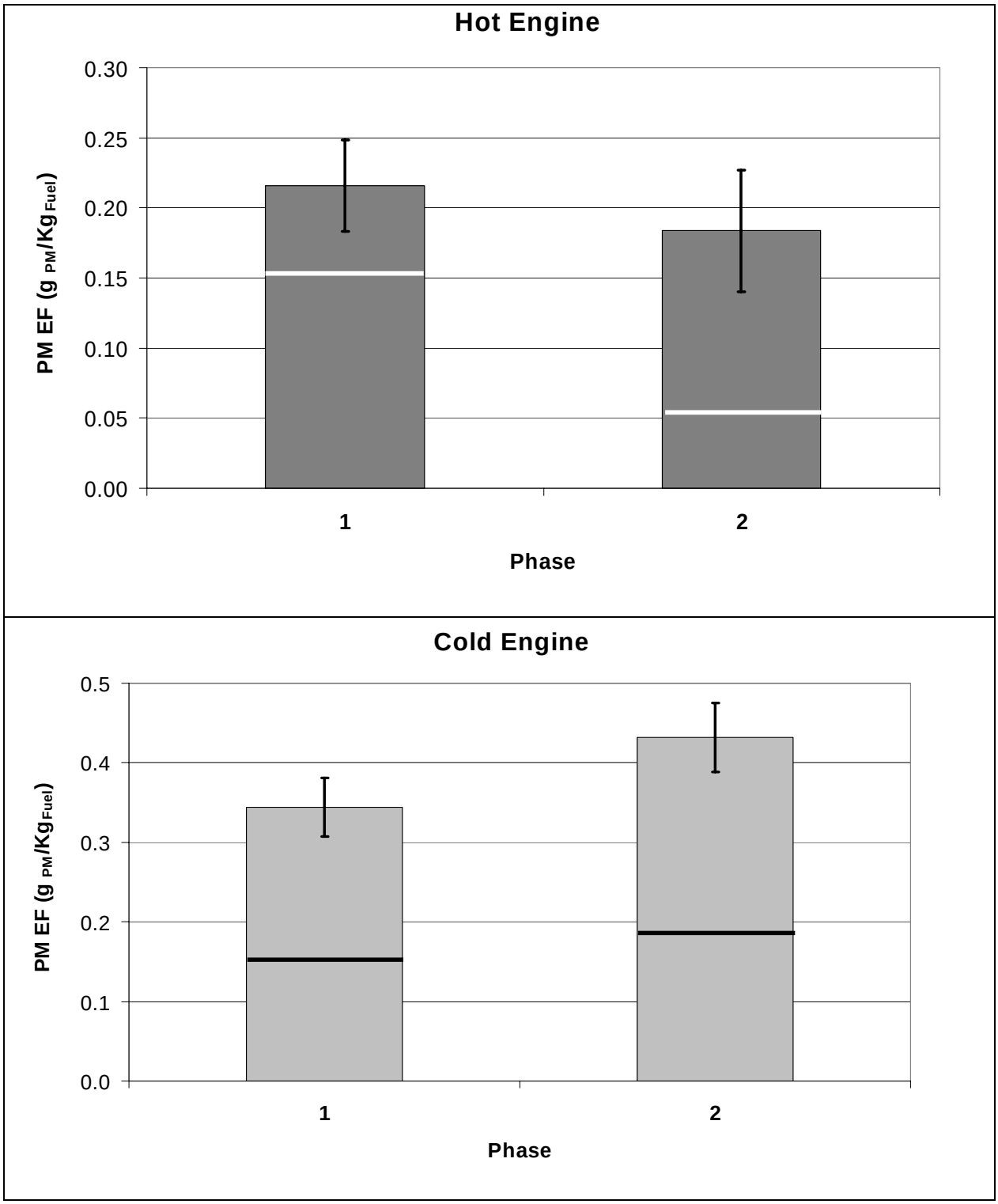

Figure 5-9. Average and median PM emission factors for cars at the Lanark Road site. The columns represent the average emission factors, while the error bars are the standard error of the mean. The horizontal lines represent the median emission factors. For both the hot and the cold engine cases the differences between average emission factors for phase I and phase II are not significant at the 95% confidence level.

5.5. Influence of Visible Steam on Measured Emissions

The presence of a visible steam plume on the outbound vehicles at the Lanark Road location was noted. Due to the camera's position, the plume could not be seen on the inbound vehicles (cold start). Steam was more prevalent during phase I (~30% of vehicle) than in phase II (~10% of vehicles). This is consistent with trends in the relative humidity. The highest density of vehicles with steam plumes was observed during the precipitation event on Thursday of phase II.

The presence of steam in the plume may degrade the emission measurements by increasing the optical opacity or by interfering with the absorption and/or backscattering measurements. An investigation of the effect of the steam on the average and median emission factors is reported in Table 5-2. When clear evidence of the presence or absence of steam was found a flag was attached to the emissions data in the database (S for steamer, and NS for non steamer). Average, median, and standard errors of the emission factors were calculated for vehicle plumes with visible steam and those without.

For all pollutants, average and median emission factors were higher in the presence of visible steam than in the absence of visible steam. During phase I, average emission factors of CO, HC, NO, and PM were all significantly higher for vehicles with steam than for those without steam. During phase II, differences were significant only for HC, NO and PM. Standard errors of the mean were higher during phase II because there were fewer vehicles with visible steam.

These results indicate that the presence of steam may introduce a bias in the measured emissions factors. At present, it is unknown if vehicles emitting steam are truly high emitters or if the steam interfered with the accuracy of the measurements.

Table 5-2. Effect of steam on gasoline passenger vehicles emission measurements. Uncertainties represent the standard error (68% confidence limit).

POLLUTANT	STATISTIC	PHASE I			PHASE II		
		All	*Steam*	*No Steam*	*All*	*Steam*	*No Steam*
CO (g_{CO}/Kg_{Fuel})	*Average*	222 ± 19	303 ± 38	188 ± 23	162 ± 17	214 ± 61	155 ± 18
	Median	90 ± 11	210 ± 56	72 ± 8	62 ± 12	88 ± 74	61 ± 11
	Number	197	59	138	185	19	166
HC (g_{HC}/Kg_{Fuel})	*Average*	17.2 ± 1.5	31.2 ± 3.8	12.2 ± 1.2	10.4 ± 1.4	21.2 ± 4.6	9.3 ± 1.4
	Median	10.9 ± 1.2	22.7 ± 7.7	9.06 ± 0.86	7.35 ± 0.66	14.0 ± 2.5	6.87 ± 0.55
	Number	172	45	127	175	16	159
NO (g_{NO}/Kg_{Fuel})	*Average*	8.9 ± 0.9	11.6 ± 2.4	7.9 ± 0.8	7.57 ± 0.63	11.1 ± 3.1	7.25 ± 0.63
	Median	5.5 ± 0.6	5.9 ± 0.7	5.4 ± 0.9	4.2 ± 0.6	5.44 ± 3.4	4.0 ± 0.8
	Number	135	38	97	170	14	156
PM (g_{PM}/Kg_{Fuel})	*Average*	0.37 ± 0.05	0.59 ± 0.13	0.28 ± 0.05	0.44 ± 0.07	0.92 ± 0.26	0.38 ± 0.07
	Median	0.19 ± 0.02	0.31 ± 0.04	0.14 ± 0.02	0.16 ± 0.05	0.52 ± 0.20	0.13 ± 0.03
	Number	153	47	106	174	16	158

5.6. School Bus Emission Factors

5.6.1. Fleet Averages and Medians

In this section the average (or mean) and median emission factors from the school buses are compared for the two phases to assess the effect of switching from petroleum diesel to a 20% biodiesel fuel mixture (B20) on emissions of CO, HC, NO, and PM. The average and median emission factors are reported in Table 5-3.

For both phases, the CO and HC emission factors were lower for buses than for gasoline vehicles, whereas NO emission factors for buses were higher than for non-buses. These results are consistent with other remote sensing studies (Kuhns et al., 2004; Mazzoleni et al., 2004). Although PM emission factors are generally higher for the buses (0.57 g/kg fuel) than for the gasoline vehicles (0.22 g/kg fuel), this difference is not as large as the comparable published values of remotely sensed vehicles in Las Vegas (1.5 g/kg fuel for diesel and 0.056 g/kg fuel for gasoline). It should be noted that the buses in this study are routinely maintained, while the fleet of diesel vehicles in Las Vegas were a variety of commercial and privately owned vehicles.

The non-bus PM emission distributions from Lanark Road were skewed (as discussed earlier) and average emission factors were strongly influenced by a few, poorly maintained, high emitters. The diesel bus emission factors instead have a lower skewness, indicating more consistent maintenance. This conclusion is also supported by the fact that the median PM emission factors for the buses are much higher than median emission factors for gasoline vehicles (Table 5-1 and Table 5-3).

Average and median emission factors of outbound vehicles were always higher than average and median emission factors of inbound vehicles. This suggests that engine temperature has an effect on emissions even though the buses do not have catalytic converters. The hot to cold emissions difference is much less pronounced than for gasoline vehicles that have catalytic converters (mid 1980 model years to the present).

Mean cold start emissions of CO, HC, and PM and hot stabilized emissions of CO and PM were higher (t-test alpha = 0.05) after the buses switched to B20. A slight but significant reduction in median cold start NO emission factors (7%) was observed after the switch. An additional slight but significant reduction in median hot stabilized CO emission factors (16%) was observed after the switch. The results of Table 5-3 are shown graphically in Figure 5-10 through Figure 5-13. The medians are reported (without uncertainties for clarity) as horizontal line across each average column plot.

From Figure 5-13, it is evident that PM emissions are almost normally distributed for petroleum diesel (i.e., the median and mean are very close to each other). The PM emission factors for the B20 case are more skewed indicating that a few higher emitters are at least partly responsible for the increased PM emissions with the B20 fuel. To investigate this hypothesis, quintile distributions were constructed by sorting the raw data by decreasing emissions. The resulting list was divided into five groups. Average emission factors and standard errors were calculated for each group. These data are shown in Figure 5-14 (hot stabilized engine) and Figure 5-15 (cold start). The lower values in the 5^{th} quintile on the right of the hot engine plot are strongly influenced by the measurement noise. There is no statistically significant difference between the 5^{th} bars for both phases in hot engine condition suggesting that the same sources of noise where affecting both measurement phases. This adds more confidence to the consistency of the measurements. The effect is less evident in the cold engine case due to the higher emission factors.

It is evident that the increase in emission factors is higher for the highest emitters, however it is significant across the distribution with the exception of the lowest quintile. Consequently, the influence of B20 on PM emissions appears to influence the entire bus fleet.

Table 5-3. Averages and medians of gases and PM emission factors for school bus fleet at the Lanark Road site.

POLLUTANT	STATISTIC	PETROLEUM DIESEL		B20	
		IN	*OUT*	*IN*	*OUT*
CO (g_{CO}/Kg_{Fuel})	*Average*	11.8 ± 0.6	18.7 ± 0.9	10.7 ± 0.7	25.0 ± 1
	Median	8.0 ± 0.4	13.3 ± 0.7	6.7 ± 0.4	17.3 ± 1
	Number	497	397	413	538
HC (g_{HC}/Kg_{Fuel})	*Average*	1.3 ± 0.1	3.4 ± 0.2	1.6 ± 0.1	3.1 ± 0.2
	Median	1.0 ± 0.1	2.8 ± 0.2	1.2 ± 0.05	2.4 ± 0.2
	Number	487	353	406	527
NO (g_{NO}/Kg_{Fuel})	*Average*	21.9 ± 0.6	25.9 ± 0.6	21.6 ± 0.5	25.7 ± 0.6
	Median	20.5 ± 0.9	24.6 ± 0.5	19.7 ± 0.5	22.9 ± 0.7
	Number	449	363	381	479
PM (g_{PM}/Kg_{Fuel})	*Average*	0.57 ± 0.03	1.05 ± 0.05	1.07 ± 0.06	1.73 ± 0.07
	Median	0.47 ± 0.03	0.92 ± 0.05	0.89 ± 0.03	1.41 ± 0.04
	Number	241	234	291	494

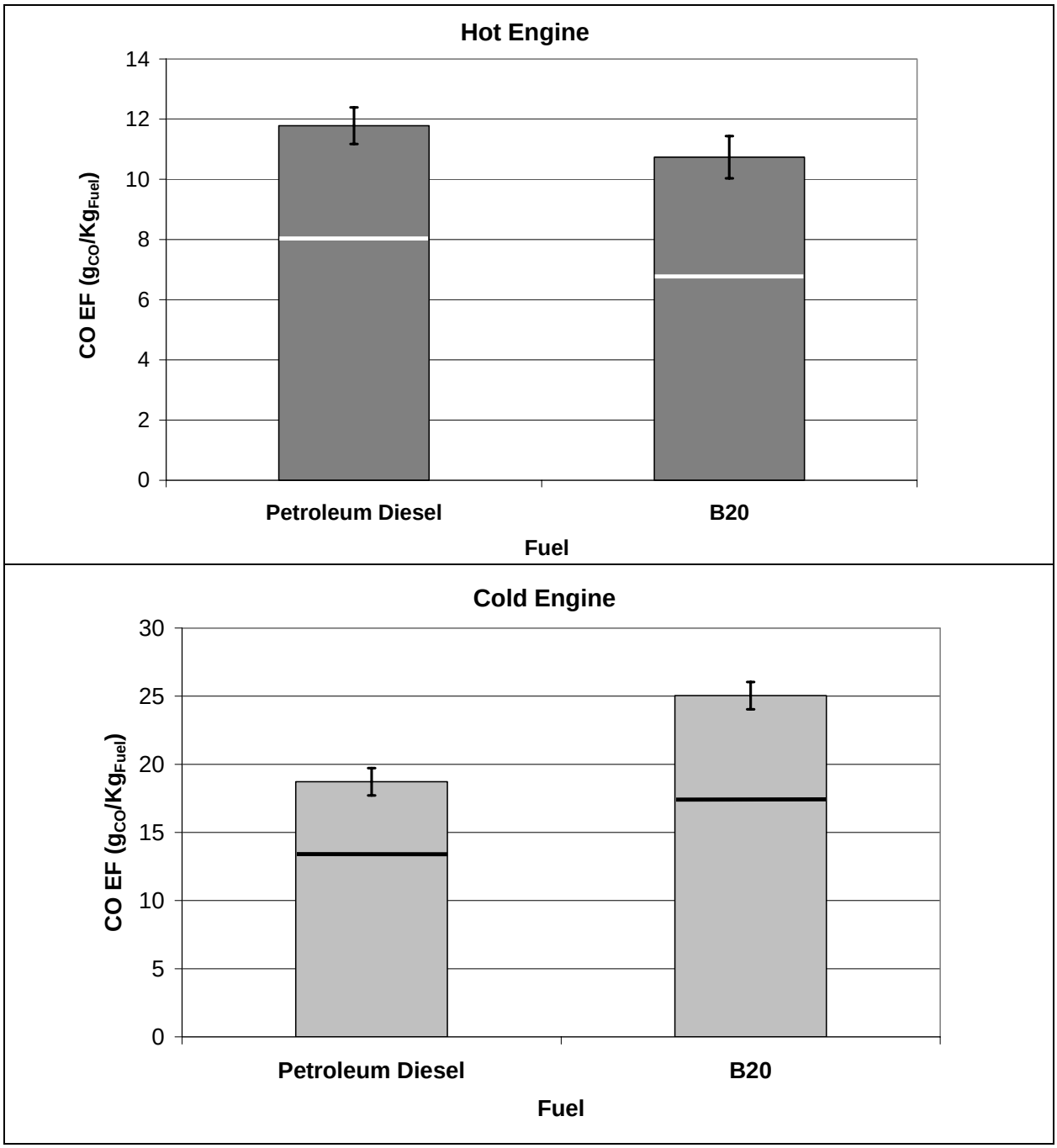

Figure 5-10. Average and median CO emission factors for buses from phase I (Petroleum Diesel) and phase II (B20). The columns represent the average emission factors, while the error bars are the standard error of the mean. The horizontal lines represent the median emission factors. For the hot engine case the difference between average emission factors for diesel petroleum and B20 is not significant at the 95% confidence level, while the CO emission factors increase for the cold start case after the switch to B20 fuel.

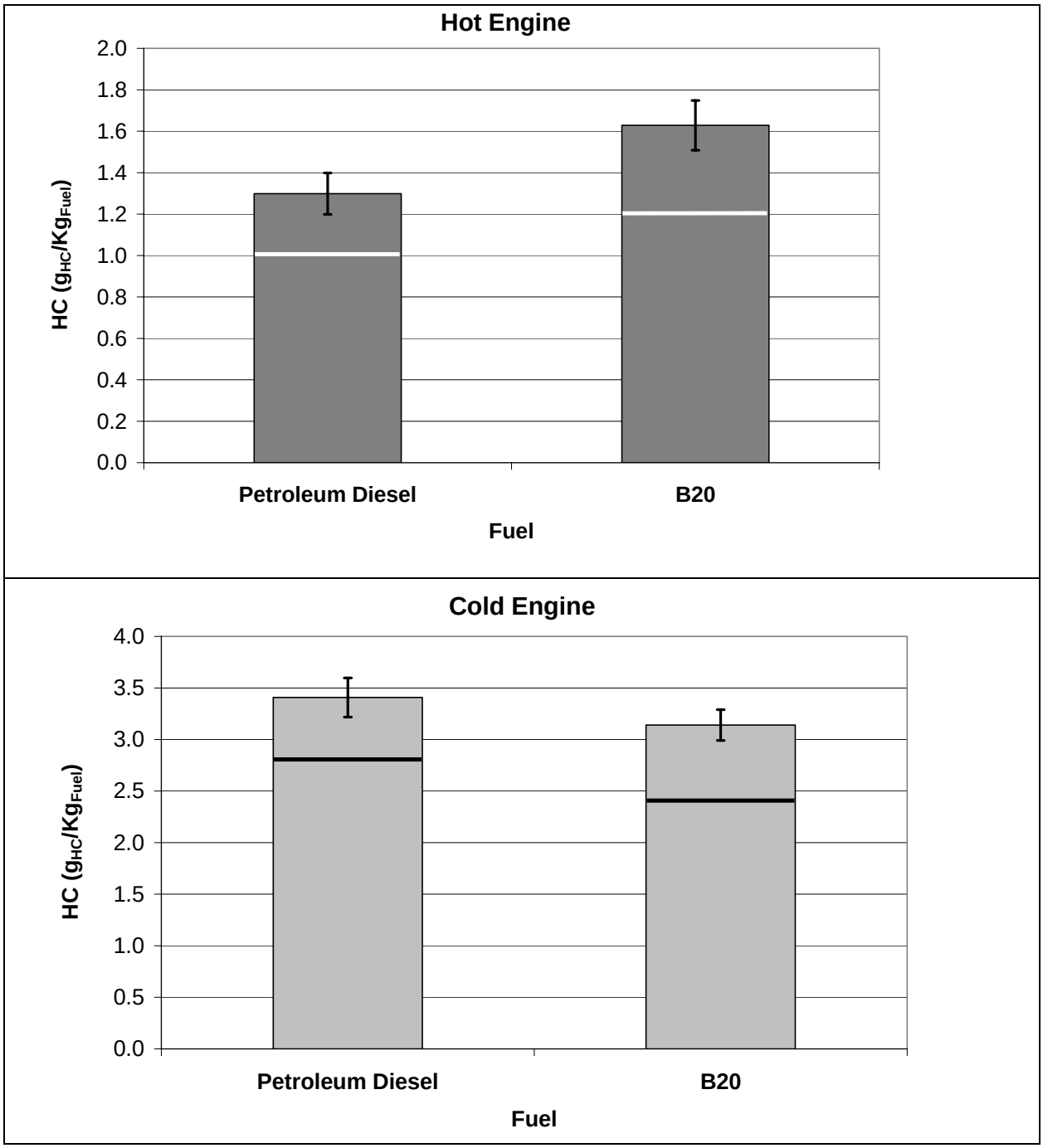

Figure 5-11. Average and median HC emission factors for buses from phase I (Petroleum Diesel) and phase II (B20). The columns represent the average emission factors, while the error bars are the standard error of the mean. The horizontal lines represent the median emission factors. For the hot stabilized case the increase of average emission factors between diesel petroleum and B20 is significant at the 95% confidence level, while the difference is not significant for the cold engine case.

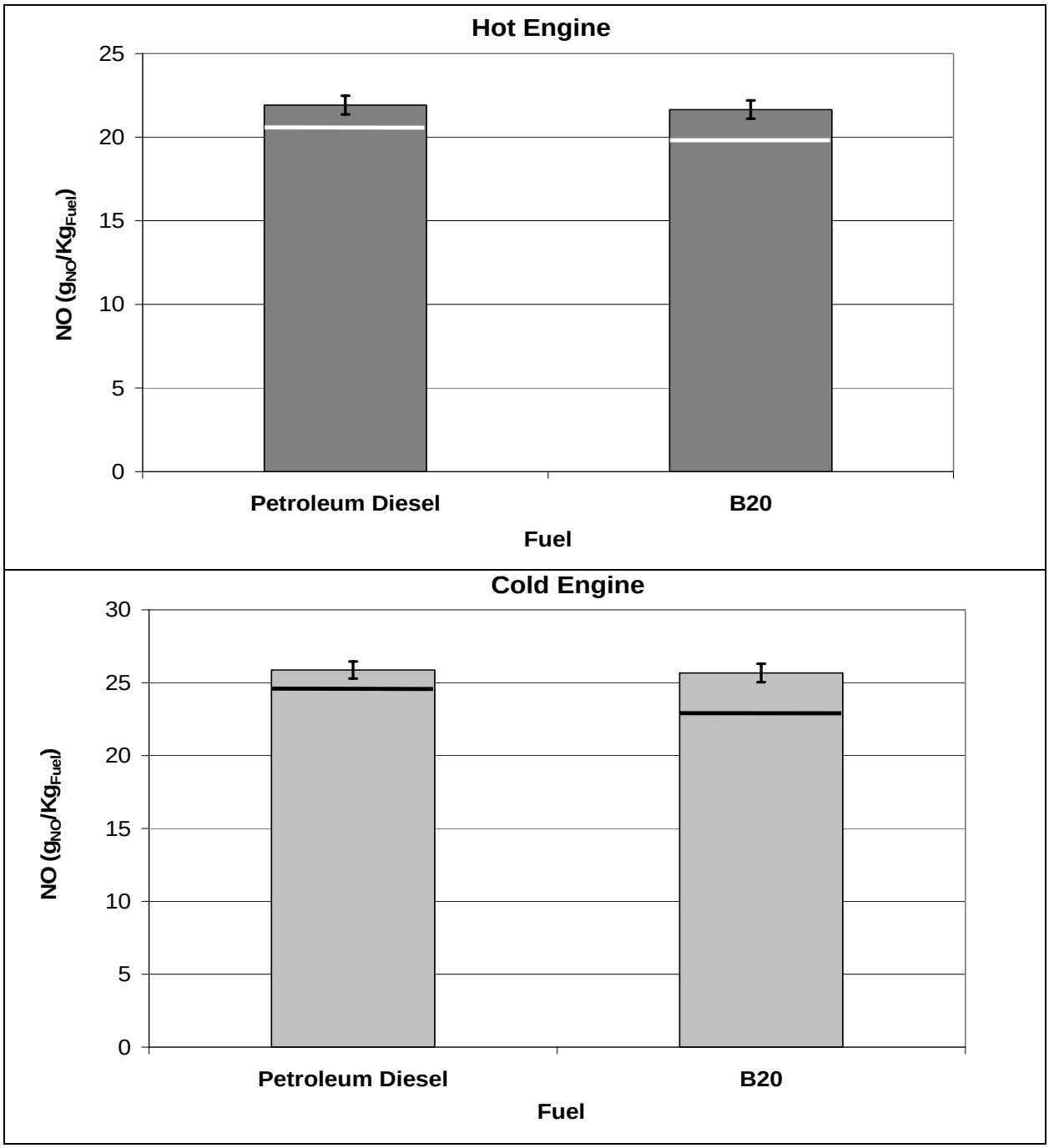

Figure 5-12. Average and median NO emission factors for buses from phase I (Petroleum Diesel) and phase II (B20). The columns represent the average emission factors, while the error bars are the standard error of the mean. The horizontal lines represent the median emission factors. For both the hot and the cold engine cases the differences of average emission factors between diesel petroleum and B20 is not significant at the 95% confidence level.

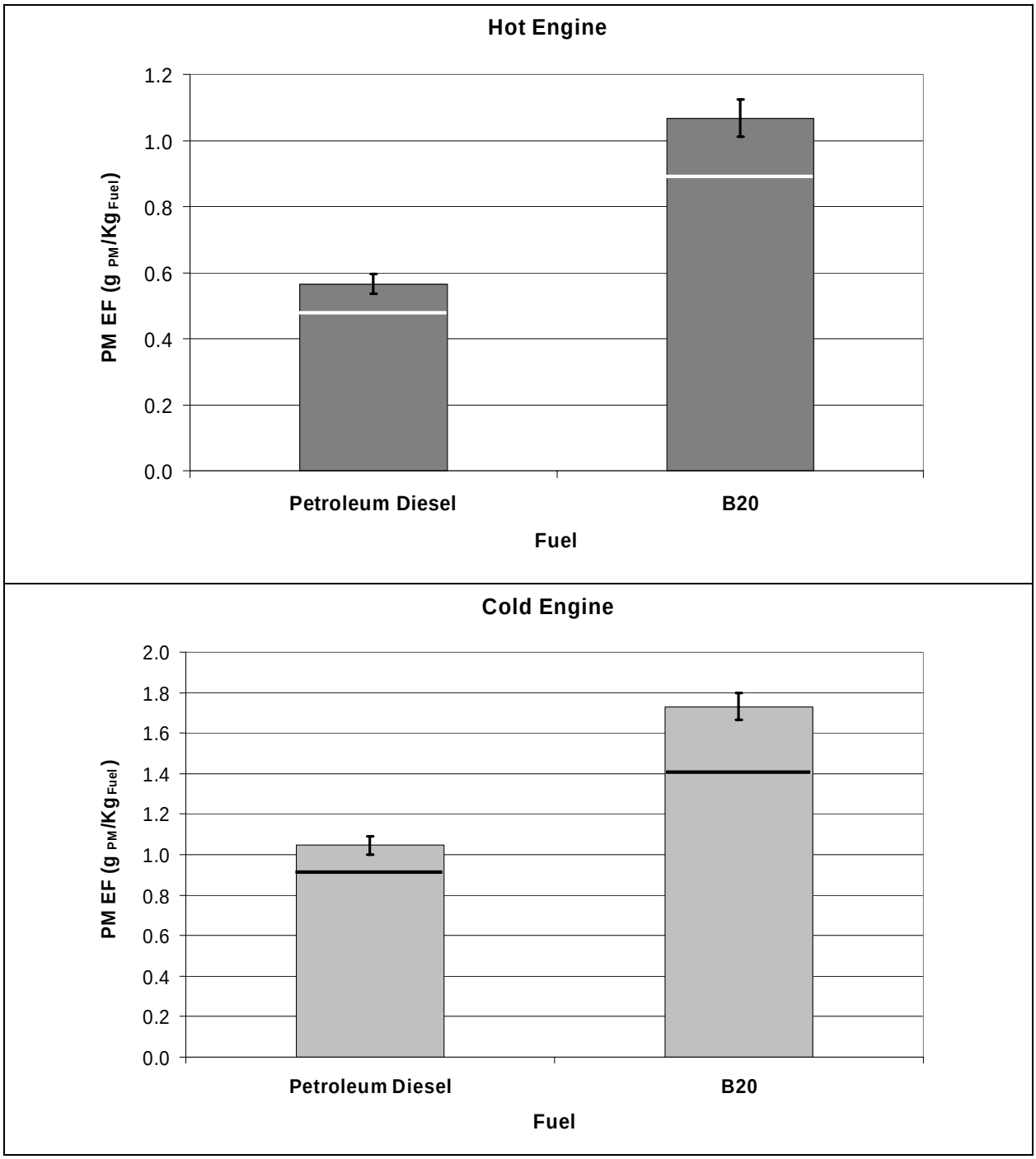

Figure 5-13. Average and median PM emission factors for buses. The columns represent the average emission factors, while the error bars are the standard error of the mean. The horizontal lines represent the median emission factors. For both the hot and the cold engine cases, the increase of average emission factors between diesel petroleum and B20 is significant at the 95% confidence level.

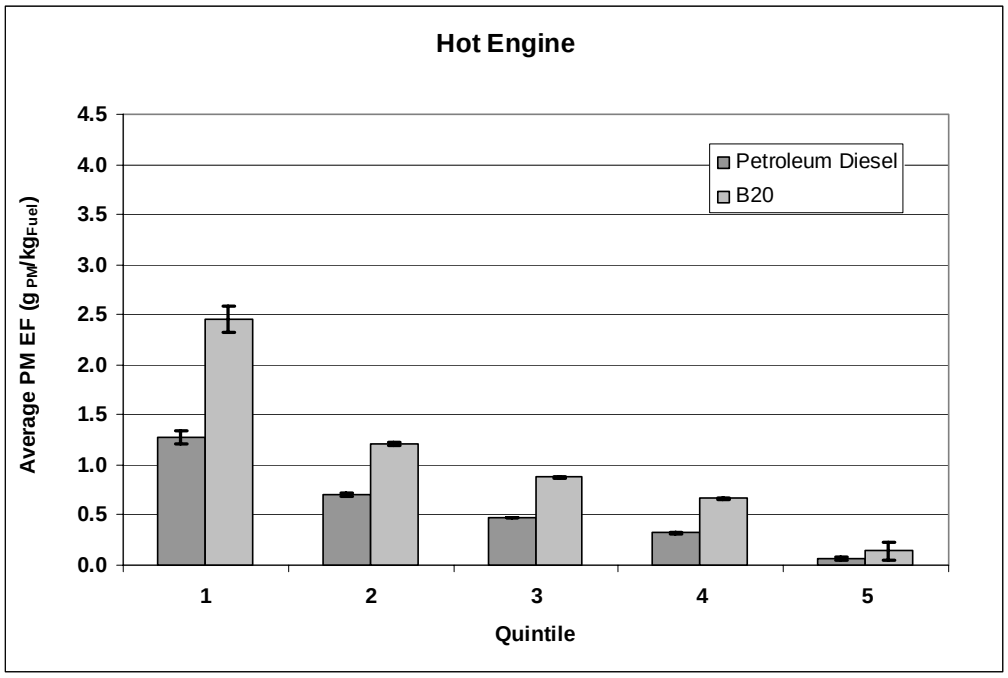

Figure 5-14. Quintile distribution of hot engine PM EFs from backscattering LIDAR inverted measurements on school buses. The error bars represent the standard error of the mean.

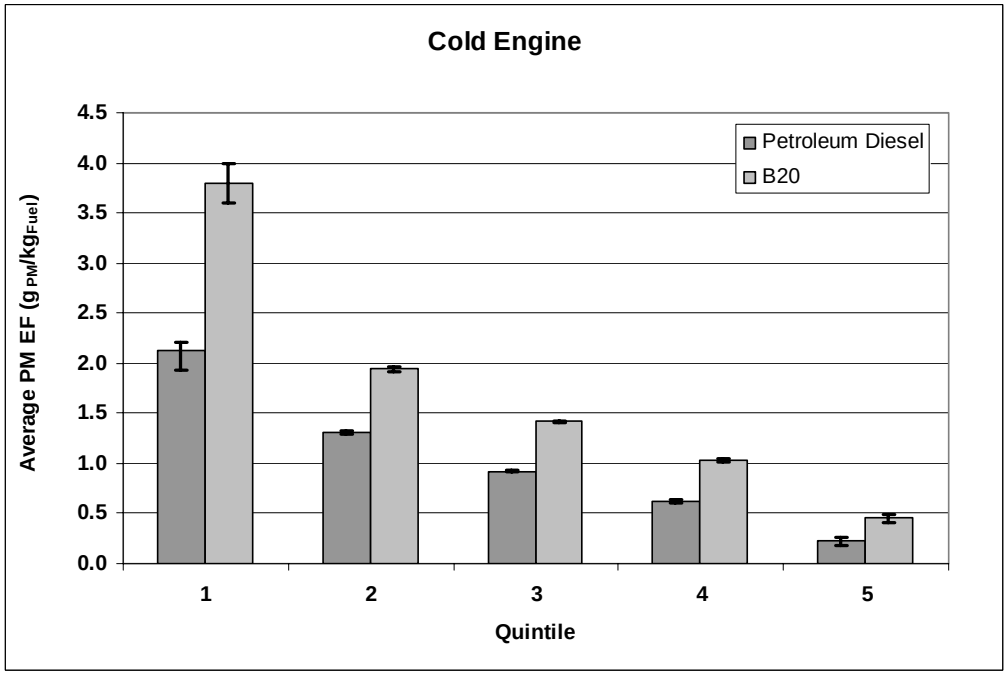

Figure 5-15. Quintile distribution of cold engine PM EFs from backscattering LIDAR inverted measurements on school buses. The error bars represent the standard error of the mean.

5.6.2. Control School Buses

Five buses (identified as #98-15, #202, #97-19, #95-5 and #03-2) from the MJSD bus fleet were switched to B20 in April 2002. A comparison of their average emission factors between phases provides additional insight into the quality and consistency of the measurements. Since these buses did not change fuels during the study, significant differences in emission factors would be associated with variations in the measurements or interferences associated with meteorological conditions. Note that the buses could only be identified during cold-start conditions.

Table 5-4 shows the average (or mean) and median cold start emission factors from these five buses. Unfortunately, the sample set is quite small leading to larger standard errors when compared to the emission factors from entire fleet. Significantly higher average CO emission factors were observed during phase II than during phase I however CO median emission factor were not different. Comparison of mean emission factors of NO, HC, and PM were not significantly different between phases.

It is worthwhile to compare the emissions of these buses with the cold start emissions of the entire fleet in Table 5-3 since the fleet of 5 buses had been operating with B20 for more than one year. No significant differences were observed in average emission factors when comparing the set of 5 buses to the entire fleet during phase II.

Average CO emission factors for the five buses were higher during phase I when compared to the entire population of cold start buses running on biodiesel in phase II, however median values were not significantly different. Median NO emission factors were higher for the five buses in phase I compared the entire fleet in phase II. No other significant differences were observed for the other pollutant species. Given the relatively small number of measurements for the five buses and the large variability of emission factors, outlier points associated with transient accelerations may bias some of these results. Caution should be exercised when drawing conclusions from these results due to the relatively small number of data points.

Table 5-4. Average and median emission factors for control buses using B20 fuel in both phases.

POLLUTANT	STATISTIC	PHASE I (B20)	PHASE II (B20)
CO (g_{CO}/Kg_{Fuel})	*Average*	16.3 ± 2.3	24.8 ± 5.5
	Median	15.9 ± 4.1	19.7 ± 2.2
	Number	11	18
HC (g_{HC}/Kg_{Fuel})	*Average*	2.46 ± 0.73	2.93 ± 0.53
	Median	3.07 ± 0.84	2.86 ± 0.36
	Number	10	18
NO (g_{NO}/Kg_{Fuel})	*Average*	23.9 ± 2.7	26.6 ± 3.2
	Median	27.5 ± 3.8	25.3 ± 2.8
	Number	11	17
PM (g_{PM}/Kg_{Fuel})	*Average*	1.62 ± 0.45	1.76 ± 0.38
	Median	1.99 ± 0.60	1.46 ± 0.21
	Number	5	11

5.6.3. School Bus Emission Factor Stratification by Model Year, Visible Steam, Odometer Reading, and Engine type

5.6.3.1 Dependence of Emission Factors on Bus Model Year

Table 5-5 shows the engine type and model year for each type of bus in the MJSD bus fleet. The bus fleet was primarily composed of buses, using two types of engines: a Cummins B-Series 5.9 liter engine with electron ignition control (model year 1990 through part of 1998) and a more modern Cummins ISB Series 5.9 liter engine (model year 1998 through 2002). An onboard computer on the ISB series buses controls the engine's air/fuel ratio and the timing. All the buses were routinely maintained by the MJSD mechanics or outside contractors.

Table 5-5. Buses engine type and respective model year

MODEL YEAR	ENGINE
1983	Detroit 8.2 l
1984	Detroit 8.2 l
1985	Detroit 8.2 l
1986	Detroit 8.2 l
1987	Detroit 8.2 l
1988	Ford Brazilian
1989	Detroit 8.2 l
1990	Cummins B-Series 5.9 l
1991	Cummins B-Series 5.9 l
1992	Cummins B-Series 5.9 l
1993	Cummins B-Series 5.9 l
1994	Cummins B-Series 5.9 l
1995	Cummins B-Series 5.9 l
1996	Cummins B-Series 5.9 l
1997	Cummins B-Series 5.9 l
1998	Cummins B-Series 5.9 l (< 98-13)
1998	Cummins ISB-Series 5.9 l Computer Controlled (> 98-13)
1999	Cummins ISB-Series 5.9 l Computer Controlled
2000	Cummins ISB-Series 5.9 l Computer Controlled
2001	Cummins ISB-Series 5.9 l Computer Controlled
2002	Cummins ISB-Series 5.9 l Computer Controlled
2003	Ford DT 466/International
2004	Caterpillar

Remote sensing studies have shown that emissions of CO, HC, NO, and PM strongly depend on light duty vehicle age (Kuhns et al., 2004). Average cold-start (outbound) school bus emission factors are plotted against vehicle model year in Figure 5-17 through Figure 5-20. Average emission factors and standard errors of the mean were calculated and plotted only for model years with at least nine valid measurements in each phase. The sample group in this case is much smaller that in the previous section since both inbound buses and buses with illegible school bus or license plate numbers were excluded from the analysis.

Average CO emission factors remained constant or slightly increased for buses with model years between 1991 and 1997. Newer buses showed a steady decrease in CO emission factors with model years 1998 and newer. Possible explanations for these reductions include (1) Technology improvements with the introduction of the new Cummins ISB (Interact System B)-Series 5.9L engine in 1998 (The new ISB turbocharged engine has 24 Valves with a Bosh VP44 electronically controlled injection pump, full electronic engine management, and high pressure injectors to meet 1998 emission requirements.) and (2) Engine deterioration (The odometer readings decrease for 1994-1995 model year and newer buses, but remain approximately constant for older models (see Figure 5-16)).

CO emission factors are significantly higher for B20 than for petroleum diesel from model year 1995 and newer. Average (or mean) HC emission factors show a marked peak around the 1996 model year and steadily decrease for newer models. Emissions are also lower than the 1995-1997 models for model year 1994 or older. Average HC emissions factors are generally equivalent or less for B20 when compared with petroleum diesel. Average NO emissions factors increase slightly with model year. Average NO emissions factors for B20 and petroleum diesel are not significantly different for model years between 1994 and 1998. B20 emissions are lower than petroleum diesel emissions for model year 1993 and older but are slightly higher for 1999 model years and newer. Average PM emission factors peak or stay stable for 1996 model years or older and decrease for newer models. Average PM emission factors are consistently higher for B20 than for petroleum diesel, with maximum differences for model years 1993 and older.

The emission factor behavior of a typical model year bus is illustrated by the median emission factor. Median CO, HC and NO EFs are plotted vs. model year in Figure 5-21, Figure 5-22, and Figure 5-23, respectively. Median CO, HC and NO EFs show similar patterns to those shown by the mean CO, HC and NO EFs. The median PM emission factors peak or remain constant for 1996 model years and older buses, but decrease substantially for newer models (Figure 5-24). Median PM emission factors are significantly higher for B20 than for petroleum diesel with the exception of the 1995 model year.

Figure 5-25 shows the frequency distributions of valid PM EFs for each model year from the 2 experiment phases. The distributions for the two phases are very close to each other implying that the overall comparison between mean and median of B20 and petroleum diesel PM emission factors is not biased by inconsistent weighting of school bus model years.

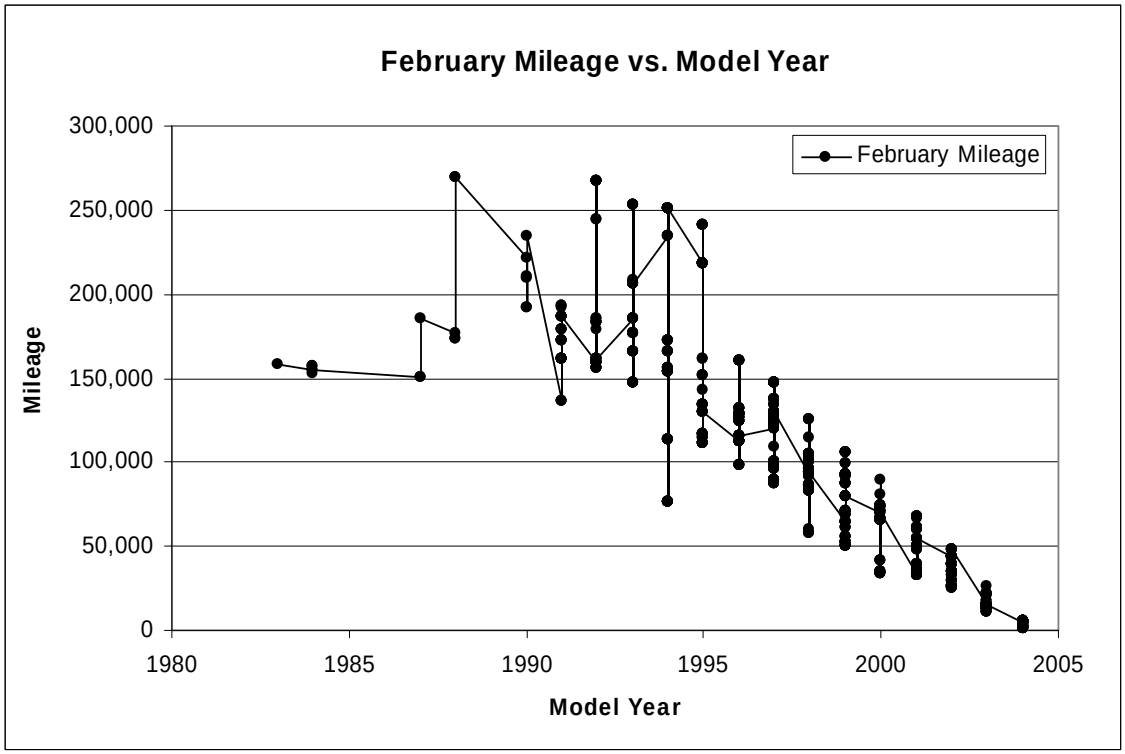

Figure 5-16. School bus odometer mileage vs. model year.

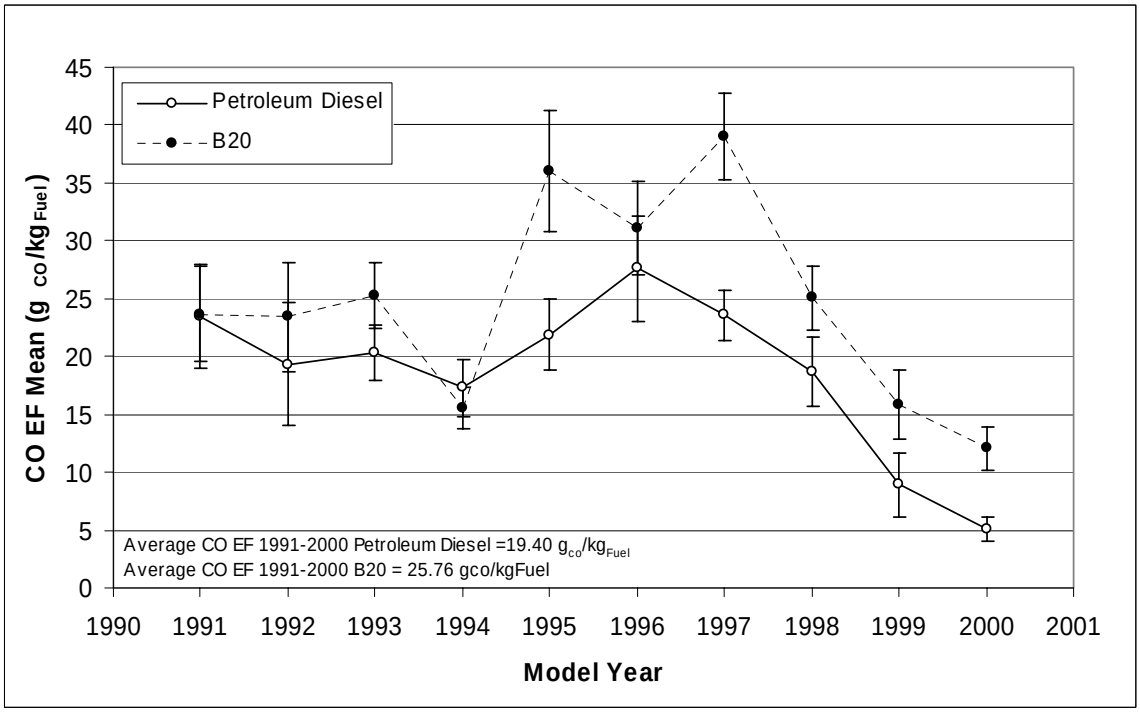

Figure 5-17. CO emission factor vs. bus model year. Each point is the average of the emissions in the respective model year group and the error bar represent the standard error of the mean.

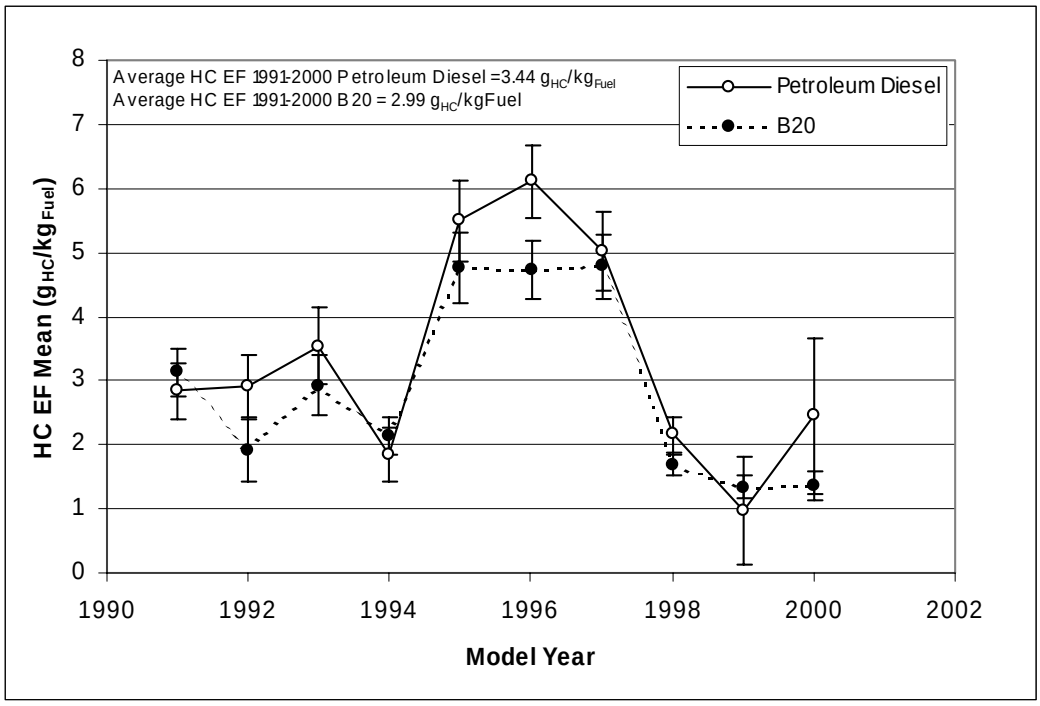

Figure 5-18. HC emission factor vs. bus model year. Each point is the average of the emissions in the respective model year group and the error bar represent the standard error of the mean.

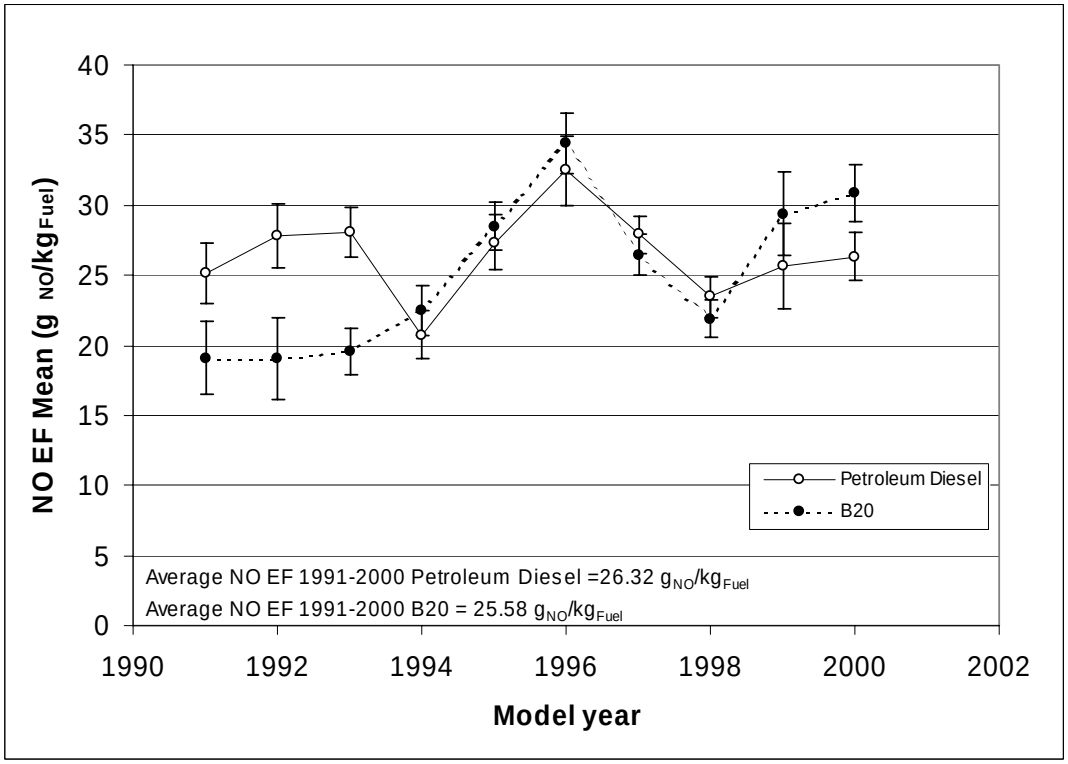

Figure 5-19. NO emission factor vs. bus model year. Each point is the average of the emissions in the respective model year group and the error bar represent the standard error of the mean.

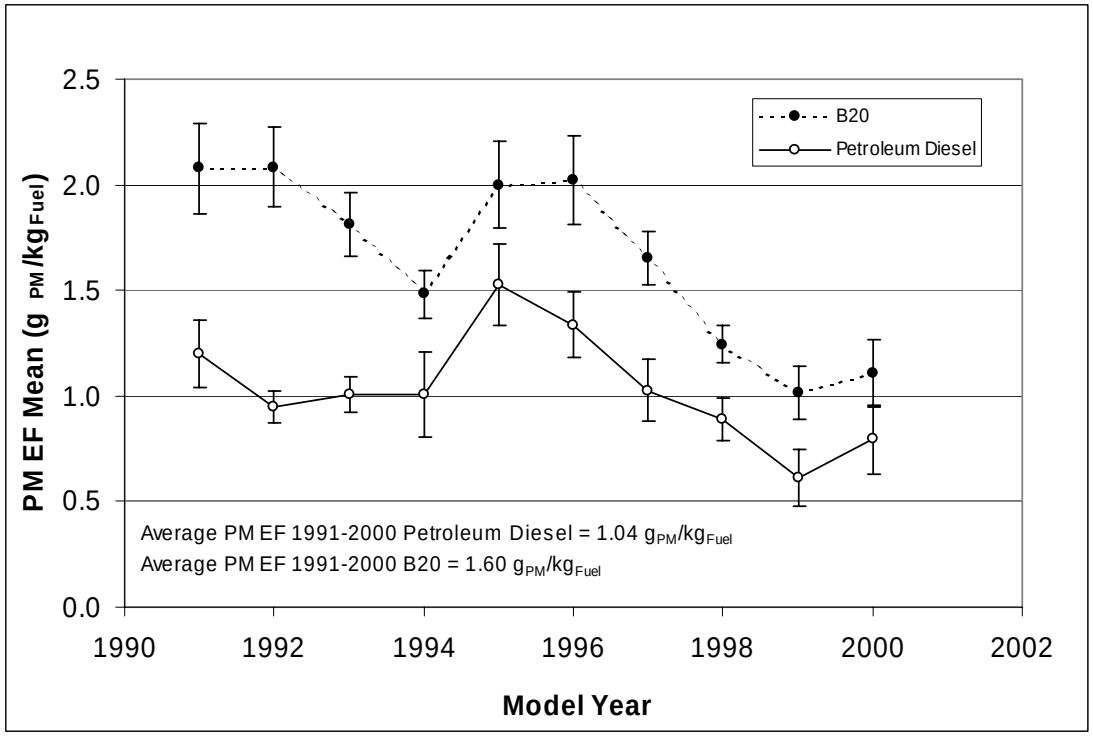

Figure 5-20. PM emission factor vs. bus model year. Each point is the average of the emissions in the respective model year group and the error bar represent the standard error of the mean.

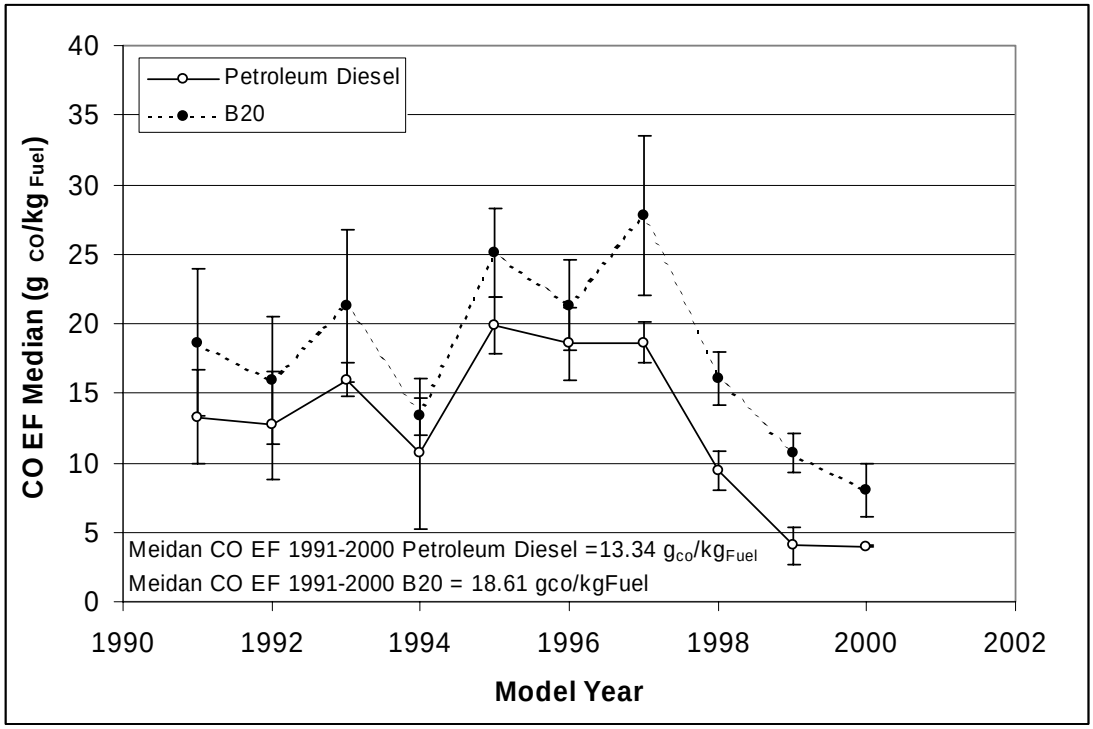

Figure 5-21: CO median emission factors vs. bus model year. Each point is the median of the emissions in the respective model year.

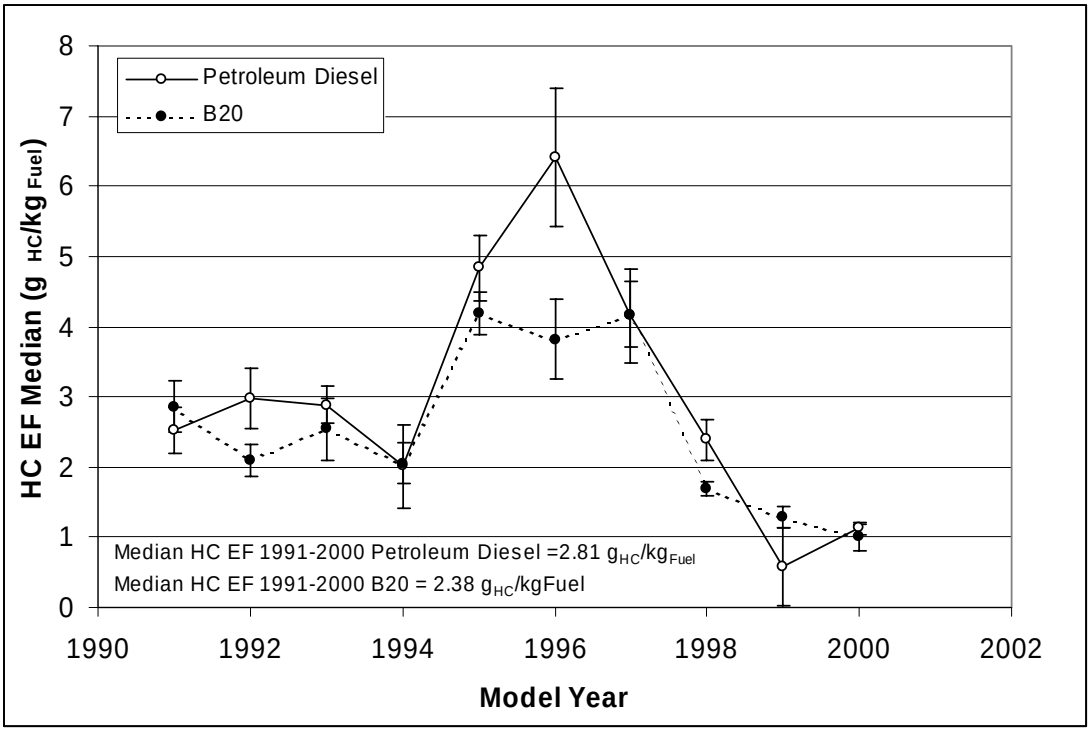

Figure 5-22: HC median emission factors vs. bus model year. Each point is the median of the emissions in the respective model year

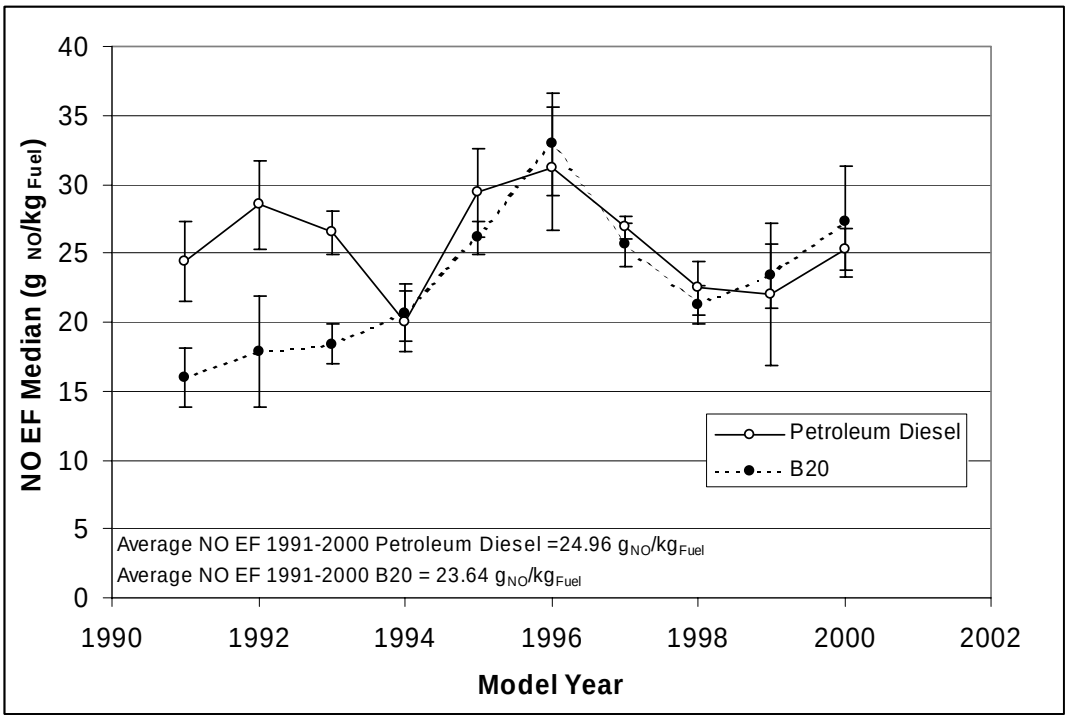

Figure 5-23: NO median emission factors vs. bus model year. Each point is the median of the emissions in the respective model year

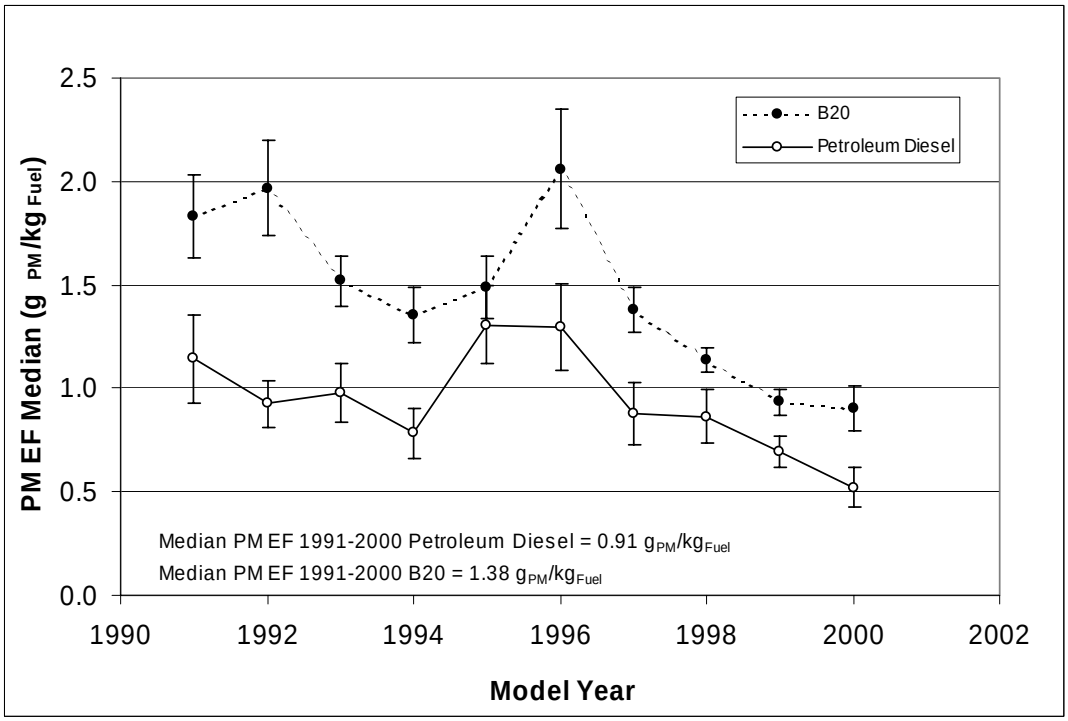

Figure 5-24. PM median emission factors vs. bus model year. Each point is the median of the emissions in the respective model year.

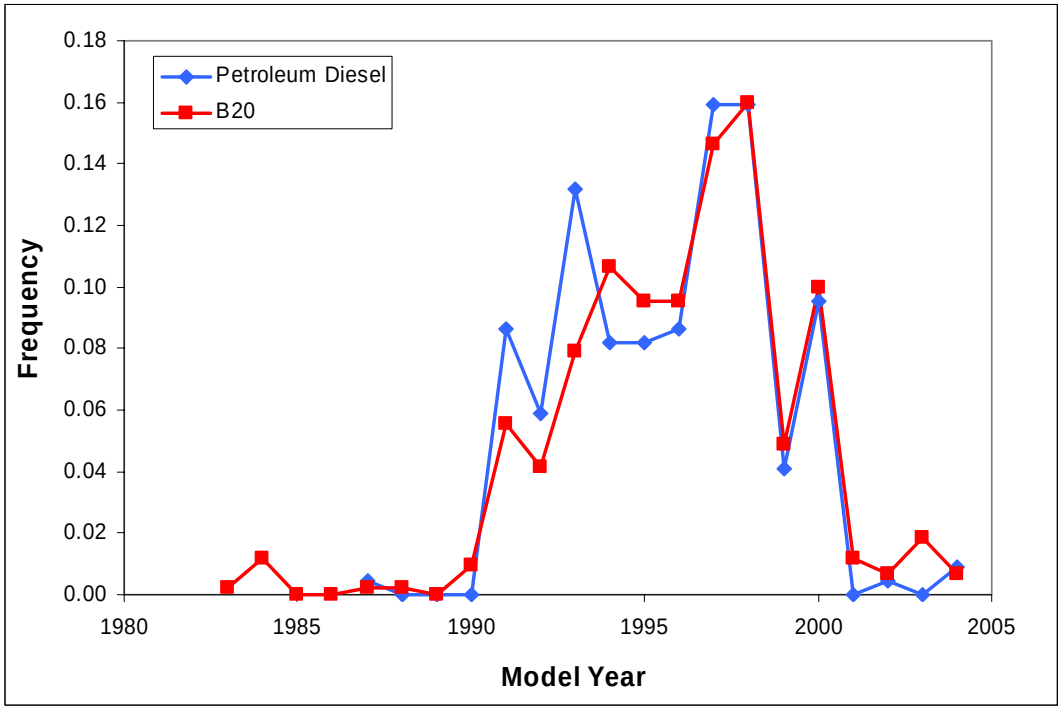

Figure 5-25. Frequency distribution of valid PM readings for each model year.

5.6.3.2 Dependence of PM Emission Factors on Engine Type

Engine type and odometer readings are generally stronger factors that influence PM EFs than are vehicle model year. The dependences of PM EFs with engine type and odometer reading are analyzed here. To exclude the possible influence of steam on the PM measurements, the average and median emission factors for the school buses were plotted versus engine type only for vehicles with no visible steam (for a discussion of the effect of steam on school buses EFs see section 5.6.3.6).

Figure 5-26 and Figure 5-24 indicate that the average and median PM emission factors are related to engine type. There is no physical differences between the Cumming B-Series engines from model years 1991-1994 and model years 1995-1998. Emissions were generally higher from the latter model year engines, so the results were stratified along what appeard to be a natural break in the data. The figures show the newer Cummins ISB series engines had lower emission factors and were less prone to increased PM emissions when using B20. The ISB engine has a computer controlled fuel injection system and may have been able to compensate for restricted fuel flows associated with off-specification B20 Fuels (see section 6 for additional details).

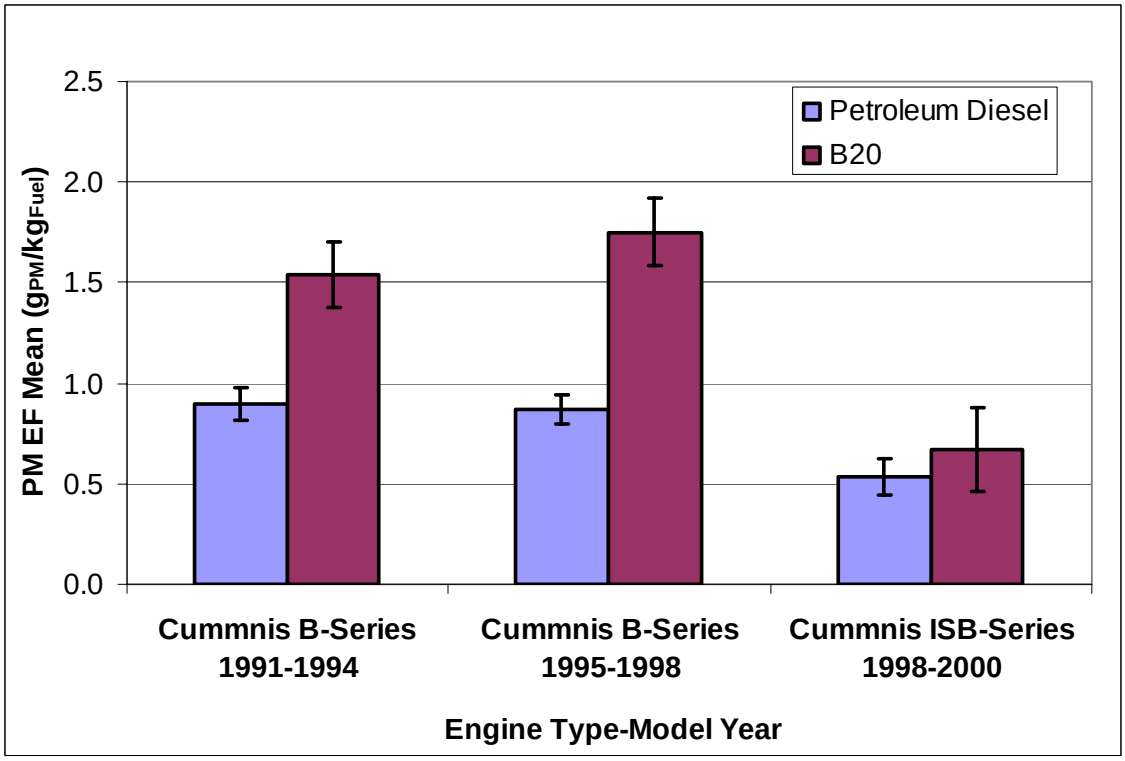

Figure 5-26. Average PM emission factors for two different engine types with no-steam emissions.

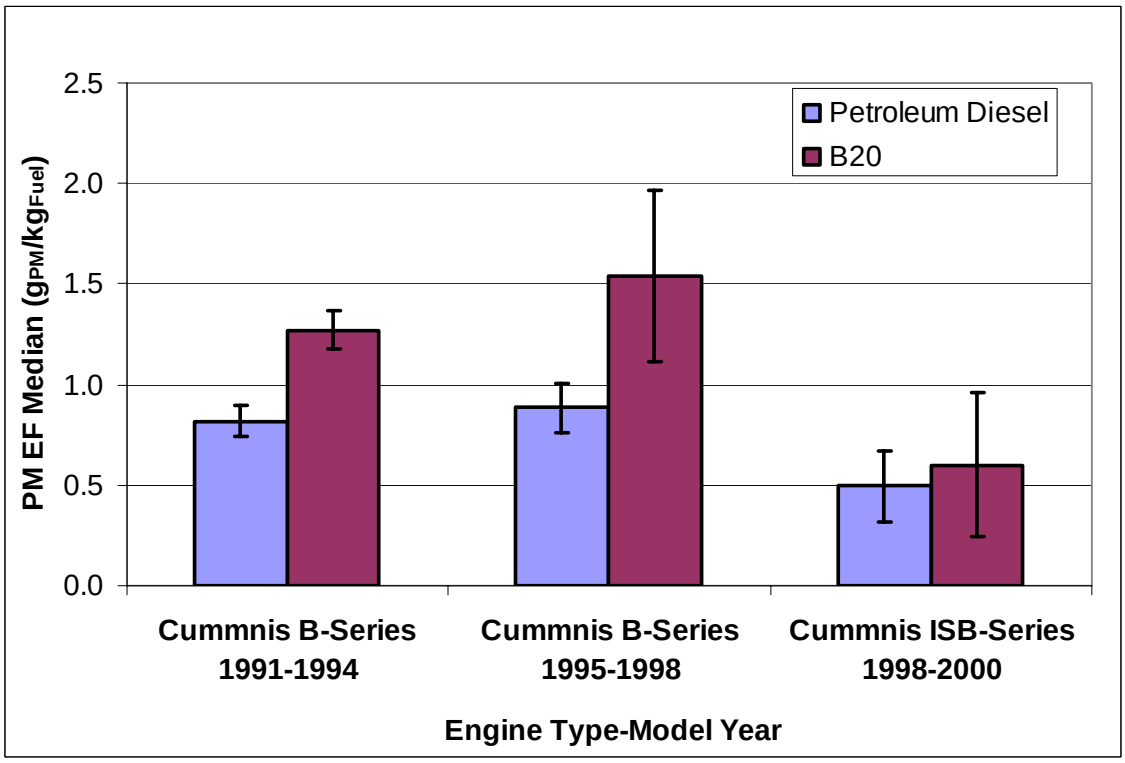

Figure 5-27. Median PM emission factors for two different engine types with no-steam emissions.

5.6.3.3 Changes in PM Emission Factors vs. Miles Traveled After Fuel Switch

PM emission factors were stratified by the number of miles that each bus traveled between the end of January and February of 2004. These mileage estimates may be biased low by as much as 50% because they do not include the distance traveled between January 15 and January 31 or the first week of March 2004. Assuming buses accumulate mileage at a consistent rate, the omissions of these days should not influence the trends in the results. The dataset was divided into ten groups based on accumulated mileage. Each group had an equal number of data points (80). The average and standard deviation of the mean of the difference in PM emission factors were calculated for each group from phase I to phase II (Figure 5-28). PM EFs were higher for vehicles that logged fewer miles in February and were lower for vehicles that logged more miles. This trend suggests that the accumulated miles after switching to B20 might be an important factor to explain the higher PM emissions. A liner regression of the averaged EFs yields a correlation coefficient (R) of 0.63.

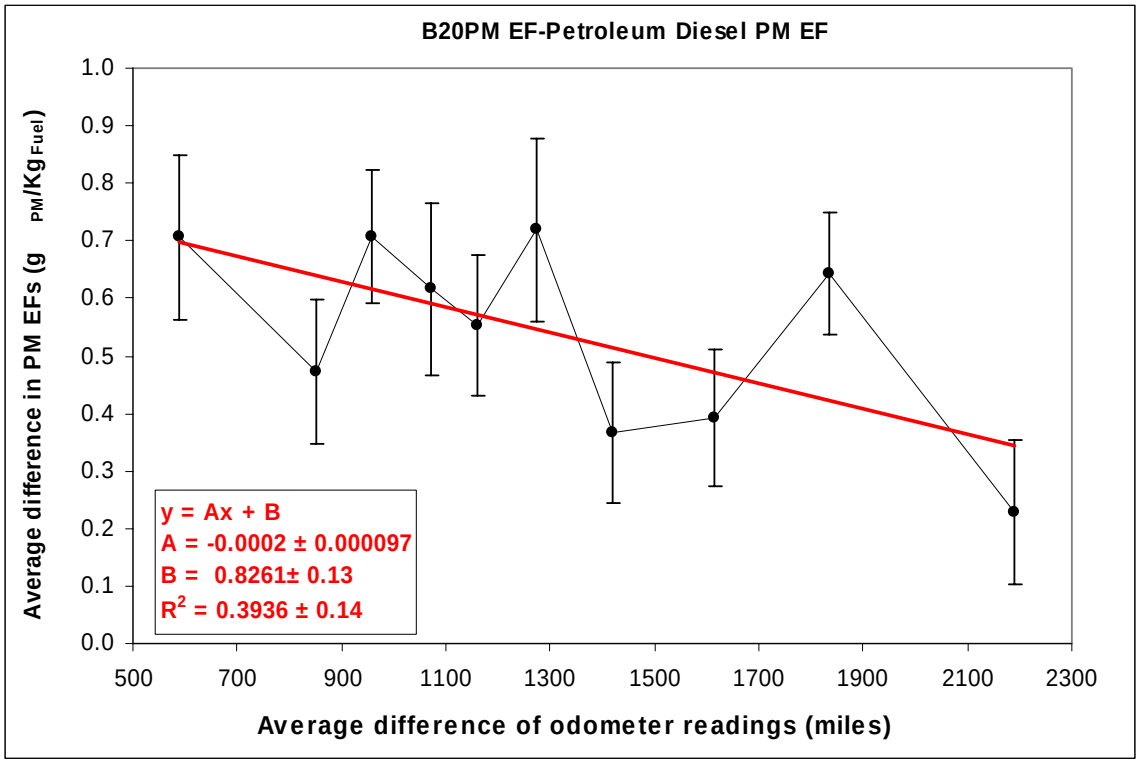

Figure 5-28. Average differences of emission factors between phase II (B20) and phase I (Petroleum Diesel) as a function of miles traveled after the fuel switch.

5.6.3.4 Sensitivity of Changes in PM Emission Factors to Composition of School Bus Fleet

Differences in the composition of the measured fleet during the two phases may have been another reason for the changes in PM emission factors. Table 5-6 shows the average emission factors for all pollutants from the two phases for exactly the same group of buses. The results reported in Table 5-6 are nearly identical with the results reported for all buses with cold engine in Table 5-3. Average and median PM emission factors were still approximately two times larger for B20 fueled buses than for petroleum diesel fueled buses.

Table 5-6. Average cold engine emissions factors on the same buses measured in phases I and II. Uncertainties are the 68% confidence intervals.

POLLUTANT	STATISTIC	PETROLEUM DIESEL	B20
CO (g_{CO}/Kg_{Fuel})	*Average*	19.9 ± 0.5	27.5 ± 0.7
	Median	13.3 ± 0.7	18.64 ± 0.03
	Number	1348	1348
HC (g_{HC}/Kg_{Fuel})	*Average*	3.4 ± 0.1	2.77 ± 0.08
	Median	2.73 ± 0.07	2.26 ± 0.07
	Number	1224	1224
NO (g_{NO}/Kg_{Fuel})	*Average*	25.9 ± 0.3	24.0 ± 0.4
	Median	24.7 ± 0.2	22.0 ± 0.3
	Number	1137	1137
PM (g_{PM}/Kg_{Fuel})	*Average*	1.054 ± 0.025	1.597 ± 0.034
	Median	0.903 ± 0.036	1.364 ± 0.023
	Number	805	805

5.6.3.5 PM Emission Factor vs. Speed and Acceleration

Emission factors from diesel vehicles may be prone to large variations dependent on the engine load. Speed and acceleration were measured for each vehicle as they passed through the VERSS test area. The speed and acceleration are instantaneous measures of the road load and may differ from the engine load due to temporal lags, the power output, and variable amounts of internal friction associated with the transmission and braking systems. Moreover, the speed and acceleration were measured in different positions with respect to the inlet of the In-Plume system. The sampling inlet perturbed normal driving conditions since drivers would slow their vehicle to roll over the inlet and then accelerate to resume their speed on the road. Figure 5-3 shows the speed and acceleration bars installed on the east side of the In-Plume system inlet. Unfortunately, the speed and acceleration bars were either installed in line with the In-Plume inlet or up to 3 meters to the east of the inlet. The exact position of the speed and acceleration bars was not consistently recorded for each day. On a freeway onramp, the relative placement of the speed and acceleration bars has little effect on the engine load since the vehicle is under moderate acceleration for an extended period of time as it is merging on the freeway.

The inconsistency of the speed and acceleration bar placements does not affect the engine mode at the time of the emissions measurements since the In-Plume inlet and the Cross-Plume analytical beam were always installed next to each other. Drivers that slowed down to pass the test section would do so when traveling in either direction, independent of the study phase.

Instantaneous measurements of speed were less sensitive to the placement of the sensor bars than were measurements of acceleration. For school buses with valid speed measurements, the average outbound speeds were very similar at 11.1 +/- 0.5 km/hr (n = 106) and 10.3 +/- 0.3 km/hr (n = 170) for phases I and II, respectively. Average inbound speeds for the buses were 11.4 +/- 0.3 km/hr and 10.7 +/- 0.3 km/hr for phases I and II, respectively. The VERSS data acquisition software automatically invalidated all bus speeds less than 8 km/hr. The validity rate for the speed and acceleration data for school buses was 20% due to the slow speed and long wheelbases of the school buses. In contrast, non-bus vehicles have a speed and acceleration data validity rate of 65%.

The consistency of the valid vehicle speeds between phases indicates that the buses were operating in a similar mode for each test phase. In addition, the presence of the In-Plume sampling inlet homogenized the operating mode of the buses at the time of the measurement since the drivers consistently slowed down when driving over the bump.

5.6.3.6 Emission Factor vs. Steam, No-Steam Flag

To assess the effect of steam on emissions measurements, emission factor measurements for buses with visible steam were separated from those with no visible steam (Table 5-7). For CO PM and HC emission factors, average and median emission factors are higher or unchanged in presence of visible steam. The opposite is true for NO emission factors.

When plumes with steam are excluded from the analysis, the comparison of petroleum diesel to biodiesel emission factors is consistent with the analysis of the entire school bus fleet. Average and median CO emission factors are significantly higher with B20. Average HC emission factors are significantly lower with B20. Emission factors for NO are unchanged with fuel type. Average and median PM emission factors are significantly higher (factor of 2) with B20 fuel.

Table 5-7. Effect of steam on the measurements of emission factors from buses.

POLLUTANT	STATISTIC	PETROLEUM DIESEL			B20		
		All	*Steam*	*No Steam*	*All*	*Steam*	*No Steam*
CO (g_{CO}/Kg_{Fuel})	*Average*	19.8 ± 1.3	25.3 ± 3.3	18.0 ± 1.3	27.0 ± 2	38.0 ± 10	25.5 ± 2
	Median	14.6 ± 1.3	19.9 ± 2.0	13.3 ± 1.3	19.3 ± 3.0	27.1 ± 12	18.7 ± 2.6
	Number	192	49	143	138	16	122
HC (g_{HC}/Kg_{Fuel})	*Average*	3.7 ± 0.3	4.2 ± 1	3.6 ± 0.25	3.6 ± 0.3	7.6 ± 1.6	3.0 ± 0.24
	Median	2.9 ± 0.24	2.8 ± 0.4	2.9 ± 0.25	2.8 ± 0.18	6.9 ± 2.2	2.63 ± 0.25
	Number	179	41	138	137	16	121
NO (g_{NO}/Kg_{Fuel})	*Average*	28.6 ± 0.8	24.5 ± 1.7	29.9 ± 0.9	27.8 ± 1.2	19.0 ± 2.9	28.9 ± 1.2
	Median	27.8 ± 1.0	23.8 ± 1.4	28.5 ± 0.7	27.0 ± 2.5	17.9 ± 0.5	28.8 ± 1.2
	Number	181	43	138	127	14	113
PM (g_{PM}/Kg_{Fuel})	*Average*	1.049 ± 0.057	1.70 ± 0.14	0.861 ± 0.049	1.84 ± 0.15	3.45 ± 1.68	1.62 ± 0.15
	Median	0.919 ± 0.042	1.64 ± 0.14	0.843 ± 0.063	1.400 ± 0.087	3.09 ± 0.86	1.322± 0.088
	Number	152	34	118	108	13	95

5.7. Repeated Measurements

Many buses were measured repeatedly during each phase of the study. To assess the reproducibility of emission factor measurements on the same vehicle, the correlation of sequential measurements was calculated. Scatter plots of sequential measurements are shown for CO in Figure 5-29 and Figure 5-30 for phase I and phase II respectively.

Figure 5-31 and Figure 5-32 show the scatter plots for PM emission factors for each of the two phases. The low correlation in these figures implies a high variability in the buses emissions associated with different operating modes as the vehicles pass through the sensors. Other differences may be due to buses leaving the lot in the afternoon when the buses are slightly warm versus a much colder start in the morning.

To visualize more directly and quantitatively the variability of repeated PM emission measurements, Figure 5-33 shows two overlapped graphs, one for petroleum diesel and a second for B20. In the figure the columns represent the mean of the repeated measurements while the extremes of the gray bars represents the maximum and minimum. High emission measurement variability is evident with both fuels.

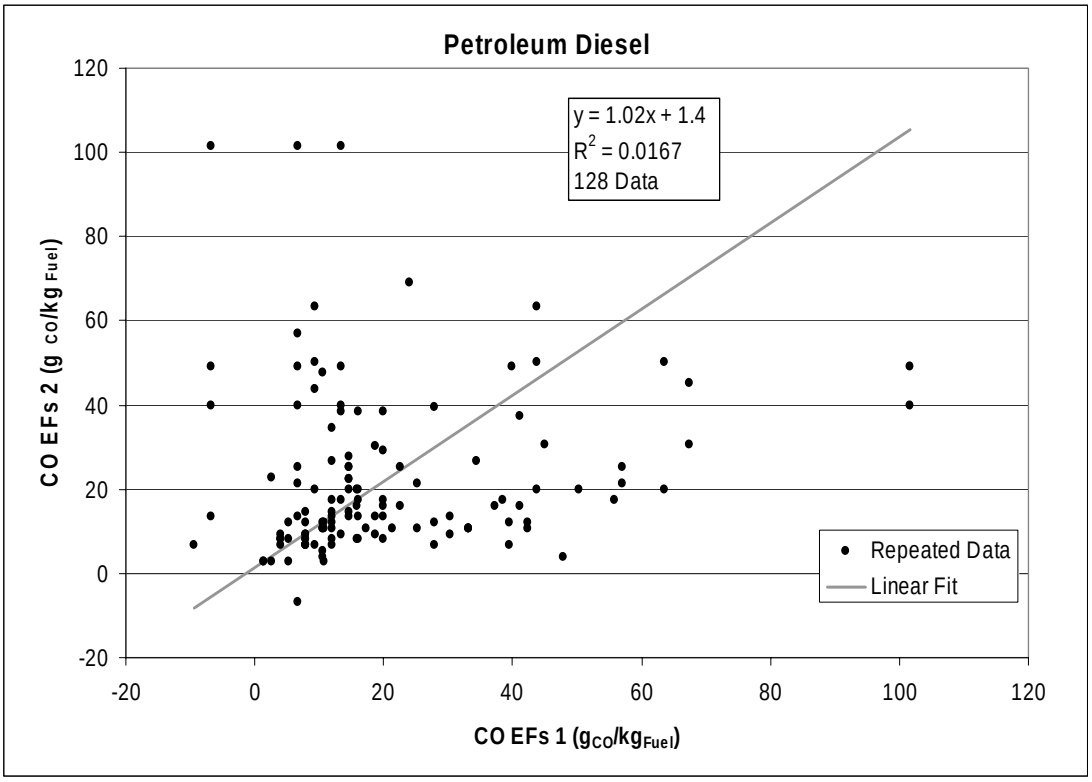

Figure 5-29. Correlation of repeated measurements for CO emission factors from buses running on petroleum diesel.

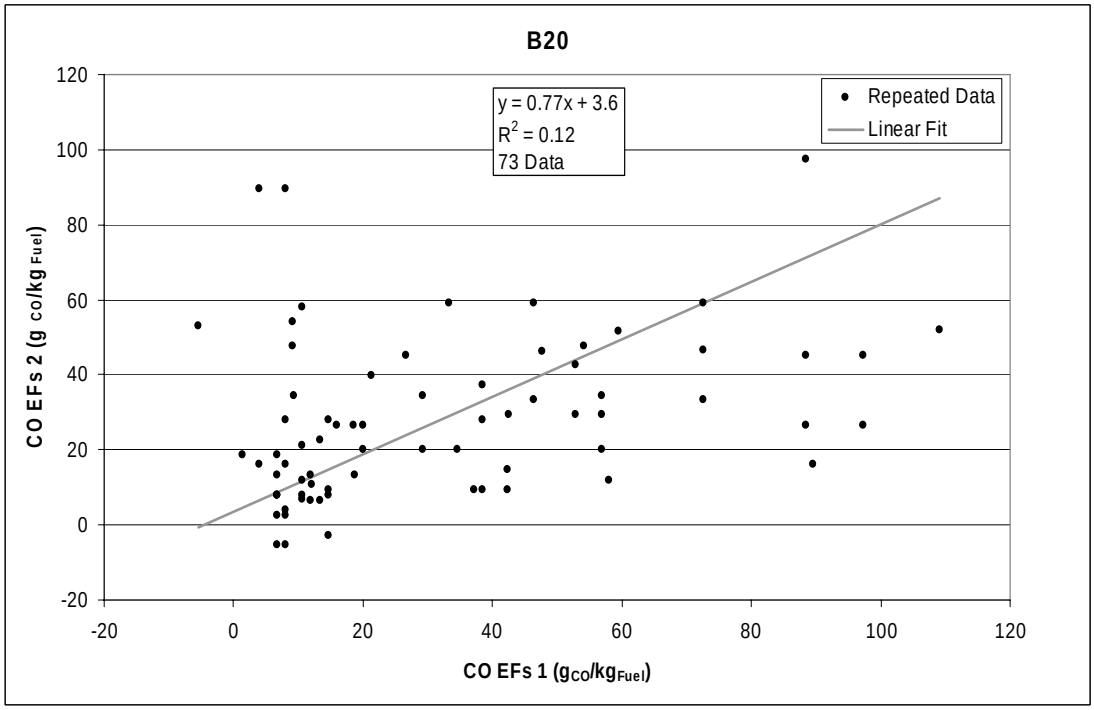

Figure 5-30. Correlation of repeated measurements for CO emission factors from buses running on B20.

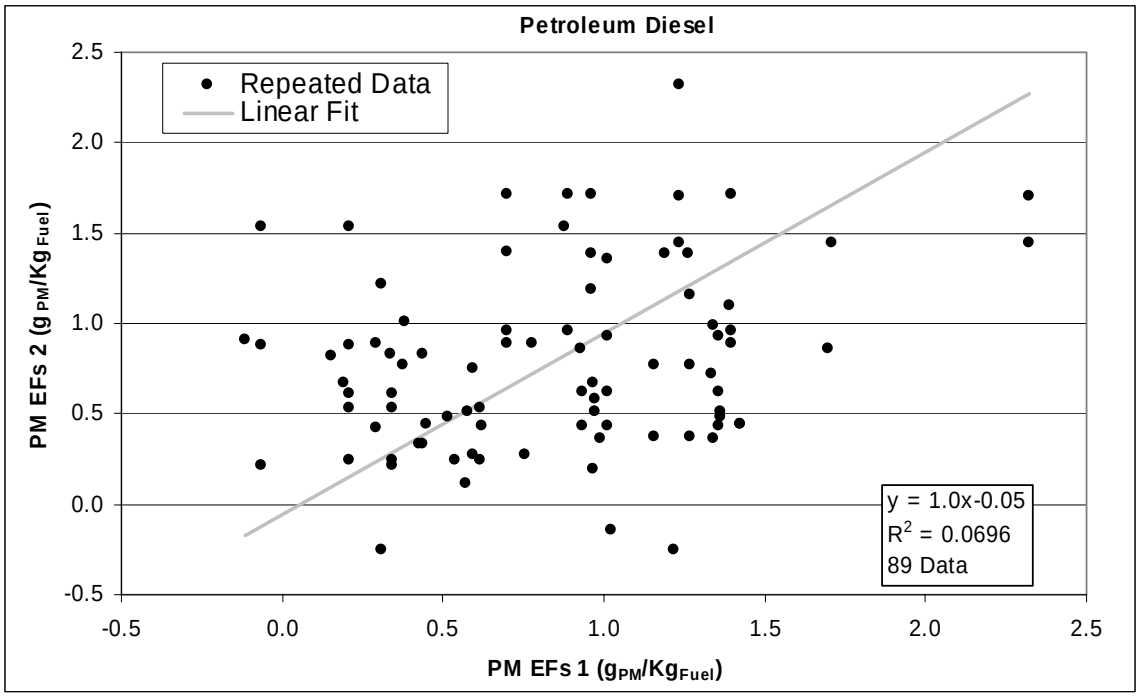

Figure 5-31. Correlation between repeated measurements of PM emission factors for Petroleum diesel.

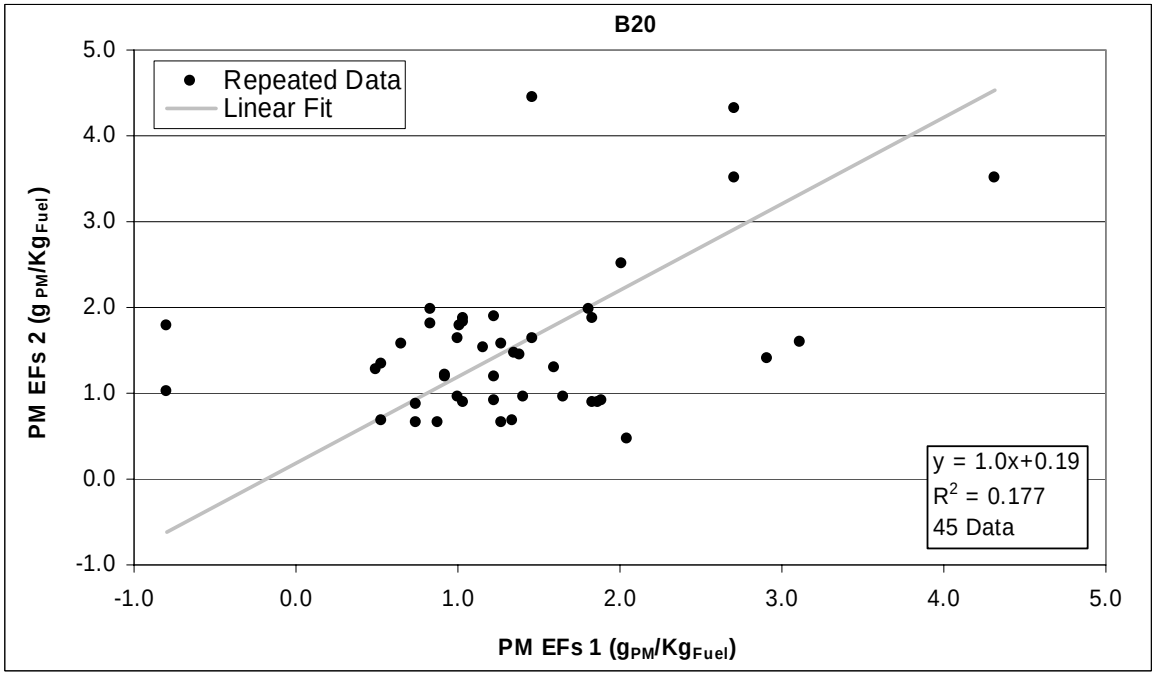

Figure 5-32. Correlation between repeated measurements of PM emission factors for B20.

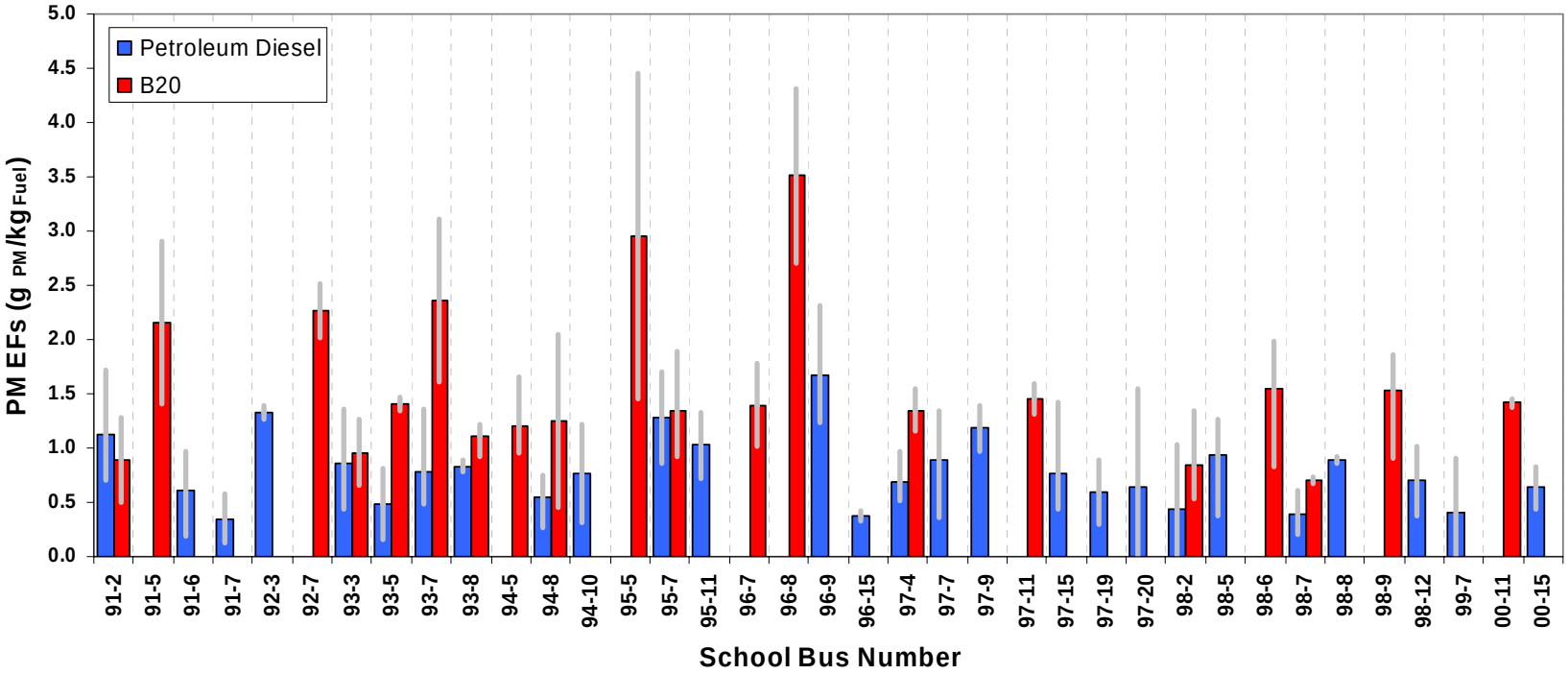

Figure 5-33. Repeated measurements of individual school buses. The columns indicate the mean of two or more repeated measurements and the gray bar represents the maximum and the minimum of the respective measurement set for each bus number.

6. Analysis of Petroleum Diesel and Biodiesel Fuels

6.1. Mechanical Problems with Buses Using B20

One possible explanation for the higher PM emission factors measured with the B20 fuel is that B20 may serve as a solvent that dislodges deposits in the engine's fuel delivery system. On older vehicles built prior to 1994, 100% biodiesel (B100) has caused fuel lines and gaskets made of rubber to dissolve. Many users of B100 have reported mechanical problems of clogged fuel filters. Many of these issues are eliminated when biodiesel is blended with petroleum diesel for a mixture of 20% biodiesel (B20) or less.

Maintenance records for the (Meridian) Joint School District #2's (MJSD's) bus fleet from December through March 2004 indicated seven incidents of failed lift pumps or fuel injector pumps in the fleet of 205 in-use buses (Table 6-1). According to the fleet's maintenance shop manager, this was an unusually large number of fuel system failures. The fuel switch from winter blend petroleum diesel to biodiesel took place on January 15, 2004, immediately after the baseline emissions measurements. The fuel pump failure that occurred on December 9, 2003 happened to one of the five buses that had been running on B20 for more than 1.5 years as part of a pilot project. With the exception of the one injector pump failure that occurred on January 9, 2004, all fuel system failures occurred after the buses had switched to B20.

Table 6-1. List of mechanical problems with the school bus fleet between December 2003 and April 2004.

Bus Number	Bus Model Year	Time on B20	Failure Date	Driver Complaint	Correction
202	2002	1.5 years	2003-12-09	Low power	Replace fuel pump
95-12	1995	none	2004-01-09 (prior to fuel switch)	Injector pump failure	Replaced fuel line and fuel pump
99-11	1999	7 days	2004-01-22	Engine won't start	Replace lift pump and fuel pump
99-7	1999	29 days	2004-02-13	Shut down on road. Blue smoke coming from exhaust	Replace fuel pump
145	2001	75 days	2004-03-15	N/A	Replaced lift pump
95-5	1995	79 days	2004-03-19	Hard starting. No PSI building in fuel pump.	Fuel injection pump failure. Repair/Replace fuel pump. Valve recheck.
99-9	1999	84 days	2004-03-24	Injector pump failure	Replaced injection pump and transfer pump.

6.2. Fuels Description

The American Society of Testing and Materials (ASTM) maintain fuel standards for several grades of diesel fuel and biodiesel fuel. ASTM Standard D975 covers five grades of diesel fuel

suitable for various types of diesel engines. ASTM standard D6751 applies to B100 fuels that are typically blended with petroleum diesel for use in compression ignition engines. Both ASTM D975 and D6751 are designed to ensure a consistent and reliable fuel product is delivered to consumers. The grades of petroleum diesel covered by ASTM standard D975 include both Grade Number 1-D and Grade Number 2-D. Grade Number 1-D is a special-purpose, light distillate fuel for automotive diesel engines in applications requiring higher volatility than that provided by Grade Number 2-D fuels. Grade Number 2-D is a general-purpose, middle distillate fuel for automotive diesel engines. It is also suitable for use in non-automotive applications especially in conditions of frequently varying speed and load. Prior to switching to the B20 biodiesel fuel blend, the school district's bus fleet was operating on a winter fuel blend of 70% Grade Number 2-D and 30% Grade Number 1-D. The winter blend is used to avoid problems associated with clouding and gelling of fuels in very cold weather.

To further investigate the cause of the mechanical problems and the emission factor change after the school buses were switched from a winter blend diesel fuel to B20 (20% Biodiesel, 80% Grade Number 2-D, plus an antigelling agent at < 0.5%), multiple fuel samples were sent to Intertek Caleb Bret Laboratories in Deer Park, Texas for analysis. Samples of fuel and additives were selected to represent a variety of handling processes as the biodiesel is transported from the manufacturer to the point of use. A description of each fuel sample and the reason for sampling is provided in Table 6-2.

6.3. Fuels Analyses

Each fuel sample was analyzed for one or more properties listed below. The properties are described here to illustrate how they may influence maintenance cycles and engine performance and/or emissions.

1. ***Boiling Point Distillation*** – The T90 (i.e. temperature at which 90% of original sample is distilled) distillation specification was incorporated to ensure that fuels have not been contaminated with high boiling materials such as used motor oil. B100 exhibits a boiling point rather than a distillation curve. The fatty acids from which biodiesel is produced are mainly straight chain hydrocarbons with 16 to 18 carbons that have close boiling temperatures. The atmospheric boiling point of biodiesel generally ranges from 330°C to 357°C. Fuels that volatilize at low temperatures tend to burn with less smoke and odor.
2. ***Copper Corrosion*** – The copper strip corrosion test is used to indicate potential difficulties with copper and bronze fuel system components. The requirements for B100 and conventional diesel are identical, and biodiesel meeting other D6751 specifications always passes this test. While copper and bronze may not corrode in the presence of biodiesel fuel, prolonged contact with these catalysts can cause fuel degradation and sediment formation.
3. ***Cloud Point*** – Cloud point is important for ensuring good performance in cold temperatures. B100 cloud point is typically higher than the cloud point of conventional diesel.
4. ***Sulfur Content*** – Sulfur is limited to reduce sulfate and sulfuric acid pollutant emissions and to protect exhaust catalyst systems when they are deployed on diesel engines in the future. B100 generally contains less than 15 ppm sulfur. No exhaust catalyst systems were present on the school bus fleet.

5. ***Sediment and Water Content*** – Water and sediment refers to the presence of free water droplets and sediment particles. The allowable level for B100 is set at the same level allowed for conventional diesel fuel. Poor drying techniques during manufacturing or contact with excessive water during transport or storage can cause B100 to be out of specification for water content. Excess water can lead to corrosion and provides an environment for microorganisms. Fuel oxidation can also raise sediment levels, so this test can be used in conjunction with acid number and viscosity to determine if fuels have oxidized too much during storage.
6. ***Viscosity at 40 deg C*** - A minimum viscosity is required for some engines because of the potential for power loss caused by injection pump and injector leakage. This is not an issue for B100 and the minimum is set at the same level as for petroleum diesel. The maximum viscosity is limited by the design of engine fuel injection systems. Higher viscosity fuels can cause poor fuel combustion that leads to deposit formation as well as higher in-cylinder penetration of the fuel spray which can result in elevated engine oil dilution with fuel. The maximum allowable viscosity in ASTM D975 for Grade Number 2-D diesel is 4.1 mm^2/s at 40°C although most engines are designed to operate on fuels of higher viscosity than 4.1 mm^2/s. ASTM D6751 allows for slightly higher viscosity than D975 primarily because that is where the normal viscosity of B100 lies.
7. ***Micro-Carbon Residue*** – Carbon residue gives a measure of the carbon-depositing tendency of a fuel and is an approximation of the tendency for carbon deposits to form in an engine. For conventional diesel fuel the carbon residue is measured on the 10% distillation residue. Because B100 boils entirely in the high end of diesel fuel's range and at approximately the same temperature, it is difficult to leave only a 10% residual when distilling biodiesel. So biodiesel carbon residue specifies that the entire biodiesel sample be used rather than the 10% distilled residue.
8. ***Phosphorus Content*** – Phosphorus content is limited to 10 ppm maximum in biodiesel because phosphorus can damage catalytic converters. Phosphorus concentrations above 10 ppm can be present in some vegetable oils. Biodiesel produced in the United States generally has low phosphorus levels, on the order of 1 ppm.
9. ***Total Particulate Contamination and Composition*** – Although not specified in ASTM D6751, particulate contamination will coincide with a high sediment and water content. The composition of the particulate matter may indicate the source of contamination.
10. ***Total and Free Glycerin*** – Total and free glycerin numbers measure the amount of unconverted or partially converted fats and by-product glycerin present in the fuel. Incomplete conversion of the fats and oils into biodiesel can lead to high total glycerin. Incomplete removal of glycerin can lead to high free glycerin and total glycerin. If these numbers are too high, storage tank, fuel system, and engine fouling can occur. Fuels that exceed these limits are highly likely to cause filter plugging and other problems.
11. ***Average Acid Number*** – Acid number for biodiesel is primarily an indicator of free fatty acids (natural degradation products of fats and oils) and can be elevated if a fuel is not properly manufactured or has undergone oxidative degradation. Acid numbers higher than 0.80 have been associated with fuel system deposits and reduced life of fuel pumps and filters.
12. ***Sulfated Ash*** – The sulfated ash test measures the amount of residual alkali catalyst present in the biodiesel as well as any other ash forming compounds that could contribute to injector deposits or fuel system fouling.

13. ***Flash Point*** – A minimum flash point for diesel fuel is required for fire safety. B100's flash point is typically much higher than diesel fuel's (150° C compared to 70° C) to ensure that the manufacturer has removed excess methanol used in the manufacturing process. Residual methanol in the fuel is a safety issue because even very small amounts reduce the flash point. Residual methanol, which can be found in biodiesel with low, out-of-specification flash point, can also affect fuel pumps, seals and elastomers, and can result in poor combustion properties.
14. ***Cetane Index*** – An adequate cetane number is required for good engine performance. Conventional diesel must have a cetane number of at least 40 in the United States. Higher cetane numbers help ensure good cold start properties and minimize the formation of white smoke. The ASTM limit for B100 cetane number is set at 47 as this is the level identified for "Premium Diesel Fuel" by the National Conference of Weights and Measures, as well as the fact that 47 has been the lowest cetane number found in U.S. biodiesel fuels. The cetane index (ASTM D976) is not an accurate predictor of cetane number for biodiesel or biodiesel blends since it is based on a calculation using specific gravity and distillation curve, both of which are different for biodiesel than for petrodiesel.

The results of all fuels analysis are shown in Table 6-3 through Table 6-5 and discussed in the following sections.

One concern regarding the quality of biodiesel blends that is not addressed with these tests is the homogeneity of the blend. Splash mixing of biodiesel with petroleum diesel can result in a highly variable product. For an intended blend of B20 under poor mixing conditions, most vehicles would receive fuel that is less that 20% biodiesel while other could receive a more concentrated blend. Vehicles receiving fuels with higher biodiesel concentrations than 20% are more likely to encounter mechanical problems associated with their fuel systems.

Table 6-2. List of fuels sampled and analyzed to evaluate sources of contamination of biodiesel used during this study.

Sample ID 2004-004225-DRPK-***	Sample Name	Detailed Description	Reason for sampling
#1	Envirodiesel B100	B100 supplied by a national biodiesel broker directly to Caleb-Brett in a 5-gallon plastic pail.	Test purity of B100 directly from manufacturer.
#2	BM 3016 B100	B100 from Provider #2 in Boise, ID (one of two biodiesel suppliers in Boise). Provider #2 also the supplied the winter blend fuel (30% 1-D and 70% 2-D) to the MJSD's bus fleet prior to 2004/01/15.	Test purity of B100 as delivered to distributor in Boise, ID.
#3	BM 4016 B100	B100 from Provider #1 in Boise, ID. Supplier #1 was the supplier of the B20 for the MJSD's bus fleet.	Test purity of B100 as delivered to distributor in Boise, ID.
#5	BM4014	Grade Number 2-D supplied by Provider #1 from the pipeline to Boise, ID. Diesel dyed red for use in tax-exempt distribution only.	Test purity of 2-D fuel used to make B20 at distributor.
#6	BM 4013	Grade Number 2-D supplied by Provider #1 from the pipeline to Boise, ID. No dye added.	Test purity of 2-D fuel used to make B20 at distributor.
#14	BM 2006 D2 Public Pump	Grade Number 2-D from a public pump on Franklin Road in Meridian, ID. Provider #2 supplies diesel fuel for the station.	Test purity of 2-D as distributed to public in Boise, ID.
#9	BM 3009	Grade Number 2-D collected at a public pump on State Street in Boise, ID. Provider #1 supplies diesel fuel for the station.	Test purity of 2-D as distributed to public in Boise, ID.
#10	BM 2008 Jetta	Grade Number 2-D collected from fuel tank of 2002 Diesel Volkswagon Jetta (Odometer reading: 24,500 miles).	Collect baseline of 2-D fuel purity in tanks of real world vehicles.
#11	BM 2007 Ford	Grade Number 2-D collected from #1 fuel tank of 1989 Diesel Ford F-250 with dual tanks (Odometer reading 235,406 miles).	Collect baseline of 2-D fuel purity in tanks of real world vehicles.
#8	BM 5019	Power Service Arctic Express® Fuel Additive. This anti gelling agent added to the MJSD's B20 by Provider #1 at a mixture of 5 gallons agent to 15,000 gallons B20.	Test purity of anti-gelling agent added to B20.
#7	BM 5018	B20 used in MJSD's buses during the emissions study. The fuel contains an anti-gelling fuel additive and red dye red for use in tax-exempt distribution.	Test purity of B20 product delivered to bus yard during the emissions study.
#4	BM 3010	B20 sampled from the only public pump for the fuel (Kick's 66 on the corner of Five Mile Road and Emerald Road in Boise, ID. Provider #1 supplied this station with B20.	Test purity of B20 distributed to public Boise, ID.
#12	BM 1004 B20 Ford	B20 from the #2 fuel tank of a 1989 Ford F-250 (Odometer reading 235,829). Tank 2 was filled with 16.2 gallons of B20 from Kicks 66 pump and driven 155 miles using only tank #2 fuel. Tank #2 was refilled with 9.2 gallons of B20 from Kicks 66 pump and driven an additional 268 miles before sample collection on 2004/09/01.	Measure contamination that may be imparted to fuel from deposits in fuel tanks.
#13	BM 1003 VW Jetta D2 Bio	B20 from the fuel tank of 2002 Diesel VW Jetta. Vehicle operated approximately 250 miles on B20 prior to sample collection.	Measure contamination that may be imparted to fuel from deposits in fuel tanks.

*** Implies the 3-digit number listed in the first column.

6.4. Distribution of Biodiesel from Manufacturer to Boise

Samples #1 to #3 are B100 samples. Sample #1 was shipped directly from a large manufacturer and fuel broker to the Intertek Caleb-Brett laboratory. Samples #2 and #3 were collected from B20 providers in the area. The providers receive their biodiesel after it has been shipped by rail car to an intermediate distribution center, either Salt Lake City, Utah or Portland, Oregon. From there, the biodiesel is trucked by tractor-trailer into the Boise area. The results of the analysis of these samples are shown in Table 6-3.

The copper corrosion indices and the acid numbers for all three B100 samples meet ASTM D6751 standards, indicating that the biodiesel had not undergone microbial degradation during transport or storage. The sulfur content, viscosity, phosphorus content, and sulfated ash also met the ASTM D6751 standard. Total glycerin was elevated (but met ASTM D6751 standards) in both of the samples from area fuel providers, indicating incomplete removal of the glycerin byproduct from the biodiesel product by the refineries.

The cetane index was slightly lower than the ASTM D6751 standard for all three samples. As mentioned above, method D976 to measure the cetane index of a biodiesel fuel is inaccurate due to the differences in the densities of the petroleum diesel and the biodiesel.

The total particulate contamination levels in the B100 samples were higher (132 mg/L and 44 mg/L) than for the sample shipped directly from the manufacturer/broker (16 mg/L). Analysis of the filtrate indicated high concentrations of iron (45 g/kg of filtrate) in the B100 from Provider #2 (sample #2 in Table 6-2). Iron concentrations may be associated with fuel handling vessels or valves that are abraded under normal usage. It is possible that a particle from a faucet was incorporated into the sample as it was collected from a storage tank. Consequently, the high particle loading of sample #2 may not be representative of the entire batch of biodiesel from the Provider #2. Tests of the micro carbon residue were inconclusive (but lower than 0.1 % by weight) since the laboratory test was designed to determine compliance of the petroleum diesel with ASTM D975 (< 0.35 % by weight).

Free glycerin exceeded the ASTM D6751 standard for samples #2 and #3 indicating that not all of the glycerin byproduct had been successfully extracted from the biodiesel product. The glycerin byproduct can be washed from the biodiesel product by mixing the product with water and removing the aqueous fraction after separation. A centrifuge may also be used to accelerate the separation process.

The flash point of sample #2 was below the ASTM D6751 specification. This is usually attributed to substantial unreacted methanol concentrations in the biodiesel product. As mentioned above the methanol may cause fuel pump problems and dissolution of seals in the fuel system.

Table 6-3. Analysis of B100 fuels. The absence of values in the table indicates that the quantity was not measured under the current set of tests.

				2004-004225-DRPK 0**		
				#1	#2	#3
Test Method	Property		ASTM D6751 B100 Specification	Envirodiesel B100	BM 3016 B100	BM 4016 B100
D1160	IBP	°F		524.9	439.5	397.9
	5%	°F		651.3	649.8	555.4
	10%	°F		654.8	652.4	633.7
	20%	°F		656.1	657.1	640
	30%	°F		657.3	659.5	654.5
	40%	°F		659.8	666	657.2
	50%	°F		661	667.2	659.7
	60%	°F		662.2	668.4	662
	70%	°F		664.7	669.6	664.7
	80%	°F		666	670.9	667.2
	90%	°F	< 680	667	672.1	668.4
	95%	°F		668.1	674.5	669.7
	FBP	°F		714.6	684.6	678.3
	% Recovered	%		99	98	98
	% Loss	%		0	0	0
	% Residue	%		1	1.5	1.5
	% Rec. in Cold Trap	%		0	0.5	0.5
D130 (IP 154)	Copper Corrosion		< 3	1a	1a	1a
D2500	Cloud Point	°C	Must be reported	-1	-12	-5
	Cloud Point	°F		30.2	10.4	23
D2622	Sulfur	ppm (Wt.)	< 150	<3	8	41
D2709	Sediment & Water	Vol. %	< 0.050	0	0	0
D445	Kinematic Viscosity @ 40°C	cSt	1.9-6.0	3.744	4.012	3.945
D4530	Avg. Micro Carbon Residue	Wt. %	< 0.05	<0.1*	<0.1*	<0.1*
D4951	Phosphorous	Wt. %	< 0.001	0.0001	0.0001	0.0002
D5708 Mod	Arsenic	ppm (mg/kg)		<0.500	<0.500	<0.500
	Cadmium	ppm (mg/kg)		<0.100	<0.100	<0.100
	Chromium	ppm (mg/kg)		<0.1	25.2	<0.1
	Sodium	ppm (mg/kg)		1880	2780	4120
	Lead	ppm (mg/kg)		<0.500	354	<0.500
	Calcium	ppm (mg/kg)		762	1760	3880
	Vanadium	ppm (mg/kg)		46.7	33.7	25.9
	Aluminum	ppm (mg/kg)		33.5	3080	194
	Silicon	ppm (mg/kg)		72.9	540	200
	Iron	ppm (mg/kg)		90.6	45900	1230
D6217	Total Particulate Contamination	mg/L		16	132.5	44.1
D6584	Free Glycerin	Wt. %	< 0.02	0.01	>0.05	>0.05
D6584	Total Glycerin	Wt. %	< 0.24	0.09	0.07	0.1
D664 (IP 177)	Average Acid Number	mg KOH/g	< 0.80	0.05	0.29	0.21
D874 (IP 163)	Sulfated Ash	Wt. %	< 0.020	<0.005	<0.005	<0.005
D93 (IP 34)	Corrected Flash Point	°C	> 130.0	>110*	61	>110*
	Corrected Flash Point	°F		>230	141.4	>230
D976 (IP 364)	Calculated Cetane Index		> 47	45.7	46.3	46.7

*Test is inconclusive with respect to ASTM D6751 B100 Fuel Specification

6.5. Analysis of Grade Number 2-D Petroleum Diesel

Petroleum diesel samples were analyzed as part of this study for two main reasons. First, the analysis was conducted to determine if the blending fuel in the B20 was within ASTM specifications. Second, the analysis served as a control for comparison with blended B20 from storage tanks and vehicle fuel tanks.

For the tests conducted, all measurements were within the range of ASTM D975 standards. Total particulate contamination was consistently less than 5 mg/L for all samples. These results indicate the supply of petroleum diesel does not undergo significant contamination from the area's point of deliver to the point of use in the fuel tanks of vehicles. This could be a result of the underground fuel pipeline distribution system. Almost all of the petroleum fuel in the Boise area comes from Salt Lake City, Utah refineries via a pipeline.

Table 6-4. Analysis of Grade Number 2-D petroleum diesel. The absence of values in the table indicates that the quantity was not measured under the current set of tests.

			ASTM D975-03 Diesel Specifications		2004-004225-DRPK 0**					
					#5	#6	#14	#9	#10	#11
Test Method	Property		Low Sulfur No. 2-D	No. 2-D	BM 4014	BM 4013	BM 2006 D2 Public Pump	BM 3009	BM 2008 Jetta	BM 2007 Ford
D1160	IBP	°F	>540	>540						
	5%	°F	< 640	< 640						
	10%	°F								
	20%	°F								
	30%	°F								
	40%	°F								
	50%	°F								
	60%	°F								
	70%	°F								
	80%	°F								
	90%	°F								
	95%	°F								
	FBP	°F								
	% Recovered	%								
	% Loss	%								
	% Residue	%								
	% Rec. in Cold Trap	%								
D130 (IP 154)	Copper Corrosion		< 3	< 3						
D2500	Cloud Point	°C			-3	-6	-7	-8	-12	-10
	Cloud Point	°F			26.6	21.2	19.4	17.6	10.4	14
D2622	Sulfur	ppm (Wt.)	< 500	NA						
D2709	Sediment & Water	Vol. %	< 0.05	< 0.05						
D445	Kinematic Viscosity @ 40°C	cSt	1.9-4.1	1.9-4.1						
D4530	Avg. Micro Carbon Residue	Wt. %	<0.35	<0.35	0.07	0.03	0.09	0.1	0.11	0.08
D4951	Phosphorous	Wt. %								
D5708 Mod	Arsenic	ppm (mg/kg)			<0.500	<0.500	<0.500	<0.500	<0.500	<0.500
	Cadmium	ppm (mg/kg)			<0.100	<0.100	<0.100	<0.100	<0.100	<0.100
	Chromium	ppm (mg/kg)			<0.1	<0.1	<0.1	<0.1	94.6	<0.1
	Sodium	ppm (mg/kg)			15300	8520	15800	17500	16600	27300
	Lead	ppm (mg/kg)			<0.500	<0.500	<0.500	34.8	24.7	1670
	Calcium	ppm (mg/kg)			3740	4220	9630	11100	4930	15300
	Vanadium	ppm (mg/kg)			<0.100	112	<0.100	301	152	<0.100
	Aluminum	ppm (mg/kg)			449	2170	474	1800	640	2270
	Silicon	ppm (mg/kg)			376	200	494	1950	1270	3360
	Iron	ppm (mg/kg)			1730	1510	231	1040	3360	41300
D6217	Total Particulate Contamination	mg/L			1.2	2	2.2	1.2	4.6	1
D6584	Free Glycerin	Wt. %								
D6584	Total Glycerin	Wt. %								
D664 (IP 177)	Average Acid Number	mg KOH/g								
D874 (IP 163)	Sulfated Ash	Wt. %	< 0.01	< 0.01	<0.005	<0.005	<0.005	<0.005	<0.005	<0.005
D93 (IP 34)	Corrected Flash Point	°C	> 52	> 52	68	68	72	63	62	65
	Corrected Flash Point	°F	> 126	> 126	154.2	154.2	161.4	145.2	143.4	148.8
D976 (IP 364)	Calculated Cetane Index		> 40	> 40						

*Test is inconclusive with respect to ASTM D975-03 D2 Fuel Specification

6.6. Analysis of B20 Fuels

Four samples of B20 were collected and analyzed as part of this study. Table 6-5 displays the results of analysis. Sample #7 was the B20 fuel delivered to the MJSD bus fleet, sample #4 was B20 collected at a public pump, and samples #12 and #13 were B20 collected from the fuel tanks of diesel vehicles. Samples #12 and #13 were taken to determine if fuel tank deposits had been dissolved due to contact with the B20 fuel. There is currently no ASTM standard for B20 fuel. However, the lack of compliance of the parent B100 feedstock with ASTM D6751 may be inferred based on the results of some of these analyses. If a compound in the B20 (that does not exist as measurable quantities in petroleum fuel) is measured at a level that exceeds 20% of the B100 ASTM standard, then it is highly likely that the B100 used for blending was noncompliant with ASTM D6751.

Petroleum diesel fuels have negligible levels of glycerin, since it is not a byproduct of the petro-diesel distillation process. Glycerin is a major byproduct of the trans-esterification process used to make biodiesel. The free and total glycerin analyses of Sample #4 (from the public pump) indicated that the B20 sample exceeded both the free and total glycerin standards for B100. Based on the assumption there is no glycerin in the petroleum diesel, the B100 parent fuel had a free glycerin concentration of 0.1 mg/L and a total glycerin concentration of >1.0 mg/L, more than 5 times the ASTM D6751 standards. Large uncertainties are associated with the glycerin analyses on biodiesel-petrodiesel blends. For the chromatography analysis, components within the petroleum diesel elute at the same location as the glycerin in the biodiesel. Due to the limitations of the glycerin analyses, it was not possible to determine if Sample #7 used in the bus fleet was in excess of the ASTM biodiesel glycerin standard.

Glycerin tests were not conducted on the samples collected in the vehicle fuel tanks (samples #12 and #13). Filter analysis (ASTM method D6217) of the fuel in the fuel tanks of the two diesel vehicles showed no increase in filterable mass when compared to the B20 from the public pump (Sample #4). Cloud points (ASTM method D2500) were slightly higher in the fuel tank samples (-2 °C) than in the sample from the public pump (-6 °C).

The glycerin standards in ASTM D6751 are intended to prevent glycerin collecting in fuel filters and clogging fuel injectors. According to the National Biodiesel Board (NBB, 2005), incidences of clogged fuel filters after diesel engines are switched to biodiesel are a commonly reported problem. The clog appears to be associated with dissolved deposits from the fuel tank that have migrated to the fuel filter. The sources of these data are not well documented and may have been an assemblage of reports from individual vehicle operators. Systematic studies are needed to determine if the fuel filter-clogging symptom is due to the mobilization of deposits in the fuel handling system or due to the use of off-specification biodiesel.

6.7. Summary of fuels analysis

The B100 fuel stock delivered to the study area appeared to have been non-compliant with ASTM B100 standard D6751 due to high concentrations of either free or total glycerin. Moreover, the low flash point on a local B100 sample implies that residual methanol was present is some of the biodiesel fuels delivered to the Treasure Valley. Although the B100 used in the buses had a flashpoint of >110 degrees C, the elevated glycerin detected in the B100 feed stock may be the reason for the lift pump failures from the six school buses observed during this study.

Table 6-5. Analysis of B20 fuels samples (and an anti-gelling agent). The absence of values in the table indicates that the quantity was not measured under the current set of tests.

			ASTM D6751 B100 Specification	ASTM D975-03 Diesel Specifications		2004-004225-DRPK 0**				
						#7	#4	#12	#13	#8
Test Method	Property		B100	Low Sulfur No. 2-D	No. 2-D	BM 5018	BM 3010	BM 1004 B20 Ford	BM 1003 VW Jetta D2 Bio	BM 5019 Arctic Express
D1160	IBP	°F		>540	>540					
	5%	°F		< 640	< 640					
	10%	°F								
	20%	°F								
	30%	°F								
	40%	°F								
	50%	°F								
	60%	°F								
	70%	°F								
	80%	°F								
	90%	°F	< 680							
	95%	°F								
	FBP	°F								
	% Recovered	%								
	% Loss	%								
	% Residue	%								
	% Rec. in Cold Trap	%								
D130 (IP 154)	Copper Corrosion		< 3	< 3	< 3	1a	1a			
D2500	Cloud Point	°C	Must be reported			-13	-6	-2	-2	9
	Cloud Point	°F				8.6	21.2	28.4	28.4	48.2
D2622	Sulfur	ppm (Wt.)	< 150	< 0.05	NA					
D2709	Sediment & Water	Vol. %	< 0.050	< 0.05	< 0.05					
D445	Kinematic Viscosity @ 40°C	cSt	1.9-6.0	1.9-4.1	1.9-4.1					
D4530	Avg. Micro Carbon Residue	Wt. %	< 0.05	<0.35	<0.35	0.06	0.09	0.06	0.06	0.19
D4951	Phosphorous	Wt. %	< 0.001							
D5708 Mod	Arsenic	ppm (mg/kg)				<0.500	<0.500	<0.500	<0.500	<0.500
	Cadmium	ppm (mg/kg)				<0.100	<0.100	<0.100	<0.100	<0.100
	Chromium	ppm (mg/kg)				<0.1	<0.1	<0.1	<0.1	<0.1
	Sodium	ppm (mg/kg)				21600	12900	8370	14600	4220
	Lead	ppm (mg/kg)				<0.500	<0.500	3340	<0.500	<0.500
	Calcium	ppm (mg/kg)				14700	4420	4440	3770	638
	Vanadium	ppm (mg/kg)				184	142	104	<0.100	19.2
	Aluminum	ppm (mg/kg)				742	1580	376	5880	64.1
	Silicon	ppm (mg/kg)				857	735	758	1420	157
	Iron	ppm (mg/kg)				1690	438	882	1310	20.9
D6217	Total Particulate Contamination	mg/L				3.2	5.6	2.6	2.8	1525
D6584	Free Glycerin	Wt. %	< 0.02			<0.01	0.02			
D6584	Total Glycerin	Wt. %	< 0.24			<0.2	>0.2			
D664 (IP 177)	Average Acid Number	mg KOH/g	< 0.80			0.14	<0.05			
D874 (IP 163)	Sulfated Ash	Wt. %	< 0.020	< 0.01	< 0.01	<0.005	<0.005	<0.005	<0.005	<0.005
D93 (IP 34)	Corrected Flash Point	°C	> 130.0	> 52	> 52	71	66	71	71	<40
	Corrected Flash Point	°F		> 126	> 126	159.6	150.6	159.6	159.6	<104.0
D976 (IP 364)	Calculated Cetane Index		> 47	> 40	> 40					

*Test is inconclusive with respect to ASTM D975-03 D2 Fuel Specification

7. Conclusions

The objective of this study was to measure exhaust emission changes associated with switching the (Meridian) Joint School District #2 (MJSD) bus fleet from petroleum diesel to a 20% mix of biodiesel and 80% petroleum diesel (B20).

A literature review was performed and found that engine dynamometer tests have shown decrease emissions of CO, HC, and PM when engines are switched to biodiesel. Both emission factor increases and decreases were found when tests were conducted using chassis dynamometers. The comparison of these results suggested that testing conditions might play an important roll in the outcome of the test.

A field study was conducted in two phases to measure the change in emissions factors after the fuel switch from the fleet of 205 school buses with model years ranging from 1983 to 2004. Measurements were conducted for buses returning and leaving the school bus depot on Lanark Road in Meridian, Idaho. Primarily light duty gasoline vehicles driven by the school bus drivers, school district employees, and the students of a nearby high school were also measured during the study. The first data collection phase took place between January 11 and January 15, 2004 when the buses were running on 100% petroleum diesel. On January 16, 2004, the fuel storage tank at the bus depot was filled with B20. Emissions from the buses were measured again between March 1, 2004 and March 4, 2004.

A commercial remote sensing device was used to measured CO, HC, and NO emissions of the buses as they left and returned to the bus depot. A novel LIDAR system developed by DRI was used to measure PM in the exhaust of the passing buses. A redundant In-Plume emissions measurement system sampled exhaust plumes from the center of the roadway for comparison with the remotely sensed measurements. A video camera was used to record the license plates of the westbound vehicles, however only gross vehicle classification could be performed on the eastbound vehicles (i.e. school bus, car, pickup, SUV, etc). Average sampling temperatures and relative humidities during the study were -5 °C and 85% for phase I and 2 °C and 70% for phase II.

Factors such as engine load, ambient meteorological conditions, instrument drift, and insufficient sampling may introduce bias (or error) into a field study of this type. The underling assumption in the study's design was that changes in emission factors between phases I and II are solely due to the change in fuels. To evaluate the validity of this assumption, numerous control tests were applied.

With respect to engine load, the average school bus speeds through the test site were generally consistent during both phases (11.2 km/hr for phase I and 10.5 km/hr for phase II). The consistency of the valid vehicle speeds between data collection phases indicates that the buses were operating in a similar mode during each test phase. In addition, the presence of the In-Plume sampling inlet homogenized the operating mode of the buses, since the drivers consistently slowed down when driving over the bump in the road it created.

Under cold and humid conditions, many vehicles passing the test site emitted visible steam. Due to the placement of the video camera, the presence of steam was only noted when vehicles were traveling westbound (i.e. cold start conditions) through the test section. For light duty vehicles, emissions of all species were significantly higher when visible steam was observed. At present,

it is uncertain if this increase is an artifact of steam interference or if the emission factors were actually higher. Non-bus vehicles emitted 31% +/- 20% more hydrocarbons in phase I than during phase II when steam was present in the exhaust plumes. Average emission factors of CO, NO, and PM for light duty vehicles without steam were not significantly different (t-test, alpha = 0.05) between phases I and II.

Large differences were observed in the emission factors between eastbound vehicles (cold engine) and the westbound vehicles (hot-stabilized engine) for all vehicle types. Daily average PM emission factor measurements with the In-Plume system were in very good agreement with the remotely sensed PM emission factor measurements. This agreement suggests that both systems were accurately measuring the PM emissions from the passing vehicles and that measured differences are not associated with instrument variation. A comparison of emissions measurements from individual vehicles also indicated excellent agreement between the CO and NO emission factors measured by the In-Plume system and the remote sensing Cross-Plume system.

Prior to the beginning of the study, a subset of five buses had been operating on B20 since March 1, 2003. With the exception of CO, emissions factors of these buses were not significantly different between phases I and II. CO emission factors for the control set of school buses running on B20 were 52% +/- 37% higher during phase II than during phase I.

The presence of non-bus vehicles at the testing area also provided an additional control measurement for the consistency of the instrumentation between phases I and II. Average emission factors for light duty vehicles at the Lanark Road site were not significantly different between test phases with the exception of CO (96% +/- 36% higher for hot stabilized conditions during phase II), HC (45% +/- 13% higher for cold start conditions during phase I), and PM (26% +/- 17% higher for cold start during phase II). Emissions from light duty gasoline vehicles are highly skewed and average values are susceptible to influence by a small number of very high emitting vehicles. As a result, median emission factors from gasoline-powered vehicles were in better agreement between the two phases.

Average emission factors for the diesel school buses were much less skewed than the emission factors from the light duty gasoline vehicles. Consequently the confidence limits of the average (or mean) emission factors for the buses are lower than for the light duty gasoline vehicles. For the school buses, cold start emissions of CO were 34% +/- 7% higher after the switch to B20. Average hot-stabilized CO emissions factors were not significantly different after the switch to B20. Average hot-stabilized HC emission factors increased 23% +/- 11% after the switch to B20, but differences in cold-start HC emission factors were indistinguishable. Emission factors of NO for buses running on both fuels were not significantly different (<1% change). The largest changes in emission factors were observed for PM. Hot stabilized PM emission factors were 88% +/- 11% higher with B20 and cold start PM emission factors were 65% +/- 8% higher after the buses switched to B20.

Comparisons of average emissions factors were conducted by grouping emissions by engine type, engine age, odometer reading, and total miles traveled using B20. Additional analyses were conducted to ensure that groups of the same buses were compared. All analyses were consistent in finding higher PM emission factors for the buses using B20. These results are in disagreement with the majority of dynamometer biodiesel studies that show a decrease in CO, HC, and PM emission factors with biodiesel use.

In addition to the higher PM emission factors observed after a switch to biodiesel, a number of mechanical problems forced six buses temporarily out of service. Each of these buses had failures of either a lift pump or fuel pump, which delivers fuel to the injectors. One of these failures occurred prior to the fuel switch on a control buses that had been using biodiesel for ~1.5 years.

These conflicting emissions measurements prompted the analysis of the fuels available in Idaho's Treasure Valley. Samples of B100, B20, and petroleum diesel were collected directly from a B100 manufacturer/distributor and at several distribution points around the valley. The samples were sent to Caleb Brett Laboratories in Deer Park, Texas for testing. Analyses of these fuels indicated that the biodiesel used in the Treasure Valley was not in compliance with the newly published ASTM standard for B100 (D6751). All of the biodiesel samples collected had elevated levels of glycerin (a byproduct of the biodiesel trans-esterification process). In addition, one of the B100 samples had a low flash point that is usually associated with residual methanol in the biodiesel. Based on the U.S. Department of Energy's "Biodiesel Handling and Use Guidelines", these deficiencies can cause fuel system failure and poor combustion characteristics. The findings of increased PM emission factors and fuel systems failures are consistent with B20 made from off-specification biodiesel fuel.

This study differed from many previous laboratory studies in that the effects of a fuel switch under real world conditions were tested. The analysis identified that the use of off-spec fuel can reverse the some of beneficial effects of using biodiesel.

7.1. Recommendations for Future Studies

The goal of this study was to measure the change in emissions from school buses after they switch to biodiesel. As mentioned above, the measurements indicated that emissions of CO, HC, and PM increased with the use of the biodiesel blend. It is unclear if the increases in emissions and reported mechanical problems are associated with the dissolution of material build-up in the buses' fuel system components or if the problems are associated with using biodiesel that is off-specification with respect to the ASTM D6751 standards. Moreover, it is currently unknown how pervasive off-specification fuels are in the biodiesel production industry.

Future studies could address these uncertainties by:

- continuously collecting samples of petroleum diesel and biodiesel fuel during an emissions field study
- performing controlled experiments on a representative number of vehicles to determine if fuel filter replacement and tank cleaning prior to switching to B20 influences vehicle emissions
- conducting a biodiesel fuel quality analysis to determine if off-specification fuels are commonly distributed

7.2. Recommendations for Using Biodiesel

Mixing waste cooking oils with alcohol in the presence of a catalyst produces biodiesel. This simple process separates biodiesel from a more dense glycerin phase. Because of this, biodiesel can be made on very small scales with little quality control. Failure to completely react and separate the glycerin phase from the biodiesel product can result in fuels that will not meet the newly published ASTM D6751 biodiesel (or B100) specifications.

At present, ASTM D6751 is a guideline for biodiesel producers. This study has shown that use of biodiesel not able to meet ASTM D6751 may increase PM, CO, and HC emissions and cause fuel system failures.

It is recommended that fleet managers considering switching to biodiesel blends adhere to the guidelines established in the Department of Energy's National Renewable Energy Laboratory document "*2004 Biodiesel Handling and Use Guidelines*" available at:

http://www.nrel.gov/vehiclesandfuels/npbf/pdfs/tp36182.pdf

For B100 usage, these guidelines recommend "Plan and budget for the time and expense of increased fuel filter changes or cleaning your fuel system when first starting to use B100." It is generally thought that use of the more dilute B20 will not incur these expenses. Unfortunately, the mixing ratio of biodiesel to petroleum diesel to produce B20 is not regulated under the ASTM D6751 standards. Splash mixing of the two fuels may result in blends that are very different than B20. Consequently, the precautions recommended to users of B100 (i.e. fuel filter changes and fuel system cleaning) may reduce the occurrence of fuel system failures and help to ensure emissions reductions when using B20.

8. References

Abdul-Khalek, I. S., D. B. Kittelson and F. Brear (2003). The influence of dilution conditions on diesel exhaust particle size distribution measurements (SAE 982599), Warrendale, PA, Society of Automotive Engineers.

Barber, P. W., H. Moosmüller, R. E. Keislar, H. D. Kuhns, C. Mazzoleni and J. G. Watson (2004). "On-Road Measurement of Automotive Particle Emissions by Ultraviolet Lidar and Transmissometer: Theory." Measurement Science and Technology, submitted for publication.

Baum, M. M., E. S. Kiyomiya, S. Kumar, A. M. Lappas and H. C. Lord, III (2000). "Multicomponent remote sensing of vehicle exhaust by dispersive absorption spectroscopy 1. Effect of fuel type and catalyst performance." Environmental Science & Technology 34(13): 2851-2858.

Baum, M. M., E. S. Kiyomiya, S. Kumar, A. M. Lappas, V. A. Kapinus and H. C. Lord, III (2001). "Multicomponent remote sensing of vehicle exhaust by dispersive absorption spectroscopy - 2. Direct on-road ammonia measurements." Environmental Science & Technology 35(18): 3735-3741.

Bessagnet, B. and R. Rosset (2001). "Fractal modelling of carbonaceous aerosols - Application to car exhaust plumes." Atmospheric Environment 35(28): 4751-4762.

Bishop, G. A., J. A. Morris and D. H. Stedman (2001). "Snowmobile contributions to mobile source emissions in Yellowstone National Park." Environmental Science & Technology 35(14): 2874-2881.

Bishop, G. A., S. E. McLaren, D. H. Stedman, W. R. Pierson, R. B. Zweidinger and W. Ray (1996). "Method comparisons of vehicle emissions measurements in the Fort McHenry and Tuscarora mountain tunnels." Atmospheric Environment 30(12): 2307-2316.

Brown, J. E., F. G. King, Jr., W. A. Mitchell, W. C. Squier, D. B. Harris and J. S. Kinsey (2002). "On-road facility to measure and characterize emissions from heavy-duty diesel vehicles." Journal of the Air & Waste Management Association 52(4): 388-395.

Brown, J. E., M. J. Clayton, D. B. Harris and F. G. King, Jr. (2000). "Comparison of particle size distribution of heavy duty diesel exhaust using a dilution tailpipe sampler and an in-plume sampler during on-road operations." Journal of the Air & Waste Management Association 50(8): 1407-1416.

Cadle, S. H., R. A. Gorse, Jr., B. K. Bailey and D. R. Lawson (2003). "Real-world vehicle emissions: A summary of the twelfth Coordinating Research Council On-Road Vehicle Emission Workshop." Journal of the Air & Waste Management Association 53(2): 152-167.

Calvert, J. G., J. B. Heywood, R. F. Sawyer and J. H. Seinfeld (1993). "Achieving acceptable air quality: Some reflections on controlling vehicle emissions." Science J1 - sci 261: 37-45.

Canakci, M. and J. H. Van Gerpen (2003). "Comparison of engine performance and emissions for petroleum diesel fuel, yellow grease biodiesel, and soybean oil biodiesel." Transactions of the ASAE 46(4): 937-944.

Cardone, M., M. V. Prati, V. Rocco, M. Seggiani, A. Senatore and S. Vitolo (2002). "Brassica carinata as an alternative oil crop for the production of biodiesel in Italy: Engine performance

and regulated and unregulated exhaust emissions." Environmental Science & Technology 36(21): 4656-4662.

Chen, Y. C. and C. H. Wu (2002). "Emissions of submicron particles from a direct injection diesel engine by using biodiesel." Journal of Environmental Science and Health Part A-Toxic/Hazardous Substances & Environmental Engineering 37(5): 829-843.

Durbin, T. D. and J. M. Norbeck (2002). "Effects of biodiesel blends and ARCO EC-diesel on emissions from light heavy-duty diesel vehicles." Environmental Science & Technology 36(8): 1686-1691.

Durbin, T. D., J. R. Collins, J. M. Norbeck and M. R. Smith (2000). "Effects of biodiesel, biodiesel blends, and a synthetic diesel on emissions from light heavy-duty diesel vehicles." Environmental Science & Technology 34(3): 349-355.

Gillies, J. A. and A. W. Gertler (2000). "Comparison and evaluation of chemically speciated mobile source PM2.5 profiles." Journal of the Air & Waste Management Association 50(8): 1459-1480.

Guenther, P. L., D. H. Stedman, G. A. Bishop, S. P. Beaton, J. H. Bean and R. W. Quine (1995). "A hydrocarbon detector for the remote sensing of vehicle exhaust emissions." Review of Scientific Instruments 66: 3024-3029.

Guenther, P. L., G. A. Bishop, J. E. Peterson and D. H. Stedman (1994). "Emissions from 200,000 vehicles: A remote sensing study." Science of the Total Environment 146/147: 297-302.

Hansen, A. D. A. and H. Rosen (1990). "Individual measurements of the emission factor of aerosol black carbon in automobile plumes." Journal of the Air & Waste Management Association 40(12): 1654-1657.

Horvath, H. (1993). "Atmospheric light absorption - A review." Atmospheric Environment 27A(3): 293-317.

Jimenez, J. L., J. B. McManus, J. H. Shorter, D. D. Nelson, M. S. Zahniser, M. Koplow, G. J. McRae and C. E. Kolb (2000). "Cross road and mobile tunable infrared laser measurements of nitrous oxide emissions from motor vehicles." Chemosphere - Global Change Science 2(3-4): 397-412.

Kirchstetter, T. W., R. A. Harley, et al. (1999). "On-road measurement of fine particle and nitrogen oxide emissions from light- and heavy-duty motor vehicles." Atmospheric Environment 33(18): 2955-2968.

Kittelson, D. B. (1998). "Engines and nanoparticles: A review." 29(5/6): 575-588.

Kleeman, M. J., J. J. Schauer and G. R. Cass (2000). "Size and composition distribution of fine particulate matter emitted from motor vehicles." Environmental Science & Technology 34(7): 1132-1142.

Knapp, K. T. (1992). Dynamometer testing of on-road vehicles from the Los Angeles in-use emissions study. Transactions, PM10: Standards and Nontraditional Particulate Source Controls. J. C. Chow and D. M. Ono. Pittsburgh, PA, Air & Waste Management Association: 871-884.

Kuhns, H. D., C. Mazzoleni, H. Moosm ller, D. Nikolic, R. E. Keislar, P. W. Barber, Z. Li, V. Etyemezian and J. G. Watson (2004). "Remote sensing of PM, NO, CO, and HC emission factors

for on-road gasoline and diesel engine vehicles in Las Vegas, NV." Science of the Total Environment, 322, 123-137.

Kuhns, H., V. Etyemezian, D. Landwehr, C. MacDougall, M. Pitchford and M. Green (2001). "Testing Re-entrained Aerosol Kinetic Emissions from Roads (TRAKER): a new approach to infer silt loading on roadways." Atmospheric Environment 35(16): 2815-2825.

Lawson, D. R. (1995). "The costs of "M" in I/M - Reflections on inspection/maintenance programs." Journal of the Air & Waste Management Association 45(6): 468-476.

Lawson, D. R., P. J. Groblicki, D. H. Stedman, G. A. Bishop and P. L. Guenther (1990). "Emissions from in-use motor vehicles in Los Angeles: A pilot study of remote sensing and the inspection and maintenance program." Journal of the Air & Waste Management Association 40(8): 1096-1105.

Lindhjem, C. and A. J. Pollack (2003). Task 1 - Incorporate Biodiesel Data into Vehicle Emissions Databases for Modeling. Impact of Biodiesel Fuels on Air Quality and Human Health. K. S. Tyson and R. A. McCormick. Golden, CO, National Renewable Energy Laboratory: 46.

Lue, Y. F., Y. Y. Yeh and C. H. Wu (2001). "The emission characteristics of a small DI diesel engine using biodiesel blended fuels." Journal of Environmental Science and Health Part a-Toxic/Hazardous Substances & Environmental Engineering 36(5): 845-859.

Martins, J. V., P. Artaxo, C. Liousse, J. S. Reid, P. V. Hobbs and Y. J. Kaufman (1998). "Effects of black carbon content, particle size, and mixing on light absorption by aerosols from biomass burning in Brazil." Journal of Geophysical Research 103(D24): 32041-32050.

Mazzoleni, C., H. D. Kuhns, H. Moosm ller, R. E. Keislar, P. W. Barber, N. F. Robinson, D. Nikolic and J. G. Watson (2004). "On-road vehicle particulate matter and gaseous emission distributions in Las Vegas, NV and comparison with other areas " Journal of the Air & Waste Management Association: in press.

Mazzoleni, C., H. Moosmuller, N. J. Nussbaum, H. D. Kuhns, R. E. Keislar, P. W. Barber, V. Hiltunen and J. G. Watson (2004). "Effectiveness of inspection and maintenance programs for estimating real world emissions." Transportation Research Part A-Policy and Practice(in preparation).

McClintock, P. (1999). Remote Sensing of Real World High Exhaust Emitters -. CRC Project Number E-23. I. Applied Analysis. Tiburon, CA, Coordinating Research Council, Inc. and the Colorado Department of Public Health and Environment.

McCormick, R. L., M. S. Graboski, T. L. Alleman, A. M. Herring and K. S. Tyson (2001). "Impact of biodiesel source material and chemical structure on emissions of criteria pollutants from a heavy-duty engine." Environmental Science & Technology 35(9): 1742-1747.

Mie, G. (1908). "Beitr„ge zur optik truber medien." 2(25): 376-445.

Moosmüller, H., C. Mazzoleni, R. E. Keislar, P. W. Barber, H. D. Kuhns and J. G. Watson (2003). "On-Road Measurement of Automotive Particle Emissions by Ultraviolet Lidar and Transmissometer: Instrument." Environ. Sci. Technol. 37: 4971-4978.

Moosmuller, H., W. P. Arnott, C. F. Rogers, J. L. Bowen, J. A. Gillies, W. R. Pierson, J. F. Collins, T. D. Durbin and J. M. Norbeck (2001a). "Time resolved characterization of diesel

particulate emissions 1. Instruments for particle mass measurements." Environmental Science & Technology 35(4): 781-787.

Moosmuller, H., W. P. Arnott, C. F. Rogers, J. L. Bowen, J. A. Gillies, W. R. Pierson, J. F. Collins, T. D. Durbin and J. M. Norbeck (2001b). "Time resolved characterization of diesel particulate emissions 2. Instruments for elemental and organic carbon measurements." Environmental Science & Technology 35(10): 1935-1942.

Morris, J. A., G. A. Bishop and D. H. Stedman (1998). On-road remote sensing of heavy-duty diesel truck emissions in the Austin-San Marcos area, University of Denver.

Morris, J. A., G. A. Bishop, D. H. Stedman, P. Maly, S. Scherer, R. J. Countess, L. H. Cohen, S. J. Countess and R. Romon (1999). Remote sensing and comparison of emissions from heavy-duty diesel trucks, Atlanta, GA, Coordinating Research Council, Inc.

Nelson, D. D., M. S. Zahniser, J. B. McManus, C. E. Kolb and J. L. Jimenez (1998). "A tunable diode laser system for the remote sensing of on-road vehicle emissions." B67: 433-441.

Pierson, W. R., A. W. Gertler, et al. (1996). "Real-world automotive emissions - Summary of studies in the Fort McHenry and Tuscarora Mountain tunnels." Atmospheric Environment 30(12): 2233-2256.

Pokharel, S. S., G. A. Bishop and D. H. Stedman (2002). "An on-road motor vehicle emissions inventory for Denver: An efficient alternative to modeling." Atmospheric Environment 36(33): 5177-5184.

Popp, P. J., G. A. Bishop and D. H. Stedman (1999). "Development of a high-speed ultraviolet spectrometer for remote sensing of mobile source nitric oxide emissions." Journal of the Air & Waste Management Association 49(12): 1463-1468.

SAE (1996). Snap-acceleration smoke test procedure for heavy-duty diesel powered vehicles (SAE standard J1667). Warrendale, PA, Society of Automotive Engineers.

Schwartz, J. (1998). Remote Sensing of Vehicle Emissions: State of the Technology, Potential Applications, Cost Estimates, and Recommendations., California Inspection and Maintenance Review Committee.

Shi, J. P., D. Mark and R. M. Harrison (2000). "Characterization of particles from a current technology heavy-duty diesel engine." Environmental Science & Technology 34(5): 748-755.

Singer, B. C., R. A. Harley, D. Littlejohn, J. Ho and T. Vo (1998). "Scaling of infrared remote sensor hydrocarbon measurements for motor vehicle emission inventory calculations." Environmental Science & Technology 32(21): 3241-3248.

Stephens, R. D. (1994). "Remote sensing data and a potential model of vehicle exhaust emissions." Journal of the Air & Waste Management Association 44(11): 1284-1292.

Stephens, R. D., S. H. Cadle and T. Z. Qian (1996). "Analysis of remote sensing errors of omission and commission under FTP conditions." Journal of the Air & Waste Management Association 46(6): 510-516.

U.S.EPA (1997). "National ambient air quality standards for particulate matter: Final rule " Federal Register 62(138): 38651 -38701

U.S.EPA (1999). "40 CFR Part 51 - Regional haze regulations: Final rule." Federal Register 64(126): 35714-35774.

van Gulijk, C., J. M. Schouten, J. C. M. Marijnissen, M. Makkee and J. A. Moulijn (2001). "Restriction for the ELPI in diesel particulate measurements." 32(9): 1117-1130.

Völger, P., J. Bösenberg and I. Schult (1996). "Scattering properties of selected model aerosols calculated at UV-wavelengths: implications for DIAL measurements of tropospheric ozone." Beitr. Phys. Atmosph. 69: 177-187.

Wang, W. G., D. W. Lyons, N. N. Clark, M. Gautam and P. M. Norton (2000). "Emissions from nine heavy trucks fueled by diesel and biodiesel blend without engine modification." Environmental Science & Technology 34(6): 933-939.

Watson, J. G., J. C. Chow, D. H. Lowenthal, L. C. Pritchett, C. A. Frazier, G. R. Neuroth and R. Robbins (1994). "Differences in the carbon composition of source profiles for diesel- and gasoline-powered vehicles." Atmospheric Environment 28(15): 2493-2505.

Zhang, Y., D. H. Stedman, G. A. Bishop, S. P. Beaton, P. L. Guenther and I. F. McVey (1996). "Enhancement of remote sensing for mobile source nitric oxide." Journal of the Air & Waste Management Association 46(1): 25-29.

Zhang, Y., G. A. Bishop and D. H. Stedman (1994). "Automobile emissions are statistically g-distributed." 28(7): 1370-1374.

Zou, L. and S. Atkinson (2003). "Characterising vehicle emissions from the burning of biodiesel made from vegetable oil." Environmental Technology 24(10): 1253-1260.

Appendix A. Remote Sensing Freeway Measurements

A secondary objective of this project was to measure emission factors from the in-use fleet of on-road vehicles operating in the Treasure Valley during winter. The analysis of these measurements provides useful quantitative information to community planners including:

- Observations of the composition and age of the in-use fleet in the Treasure Valley for comparison with the overall fleet of registered vehicles.
- Effectiveness of the vehicle emissions testing program effectiveness in Ada County.
- Reference measurements of diesel emissions for comparison with the B20 emission collected at the Lanark Road site.

A.1. Measurement of Emission Factors from Vehicles Operating on Ada and Canyon County On-ramps

In addition to the measurements collected at the Lanark Road site, the Desert Research Institute (DRI) also conducted remote sensing measurements on the Nampa Boulevard/I-84 eastbound on-ramp (Nampa Site) on January 16, 2004 and on the Franklin Road/I-184 eastbound on-ramp (Boise Site) on March 5, 2004. Both sites were chosen to measure emissions from commuters heading to work. At both sites sampling equipment was set up in time to capture the morning rush hour.

Site characteristics and data recovery statistics for the two freeway sampling sites are presented in Table A-1. Ambient temperatures were generally colder at the Nampa Site than at the Boise Site. Although vehicle speed was essentially equivalent at the two sites, vehicles at the Boise Site were accelerating harder than at the Nampa Site. The road slope was higher at the Nampa Site than the Boise Site, so the average estimated engine load (i.e. vehicle specific power described later) was approximately equal at the two sites. Traffic flows were only slightly higher at the Boise Site (522 vehicles per hour) than at the Nampa Site (441 vehicles per hour). Measurement hit rates based on the VERSS's CO_2 volume measurements (arbitrary units) were higher at the Nampa Site (88%) than at the Boise Site (74%).

License plates were transcribed by COMPASS staff and matched with registration records on file at the Idaho Transportation Department (ITD). In turn, vehicle identification numbers (VINs) supplied by ITD and the Ada County Air Quality Board were decoded to generate more detailed information about each vehicle measured with the VERSS. Variables that can affect the matching of measurements with vehicle information include visibility of the license plate in the image, transcription accuracy, and validity of the ITD database of VIN numbers. Vehicles such as heavy-duty tractor-trailers have separate license plates for the trailers. Consequently, these vehicles can't be matched with ITD records. License plate matching was very good at both sites with ~3/4 of all plates matched to ITD records. At the Nampa Site, 64% of the vehicles with matched license plates were registered in Canyon County. Similarly, at the Boise Site, 68% of vehicles with matched plates were registered in Ada County. At both sites, light duty gasoline cars and trucks accounted for more than 90% of the matched vehicles. The number of heavy-duty vehicles identified by the recorded vehicle image was substantially higher at the Nampa Site (6%) compare to the Boise Site (1%). Near the Nampa Sites was a truck stop and many eastbound freight haulers were likely to pass the site after stopping to rest or refuel. Also, the

Boise Site was located on I-184, which flows into Downtown Boise. Interstate freight haulers are more likely to refuel at a location somewhere along I-84, the most direct east/west through route, rather than drive into the city center.

Average light duty gasoline vehicle ages observed at the Boise Site were similar to the average model year observed at the Nampa Site. Nampa Site light duty gasoline vehicles (1997) were observed to be ~6 months newer than the corresponding vehicles at the Boise Site (1996.5). The observed average model years are substantially newer than those of the ITD registration database from 2002. ITD's registration database contains 252,986 passenger vehicles and 14,511 trucks in Ada County and 125,811 passenger vehicles and 11,876 trucks in Canyon County. When correcting for the 2 years difference between 2002 registration database and the current year 2004, the average model year for Ada and Canyon County vehicles is 1994.8 and 1992.7, respectively. Consequently, air quality models that use vehicle ages based on registration databases to estimate mobile emissions may over estimate emissions. Figure A-1 shows maps of the sampling system set up at the two sites.

Table A-1. Comparison of measurements validity and conditions at freeway remote sensing sites.

	Nampa 2004/01/16		Boise 2004/03/05	
Operating Time	7:07 to 14:54		7:35 to 14:02	
Ambient Temperature Range (deg C)	-7 to -2		-2 to 5	
Average Speed (km/hr) and Stdev	50.7 +/- 6.5		49.8 +/- 9.2	
Average Acceleration ((km/hr)/s) and Stdev	0.01 +/- 2.3		0.95 +/- 1.4	
Road Grade (rise/run)	5.2%		1.7%	
Average Vehicle Specific Power (kW/Mg)	11.1		10.1	
Average CO_2 Vol for valid CO_2	20 +/- 13		40 +/- 19	
Total Vehicles	3370		3438	
Matched ID License Plates	2353 (70%)		2552 (74%)	
Number of Vehicles Visually Identified at GVW > 12,000 lbs	191 (6%)		34 (1%)	
Number of Vehicles with Trailers	44 (1%)		9 (0%)	
Number of Out of State Vehicles	166 (5%)		117 (3%)	
Number of Unreadable Plates	485 (14%)		718 (21%)	
Percentage of Matched Registered in Ada/Canyon	21%/64%		68%/7%	
Number of Valid CO_2 and License Plates	2952 (88%)		2503 (73%)	
Number of Valid CO and License Plates	1982 (59%)		1862 (54%)	
Number of Valid HC and License Plates	1879 (56%)		1755 (51%)	
Number of Valid NO and License Plates	1390 (41%)		1753 (51%)	
Number of Valid PM and License Plates*	1566 (46%)		504 (15%)	
Heavy Duty Diesel Vehicles (HDDV) Number/Percentage/Average Model Year	48 (2.2%)	1999.5	114 (4.7%)	1999.8
Heavy Duty Gasoline Bus (HDGB) Number/Percentage/Average Model Year	2 (0.1%)	1997.5	4 (0.2%)	1995.5
Heavy Duty Gasoline Vehicles (HDGV) Number/Percentage/Average Model Year	68 (3.1%)	1997.2	95 (3.9%)	1998.2
Light Duty Diesel Trucks (LDDT) Number/Percentage/Average Model Year	4 (0.2%)	1994.5	3 (0.1%)	1988.3
Light Duty Diesel Vehicles (LDDV) Number/Percentage/Average Model Year	5 (0.2%)	1995.0	7 (0.3%)	1993.4
Light Duty Gasoline Truck (LDGT) Number/Percentage/Average Model Year	963 (43.5%)	1997.5	1023 (42.2%)	1996.9
Light Duty Gasoline Vehicles (LDGV) Number/Percentage/Average Model Year	1114 (50.3%)	1996.5	1162 (47.9%)	1996.0

*CO_2 Vol >25.

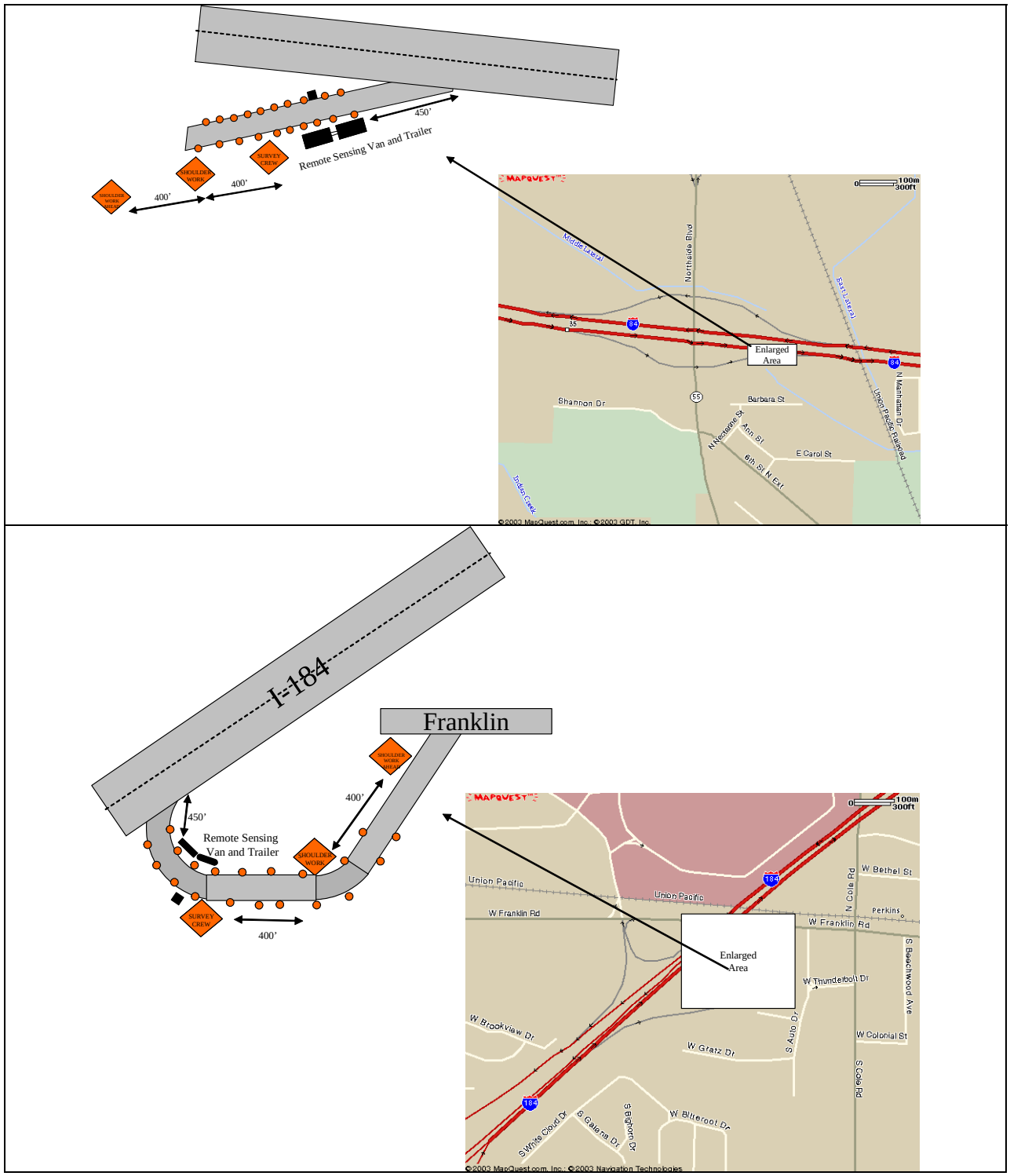

Figure A-1. Maps of sampling locations for the freeway on-ramp remote sensing tests. Upper panel shows the location sampled in Nampa on January 16, 2004. Lower panel shows the location sampled in Boise on March 5, 2004.

Previous studies by Kuhns et al. [2004] have shown the vehicle emissions are dependent on both the age of the vehicle and the Vehicle Specific Power (VSP). The VSP is a surrogate for engine load and is calculated from road slope and the instantaneous vehicle speed and acceleration as the vehicle passes through the test area. The equation used to calculate VSP is:

$$
\begin{aligned}
VSP &= \left(\frac{Power}{Mass} \right) \\
&= \left(\frac{P_{Kinetic} + P_{Potential} + P_{Rolling} + P_{Internal\,Friction} + P_{Aerodynamic}}{Mass} \right) \\
&= v \cdot a \cdot (1 + \varepsilon_i) + g \cdot grade \cdot v + g \cdot C_R \cdot v + C_{if} \cdot v + \tfrac{1}{2} \rho_a C_D \frac{A}{Mass} (v + v_W)^2 \cdot v \\
&\approx 1.1 \cdot v \cdot a + 9.81 \cdot grade \cdot v + 0.213 \cdot v + 0.000305 \cdot (v + v_W)^2 \cdot v
\end{aligned}
\qquad \text{(A-1)}
$$

The variables v and v_W are the vehicle speed and headwind speed in m/s, respectively. The variable a is the acceleration in m/s^2, and *grade* is the rise/run (i.e. arcsin(slope in degrees)). ε_i is the unitless "mass factor" that accounts for the translational mass of the rotating components (i.e. wheels, axles, crankshaft, etc.). The coefficient of rolling resistance C_R and the coefficient of aerodynamic drag C_D are unitless. C_{if} is the internal friction factor with units of m/s^2 and ρ_a is the density of air (kg/m^3). The frontal area A has units of m^2 and vehicle mass *Mass* (in kg) are based on typical values for cars or light trucks. Jimenez [1999] assumes values for all terms except v, a, and *grade* so that VSP can be calculated for each vehicle from variables measured during routine exhaust remote sensing operations.

For emissions tests conducted on dynomometers, the FTP standardized driving cycle used for the estimation of emission factors in MOBILE6 has an average VSP of 8 kW/Mg and a maximum 1 second VSP of 25 kW/Mg. Acceleration from 0 to 60 miles per hour in 15 s with a VSP of 33 kW/Mg is an example of hard acceleration that is a common mode on unobstructed freeway on-ramps. The average VERSS VSP is lower than the normal on-ramp mode because motorists tend to reduce speed and exercise caution in the vicinity of the VERSS traffic control signs and cones.

The relationships between VSP and remotely sensed emissions of CO, HC, NO, and PM for light duty gasoline vehicles (LDGVs) measured in Las Vegas are shown in Figure A-2 (Kuhns et al. [2004]). For each vehicle, the VSP was calculated using equation A-1 and rounded to the nearest even number. Even valued VSPs were chosen to incorporate more data points into each aggregate average when emission factors are grouped by VSP. Negative VSP values were replaced with 0 kW/Mg since there should be no load on the engine other than the internal friction of the engine at idle under these conditions. Engine braking is assumed to be a negligible fraction of the driving cycle since it is not detected from the remotely measured variables: speed, acceleration, and exhaust composition.

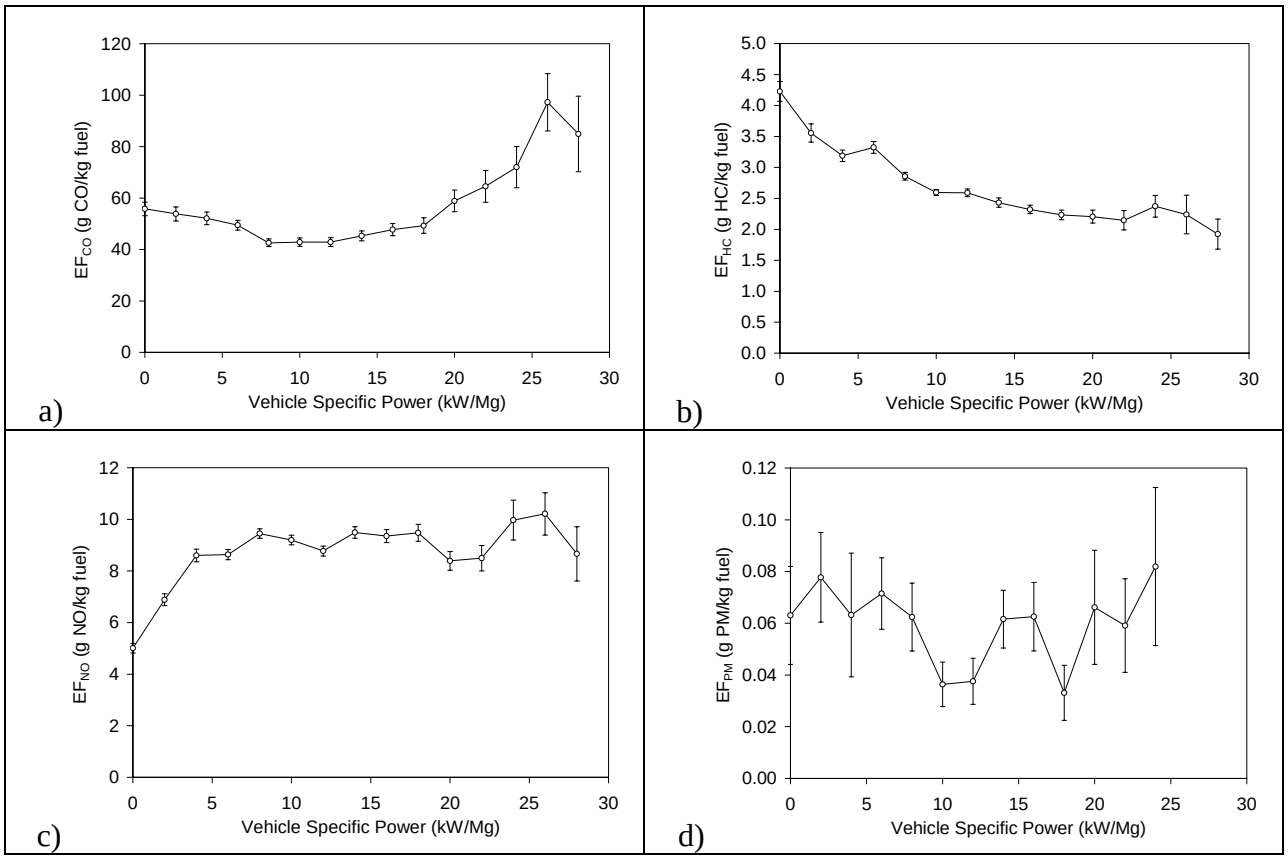

Figure A-2. Comparison of VSP versus emission factors for gasoline powered vehicles in Clark County, NV (Kuhns et al., 2004).

A.2. Fleet Distribution

Vehicle registration data may not always be indicative of the types of vehicles driven on the roadways. Owners of multiple vehicles tend to drive their newer vehicles more than their older vehicles. For the purposes of vehicle emissions modeling with EPA's MOBILE6 model, it is useful to compare the models default fleet vehicles miles traveled (VMT) distribution with a real distribution measured on local roadways.

The MOBILE6 model has 30 classes of on-road vehicles as defined in Table A-2. Vehicles with license plates matched to registration data are classified into each of these categories. As mentioned above, the number of matched heavy-duty tractors may be biased low since only the license plate on the trailer is visible from the vantage point of the remote sensing camera. The magnitude of this bias may be bounded by the fraction of vehicles visually classified as heavy duty by the license plate transcription staff: 6% of all vehicles at the Nampa Site and 1% of all vehicles at the Boise Site.

The distributions of the major vehicle types observed are shown graphically in Figure A-3. Vehicles of different tiers are grouped together under major classifications (i.e. LDGV, LDGT, LDDV/T, etc). For both Ada and Canyon County, the largest fraction of observed vehicles is light duty gasoline passenger vehicles (LDGV) followed by smaller light duty gasoline trucks (LDGT1 and LDGT2). Based on observed in-use vehicle fleet, Ada County has a slightly higher percentage of larger light duty gasoline trucks (LDGT3 and LDGT4) than Canyon County.

Table A-2. MOBILE6 Vehicle Class Definitions. GVW refers to maximum allowable fully laden weight of a vehicle and its payload defined by the manufacturer. Loaded vehicle weight refers to the weight of a vehicle plus 300 lbs.

Vehicle Class	MOBILE6 Code	Gross Vehicle Weight (GVW)	Loaded Vehicle Weight
Light-duty gasoline vehicle	LDGV	Up to 6000 lbs	
Light-duty gasoline truck 1	LDGT1	0-6000 lbs	0-3750 lbs
Light-duty gasoline truck 2	LDGT2	0-6000 lbs	>3750 lbs
Light-duty gasoline truck 3	LDGT3	6000-8500 lbs	3751-5750 lbs
Light-duty gasoline truck 4	LDGT4	6000-8500 lbs	>5750 lbs
Heavy-duty gasoline vehicle class 2B	HDGV2B	8501-10,000 lbs	
Heavy-duty gasoline vehicle class 3	HDGV3	10,001-14,000 lbs	
Heavy-duty gasoline vehicle class 4	HDGV4	14,001-16,000 lbs	
Heavy-duty gasoline vehicle class 5	HDGV5	16,001-19,500 lbs	
Heavy-duty gasoline vehicle class 6	HDGV6	19,501-26,000 lbs	
Heavy-duty gasoline vehicle class 7	HDGV7	26,001-33,000 lbs	
Heavy-duty gasoline vehicle class 8A	HDGV8A	33,001-60,000 lbs	
Heavy-duty gasoline vehicle class 8B	HDGV8B	>60,000 lbs	
Heavy-duty gasoline bus	HDGas Bus	All	
Motorcycle	Motorcycle		
Light-duty diesel vehicle	LDDV	Up to 6000 lbs	
Light-duty diesel truck 1	LDDT1	0-6000 lbs	0-3750 lbs
Light-duty diesel truck 2	LDDT2	0-6000 lbs	>3750 lbs
Light-duty diesel truck 3	LDDT3	6000-8500 lbs	3751-5750 lbs
Light-duty diesel truck 4	LDDT4	6000-8500 lbs	>5750 lbs
Heavy-duty diesel vehicle class 2B	HDDV2B	8,501-10,00 lbs	
Heavy-duty diesel vehicle class 3	HDDV3	10,001-14,000 lbs	
Heavy-duty diesel vehicle class 4	HDDV4	14,001-16,000 lbs	
Heavy-duty diesel vehicle class 5	HDDV5	16,001-19,501 lbs	
Heavy-duty diesel vehicle class 6	HDDV6	19,501-26,000 lbs	
Heavy-duty diesel vehicle class 7	HDDV7	26,001-33,000 lbs	
Heavy-duty diesel vehicle class 8A	HDDV8A	33,001-60,000 lbs	
Heavy-duty diesel vehicle class 8B	HDDV8B	>60,000 lbs	
Heavy-duty School Bus	Diesel School Bus	All	
Heavy-duty Transit Bus	Diesel Transit Bus	All	

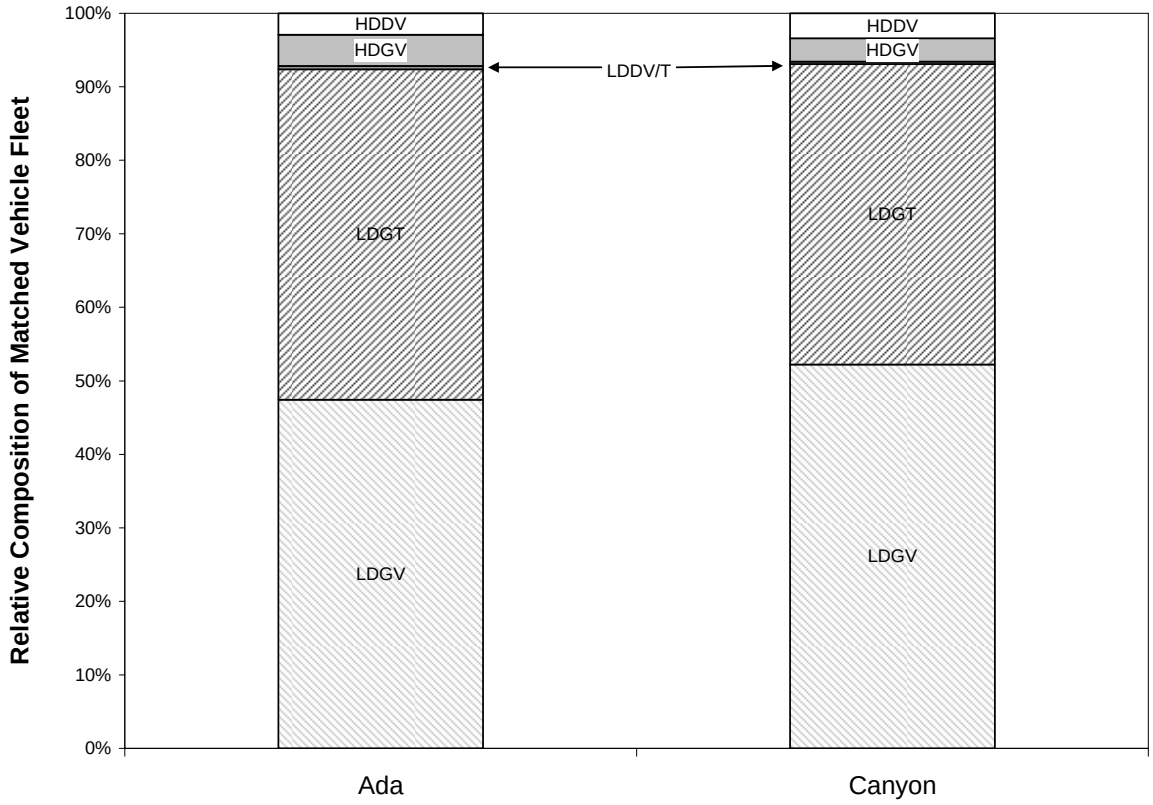

Figure A-3. Comparisons of matched county vehicle fleets from both measurement sites.

A.3. Freeway Remote Sensing Results

In the United States, the on-road fleet of vehicles is primarily composed of light duty gasoline cars and trucks. Emissions from these vehicles have reduced substantially in recent years due to the adoption of catalytic converters in the mid 1980s, computer-controlled fuel injection in the early 1990s, and on-board diagnostic (OBD) systems after 1996. Light duty gasoline vehicles (LDGV) and trucks (LDGT) built after 1996 are equipped multiple diagnostic sensors and a malfunction indicator light (MIL) on the instrument panel that alerts the driver to service the vehicle when the emission control systems are not functioning. Consequently, these vehicles tend to emit relatively small amounts of pollutants.

Emission measurements from both the Nampa and Boise Sites have been joined to assess the evolution of emission factors with vehicle age. Figure A-4 shows the distribution of emission factors with light duty gasoline vehicle and truck model year. For both CO and HC emission factors, average emissions of vehicles before 1996 are substantially higher (>95% confidence) than the group of vehicles with model years 1996 and later. Emissions of nitrogen oxides tend to trend upward continuously from the most recent model year. The pattern with the CO and HC emission factor is indicative of the effectiveness of the OBDII system introduced in all vehicles from 1996 to the present. The smooth trend with the average NO emission factors appears to be associated with the degradation of the catalytic converter's efficiency rather than the introduction of new emission control technology. Primary emissions of PM also increase with vehicle age. However, average emission factors of PM have a higher uncertainty than the other species

because there are a fewer number of valid measurements and because the emission factors for PM are generally lower than the CO, HC, and NO emission factors.

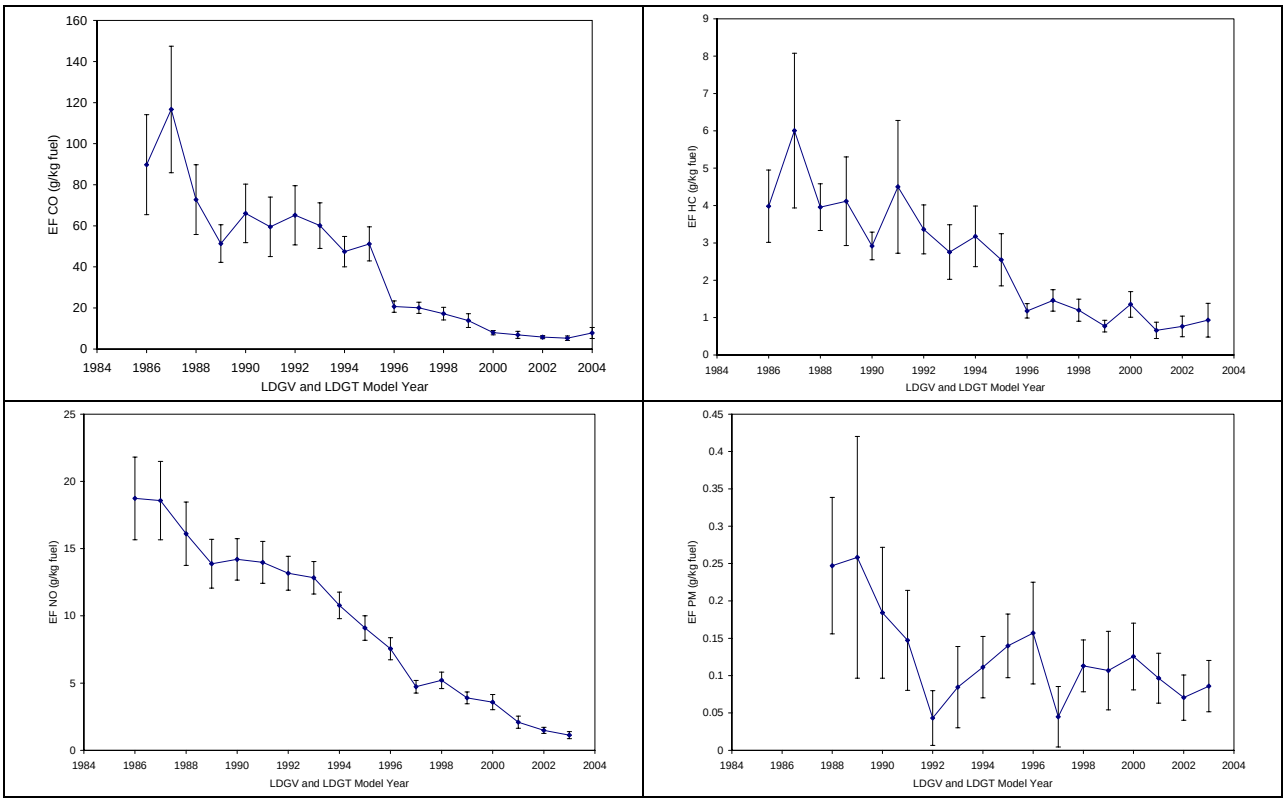

Figure A-4. Distribution of emissions based on model year for LDGV and LDGT. Each data point represents the average of at least 25 vehicles. The error bars are the standard error of the mean (i.e. standard deviation divided by the square root of the number of samples).

A.4. Comparison of Emissions Factors between Ada and Canyon County Vehicles

Ada County has implemented a decentralized vehicle inspection and maintenance program. Gasoline vehicles registered in Ada County must annually pass either a two speed idle emissions inspection or an on-board diagnostic system check. Currently, the gasoline vehicle inspection and maintenance (I/M) program only regulates CO and HC emissions. Diesel powered vehicles registered in Ada County are also required to pass an emissions test based on exhaust opacity. Vehicles registered in Canyon County are not required to participate in the I/M program. Therefore, comparison of the remote sensing results for vehicles registered in Ada and Canyon Counties provides a controlled dataset to evaluate the effectiveness of Ada County's I/M program.

EPA's Office of Transportation and Air Quality has recently finalized a report "Guidance of Use of Remote Sensing for Evaluation of I/M Program Performance" (EPA [2004]). The report outlines three methodological approaches for using remote sensing data to analyze I/M program effectiveness over the short term. The first two methods, the "step change" and

"comprehensive" methods, involve remote sensing measurements collected in an I/M area. The final method, the "reference method", compares remote sensing measurements collected in an I/M area (i.e. Ada County) with measurements collected in an external, or reference area (i.e. Canyon County). Although the dataset from this study represents only two days of sampling, it does lends itself to a reference method analysis. The uncertainty of this analysis would be improved with a larger dataset of emission factors from the in-use vehicle fleet in the Treasure Valley.

The EPA report cautions that when the distance between the reference area and the I/M program area is short. Vehicles may migrate out of an area that has an I/M program to adjacent non-I/M counties. This could be a factor in the Treasure Valley where owners of high emitting vehicles in Ada County may sell their vehicles to a new owner in Canyon County where an I/M inspection is not required. In this example, the reference method will show the I/M program is effective, but the net emissions in the Treasure Valley will show no net change in emissions. Fleet age, specific I/M policies, motor vehicle tax systems, and socioeconomic factors are important considerations to ensure that the "reference method" analysis is unbiased.

As shown earlier (Table A-1), the observed fleet of light duty gasoline cars and trucks in Canyon County has a mean model year of 1997 whereas the corresponding fleet observed from Ada County has a slightly older mean model year (1996.5). These observations of the in-use vehicle fleets are reversed from the trend in the ITD vehicle registration database. Ideally, sufficient data would exist that emission factors could be stratified by vehicle type, model year, and county. The limited sample size of the dataset precludes this type of analysis since the measured emission factors are highly variable.

The ITD database mean model year for Canyon County vehicles is 2.1 years older than that for the Ada County vehicles. Both Ada and Canyon Counties receive their fuel from the same pipeline and use the same fuel blends throughout the year. These factors reduce sources of bias associated with the fleet mix and the fuels used.

The highway remote sensing measurements were conducted in different locations at different times of the year. A higher percentage of vehicles registered in Canyon County were measured at the Nampa Site and a higher percentage of Ada County vehicles were measured on the Boise Site. To control for the influence of sampling location, emissions measurements have been grouped by county of registration (i.e. Ada or Canyon), vehicle type (i.e. LDGV or LDGT) and by sampling date/location (i.e. 20040116/Nampa or 20040305/Boise).

Figure A-5 and Figure A-6 show the average emission factors for these vehicle groups along with the standard error of the mean as error bars. When error bars of the columns do not overlap, the averages are significantly different based on a t-test with alpha = 0.05 (i.e. 95% confidence). Most comparisons of emissions from vehicles registered in Ada and Canyon Counties were inconclusive due to the relatively small sample set. A larger data set would reduce the standard error.

CO Emissions from LDGTs registered in Ada County were 47% +/- 16% and 49% +/- 33% lower than LDGTs registered in Canyon County, as measured at the Nampa and Boise Sites, respectively. No differences in CO emission factors were observed for LDGV. The average model years of the Ada County LDGTs were approximately 0.5 years newer than the Canyon County trucks at the Nampa Site and 1.5 years newer at the Boise Site. Both HC emissions from LDGVs and LDGTs were 36% +/- 35% and 31% +/- 28% lower, respectively, for Ada County

vehicles when compared to emission factors from Canyon County vehicles at the Nampa Site. However, no significant differences were observed with either LDGV or LDGT HC emission factors at the Boise Site.

Following the same pattern as the CO emission factors, NO emissions factors were 22% +/- 10 lower for Ada County LDGTs than for Canyon County LDGTs at the Boise Site and 37% +/- 25% lower at the Nampa Site. No differences were observed for NO emission factors for LDGVs. It is note worthy that average NO emissions were larger for all light duty gasoline vehicles at the Nampa Site when compared to the Boise Site. This may be related to difference in operating mode of the vehicles at the two sites. Finally, PM emission factors were generally higher at the Boise Site than at the Nampa Site. However, no significant emissions differences were measured between Ada and Canyon County registered vehicles.

In summary, Ada County's I/M program may be effective for reducing CO emission factors by ~48% and NO emission factors by ~33% from LDGTs. Differences for LDGV's CO and NO emission factors (if they exist) are likely to be less than 30%. The I/M program may reduce HC emissions from both LDGVs and LDGTs by ~31% under certain operating conditions (i.e. Nampa Site), but have a smaller effect elsewhere (i.e. Boise Site). The I/M program did not appear to significantly influence PM emissions.

Mazzoleni et al. [2004] showed a low incidence of multi-pollutant high emitting vehicles in the remote sensing fleet from Las Vegas, NV. As a result, I/M programs are effective primarily for the pollutants tested by the I/M program. Since NO and PM emissions are not directly tested by Ada County's I/M program, it is less likely that remote sensing measurements of the two fleets would show substantial differences in vehicle emissions characteristics for these species.

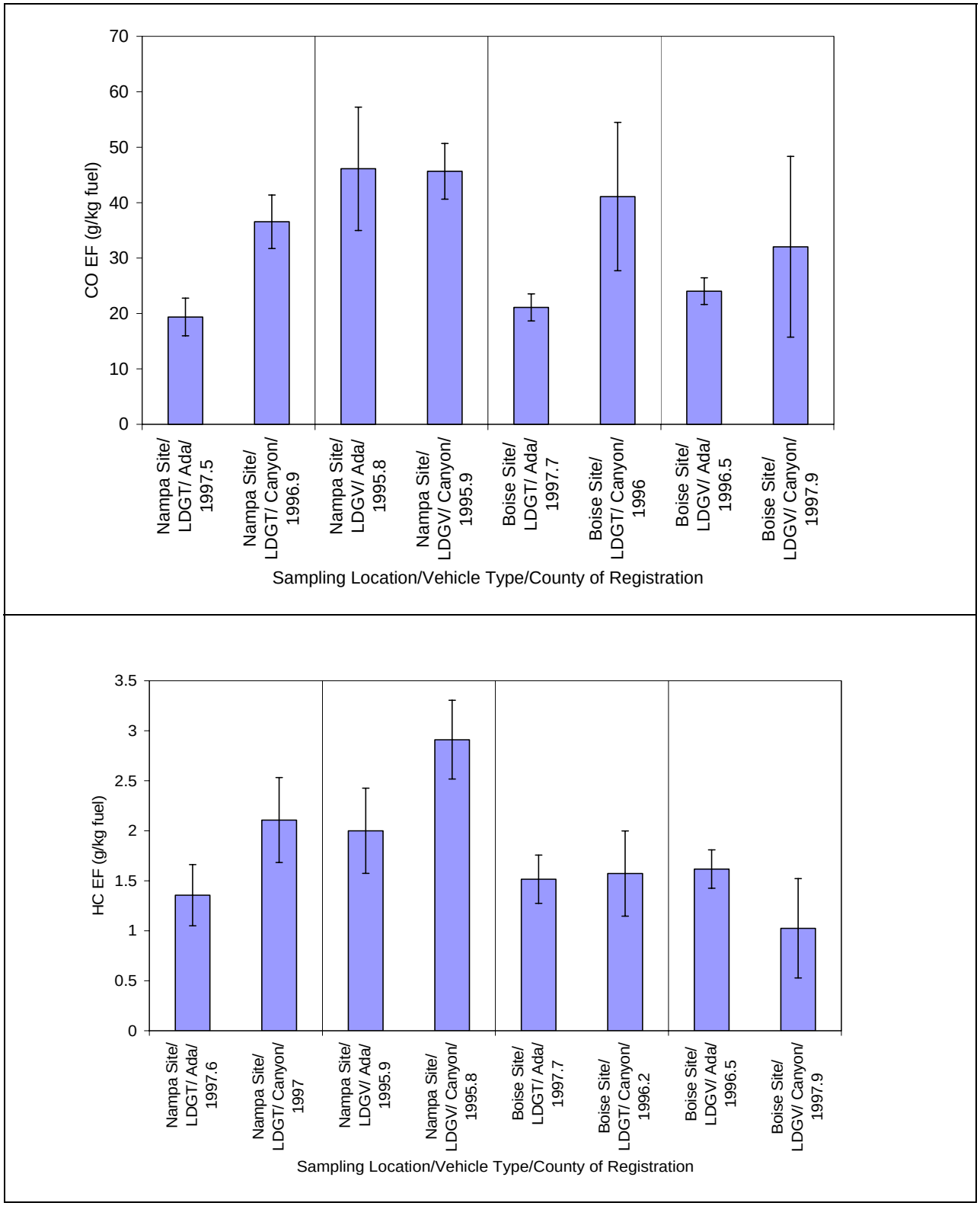

Figure A-5. Comparison of average LDGV and LDGT emissions factors of CO and HC stratified by location of measurement and county of vehicle registration.

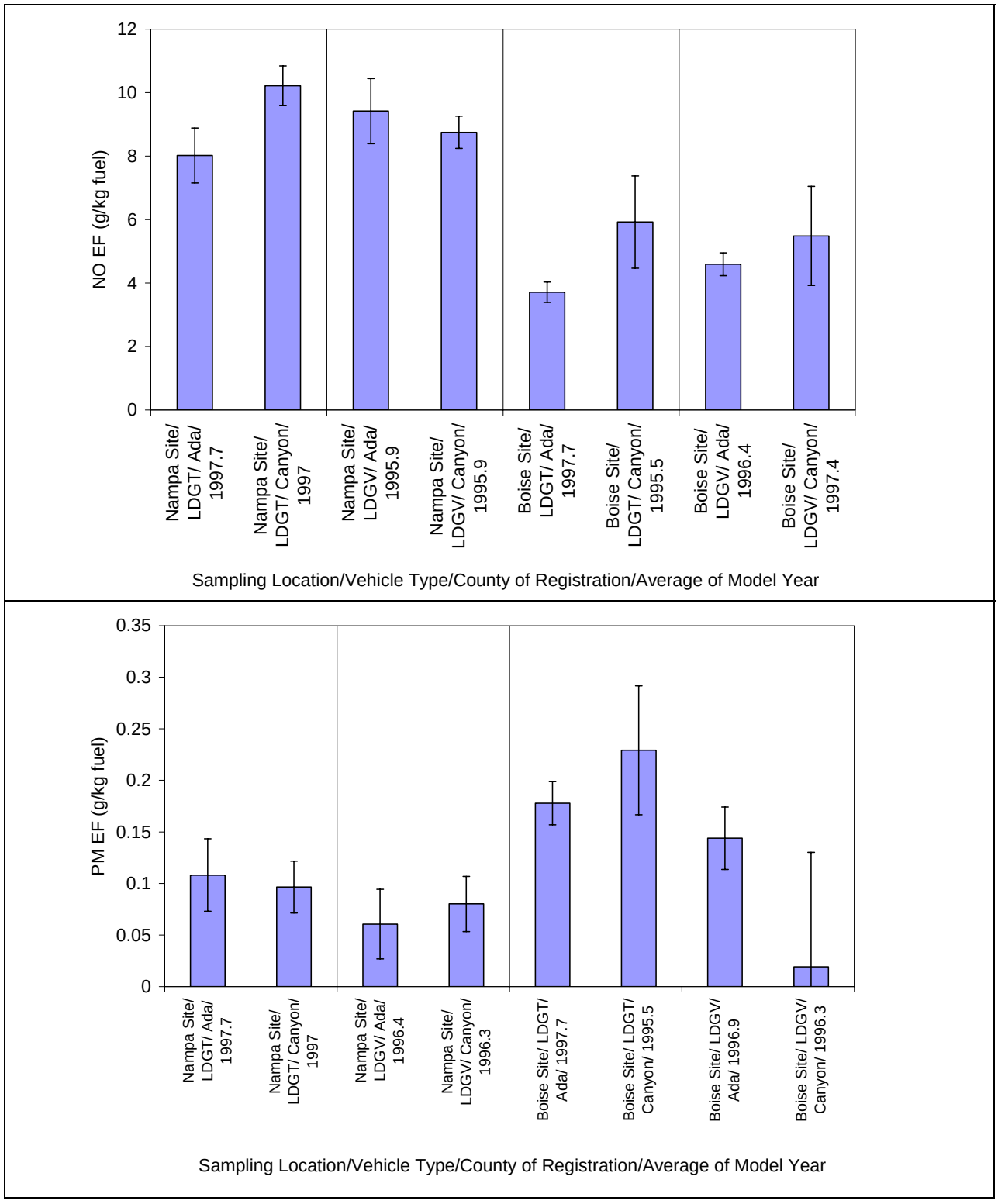

Figure A-6. Comparison of average LDGV and LDGT emissions factors of CO and HC stratified by location of measurement and county of vehicle registration.

A.5. Implications for Emissions Inventories

The MOBILE6 model produces vehicle emission factors using specified fleet age distributions. When applied to specific activity data (i.e. vehicle miles traveled), an emissions inventory for the on-road vehicle fleet operating within an airshed is produced. Ambient temperature and humidity are factored into the MOBILE6 model calculation. These terms affect the evaporative emissions of HC from fuel tanks. Low temperatures will also extend the period of time that a vehicle is operating in cold start mode (i.e. prior to the ignition of the catalytic converter). At high temperatures and humidities, drivers are more likely to use their vehicle's air conditioning unit. In turn, engine load increase and emissions per mile traveled also increase.

Emissions factors generated by MOBILE6 incorporate the emissions impacts from cold starts, where tailpipe emissions can be orders of magnitude higher than during hot stabilized operating conditions. The remote sensing emission factors measured on the freeway on-ramp correspond to the hot stabilized conditions. The cooling systems thermostat regulates the temperature of the engine under hot stabilized conditions. Under these conditions, fuel based emission factors should be invariant to ambient temperature. Therefore, these data can be used to validate MOBILE6 hot stabilized vehicle emission factors.

Fuel based emission factors (i.e. g pollutant/kg fuel) can be compared with distance based emission factors (i.e. g pollutant/mile traveled) by dividing the fuel based emission factor by the fuel economy as specified by the MOBILE6 model (i.e. km traveled/kg fuel). Specific gravities (g/cm^3) of 0.75 and 0.82 may be used to convert kg to gallons of fuel, respectively.

Table A-3 through Table A-6 show the average and standard deviation of the emission factors calculated using the measured data from the freeway on-ramps at the Boise and Nampa Sites. Data are averaged for all measured vehicles registered in Idaho, only Ada County registered vehicles, and only Canyon County registered vehicles. The comparison of these emission factors with the MOBILE6 model output is outside the scope of this project, but the data presented here offer a basis for comparing the results of a nation wide emissions model to the measured emissions from a local fleet.

Table A-3. CO emission factors for MOBILE6 vehicle classes measured on freeway on-ramps in Boise and Nampa. Uncertainties are the standard deviation. Standard errors of the mean may be calculated by dividing the standard deviation by the square root of the number of samples (n). Note: Given the large variability of emission factors within vehicle classes, appropriate caution should be applied when dealing with averages of less than 25 vehicles.

	All Counties		Ada County		Canyon County	
MOBILE6 Class	**CO EF (g/kg)**	**n**	**CO EF (g/kg)**	**n**	**CO EF (g/kg)**	**n**
HDDBS	1015 ±	1	±		1015 ±	1
HDDV2b	8 ± 12	122	11 ± 17	51	5 ± 5	43
HDDV3	3 ± 6	14	4 ± 5	6	3 ± 7	8
HDDV4	8 ± 3	3	11 ±	1	6 ± 3	2
HDDV5	9 ± 6	3	11 ± 8	2	5 ±	1
HDDV6	31 ± 28	3	31 ± 40	2	29 ±	1
HDDV7	4 ± 4	3	1 ±	1	5 ± 4	2
HDDV8a	13 ± 14	2	3 ±	1	±	
HDGB	100 ± 227	5	100 ± 227	5	±	
HDGV2b	38 ± 119	134	39 ± 114	80	43 ± 137	45
HDGV3	4 ± 11	8	5 ± 11	6	±	
HDGV4	14 ± 22	5	29 ± 34	2	±	
HDGV6	323 ±	1	323 ±	1	4 ± 13	2
LDDT12	9 ±	1	9 ±	1	4 ± 2	3
LDDT34	8 ± 3	5	9 ± 2	4	3 ±	1
LDDV	15 ± 4	3	±		16 ± 6	2
LDGT1	48 ± 117	25	15 ± 32	13	82 ± 169	11
LDGT2	30 ± 94	1096	22 ± 71	599	37 ± 115	401
LDGT3	27 ± 83	476	20 ± 52	272	39 ± 118	169
LDGT4	17 ± 37	142	15 ± 42	88	22 ± 30	44
LDGV	35 ± 101	1702	27 ± 81	925	44 ± 123	645

Table A-4. HC emission factors for MOBILE6 vehicle classes measured on freeway on-ramps in Boise and Nampa. Uncertainties are the standard deviation. Uncertainties are the standard deviation. Standard errors of the mean may be calculated by dividing the standard deviation by the square root of the number of samples (n).

	All Counties		Ada County		Canyon County	
MOBILE6 Class	**HC EF (g/kg)**	**n**	**HC EF (g/kg)**	**n**	**HC EF (g/kg)**	**n**
HDDBS	6.1 ± 1.0	1	±		6.1 ±	1
HDDV2b	2.1 ± 119.0	119	1.8 ± 3.2	49	2.3 ± 2.4	42
HDDV3	2.3 ± 13.0	13	1.1 ± 1.7	5	3.0 ± 3.6	8
HDDV4	1.4 ± 3.0	3	2.7 ±	1	0.7 ± 3.4	2
HDDV5	-0.6 ± 3.0	3	-1.5 ± 3.5	2	1.1 ±	1
HDDV6	8.0 ± 3.0	3	11.8 ± 16.2	2	0.4 ±	1
HDDV7	3.0 ± 3.0	3	1.4 ±	1	3.8 ± 3.2	2
HDDV8a	0.9 ± 1.0	1	0.9 ±	1	±	
HDGB	2.4 ± 4.0	4	2.4 ± 3.4	4	±	
HDGV2b	1.2 ± 127.0	127	1.3 ± 3.0	75	0.7 ± 2.4	43
HDGV3	2.7 ± 7.0	7	1.6 ± 2.0	6	9.3 ±	1
HDGV4	0.4 ± 5.0	5	0.2 ± 1.2	2	0.6 ± 2.0	3
HDGV6	3.1 ± 1.0	1	3.1 ±	1	±	
LDDT12	-2.5 ± 1.0	1	-2.5 ±	1	±	
LDDT34	2.4 ± 5.0	5	2.1 ± 2.4	4	3.8 ±	1
LDDV	-0.6 ± 3.0	3	±		-1.8 ± 0.5	2
LDGT1	2.2 ± 23.0	23	1.1 ± 3.0	11	3.2 ± 3.3	11
LDGT2	1.7 ± 1042.0	1042	1.4 ± 5.0	577	2.0 ± 9.8	377
LDGT3	2.0 ± 453.0	453	2.1 ± 8.6	259	2.1 ± 8.9	161
LDGT4	1.0 ± 138.0	138	0.5 ± 2.3	85	2.1 ± 4.8	43
LDGV	2.3 ± 1595.0	1597	1.7 ± 5.2	876	2.7 ± 8.6	599

Table A-5. NO emission factors for MOBILE6 vehicle classes measured on freeway on-ramps in Boise and Nampa. Uncertainties are the standard deviation. Uncertainties are the standard deviation. Standard errors of the mean may be calculated by dividing the standard deviation by the square root of the number of samples (n).

	All Counties		Ada County		Canyon County	
MOBILE6 Class	**NO EF (g/kg)**	**n**	**NO EF (g/kg)**	**n**	**NO EF (g/kg)**	**n**
HDDBS	2.5 ±	1	±		2.5 ±	1
HDDV2b	20.5 ± 10.8	110	17.9 ± 10.9	41	23.9 ± 10.5	43
HDDV3	22.3 ± 7.9	13	20.1 ± 8.6	5	23.7 ± 7.7	8
HDDV4	13.8 ± 11.4	3	22.6 ±	1	9.4 ± 11.9	2
HDDV5	29.4 ± 20.2	3	34.1 ± 26.1	2	20.1 ±	1
HDDV6	16.7 ± 9.4	3	11.4 ± 2.5	2	27.3 ±	1
HDDV7	19.7 ± 8.9	3	12.3 ±	1	23.4 ± 8.7	2
HDDV8a	14.6 ±	1	14.6 ±	1	±	
HDGB	5.0 ± 10.4	4	5.0 ± 10.4	4	±	
HDGV2b	10.4 ± 17.2	114	11.8 ± 18.8	62	9.5 ± 16.2	43
HDGV3	10.6 ± 15.5	8	4.9 ± 10.0	6	27.5 ± 20.4	2
HDGV4	5.8 ± 3.0	5	8.4 ± 0.6	2	4.1 ± 2.5	3
HDGV6	16.5 ±	1	16.5 ±	1	±	
LDDT12	6.0 ±	1	±		±	
LDDT34	7.7 ± 3.1	3	6.0 ±	1	7.2 ±	1
LDDV	12.7 ± 7.4	3	8.0 ± 4.4	2	13.2 ± 10.4	2
LDGT1	13.2 ± 14.9	23	7.4 ± 11.1	11	18.4 ± 17.1	11
LDGT2	7.3 ± 12.5	910	5.3 ± 9.7	467	10.2 ± 14.6	360
LDGT3	5.9 ± 10.0	392	4.0 ± 7.7	208	8.5 ± 12.0	155
LDGT4	6.6 ± 11.9	112	4.3 ± 9.7	66	9.9 ± 14.3	39
LDGV	6.9 ± 10.7	1362	5.5 ± 9.4	683	8.5 ± 11.7	579

Table A-6. PM emission factors for MOBILE6 vehicle classes measured on freeway on-ramps in Boise and Nampa. Uncertainties are the standard deviation. Uncertainties are the standard deviation. Standard errors of the mean may be calculated by dividing the standard deviation by the square root of the number of samples (n).

	All Counties		Ada County		Canyon County	
MOBILE6 Class	PM EF (g/kg)	n	PM EF (g/kg)	n	PM EF (g/kg)	n
HDDBS	0.22 ±	1	±		0.22 ±	1
HDDV2b	0.88 ± 1.26	97	1.45 ± 1.77	32	0.40 ± 0.60	39
HDDV3	1.04 ± 1.48	14	1.80 ± 1.78	6	0.47 ± 0.96	8
HDDV4	0.86 ± 0.75	3	1.62 ±	1	0.49 ± 0.51	2
HDDV5	0.24 ± 0.34	2	0.48 ±	1	0.00 ±	1
HDDV6	1.30 ± 0.40	2	1.02 ±	1	1.58 ±	1
HDDV7	0.22 ± 0.38	3	0.00 ±	1	0.32 ± 0.46	2
HDDV8a	0.88 ±	1	0.88 ±	1	±	
HDGB	0.11 ± 0.11	4	0.11 ± 0.11	4	±	0
HDGV2b	0.12 ± 0.54	101	0.17 ± 0.30	50	0.08 ± 0.75	44
HDGV3	0.09 ± 0.23	8	0.12 ± 0.26	6	0.01 ± 0.02	2
HDGV4	0.06 ± 0.09	6	0.09 ± 0.11	3	0.03 ± 0.08	3
HDGV6	0.00 ±	1	0.00 ±	1	±	
HDGV7	±	0	±	0	±	
LDDT34	0.86 ± 0.77	2	0.32 ±	1	1.41 ±	1
LDDV	1.02 ± 1.38	3	±		0.23 ± 0.20	2
LDGT1	0.07 ± 0.24	11	0.21 ± 0.20	4	-0.01 ± 0.24	7
LDGT2	0.11 ± 0.52	656	0.13 ± 0.43	269	0.08 ± 0.56	322
LDGT3	0.17 ± 0.49	315	0.19 ± 0.46	142	0.16 ± 0.53	147
LDGT4	0.09 ± 0.36	95	0.12 ± 0.21	50	0.05 ± 0.51	38
LDGV	0.09 ± 0.49	738	0.11 ± 0.35	244	0.08 ± 0.55	445

A.6. HDDV PM Emissions of All Vehicles vs. School Busses

The diesel vehicle PM emissions factors measured on the freeway on-ramps are generally higher than those measured on the school busses at the Lannark Road site. Hot stabilized school busses running on petroleum diesel emitted 0.57 +/- 0.03 g PM/kg fuel. Emission factors of the buses running on B20 were 1.07 +/- 0.06 g PM/kg fuel. The HDDV2b class of vehicles (Table A-6) emits 0.88 +/- 0.13 g PM/kg fuel. These differences in emission factors may be related to very different fleet maintenance practices as well as different engine loads at the measurement sites. Emissions from transient engine loadings on diesel engines can result in large variations in emission factors. The PM emissions from the buses after the switch to B20 were ~21% higher than the measured emissions from HDDV2b diesel vehicles in the area.

A.7. Conclusions

The results of this pilot study suggest that Ada Counties I/M program is effective for reducing hot stabilized emission factors of CO by ~48% and NO by ~31% in LDGTs. A significant reduction was not observed for LDGVs. HC emission factors from Ada County vehicles were ~33% lower for both LDGV and LDGT at the Nampa Site, but no significant change was observed at the Boise Site. No significant differences in PM emission factors were observed for

either LDGV or LDGT registered in Ada County with respect to similar vehicles registered in Canyon County.

The depth of analysis of the private vehicle fleet data set is limited because of its small sample size. To account for differences in vehicle class, model year, and make, larger numbers of vehicle measurements are needed. Measurements should be collected for multiple days at several sites in the Treasure Valley. A comprehensive study should also take into account the actual mileage driven by all registered vehicles over a year. This activity data is critical for accurately estimating the valley wide emission reductions achievable with an I/M program. Any additional study should follow one or more of the methods listed in EPA's document "Guidance on Use of Remote Sensing for Evaluation of I/M Program Performance".

A.8. Appendix A References:

EPA (2004). Guidance of use of remote sensing for evaluation of I/M program performance. OTAQ, EPA. EPA420-B-04-010: 63 pp.

Jimenez, J. L. (1999). Understanding and quantifying motor vehicle emissions with vehcile specific power and TDLAS Remote Sensing, Massachusetts Institute of Technology.

Kuhns, H. D., C. Mazzoleni, et al. (2004). "Remote sensing of PM, NO, CO, and HC emission factors for on-road gasoline and diesel engine vehicles in Las Vegas, NV." Science of the Total Environment: in press.

Mazzoleni, C., H. Moosm ller, et al. (2004). "Effectiveness of inspection and maintenance programs for estimating real world emissions." Transportation Research Part A-Policy and Practice(in preparation).

Appendix B. Response to Reviewer Comments

We would like to thank the following people for their time and effort spent reviewing the original draft of this report.

Dr. Jon Van Gerpen	University of Idaho
Dr. Robert McCormick	National Renewable Energy Laboratory
Donnell Rehagen	National Biodiesel Board
David Brzezinski	U.S. EPA, Office of Transportation and Air Quality
Dr. Judi Steciak	University of Idaho
Steve Howell	MARC-IV Consulting
Beth Baird	City of Boise Public Works Department
Matthew Moore	Idaho Transportation Department
Leonard Herr	Idaho Department of Environmental Quality
Rick Hardy	Idaho Department of Environmental Quality
Natalie DelRio	Idaho Department of Environmental Quality

To the best of our ability, noted typographical errors in the text have been corrected and clarifications have been added where needed. Some comments were difficult to address within the text and are addressed here for completeness. The comments have been paraphrased and consolidated here for brevity:

Comment: "The emission factor measurements are not very repeatable, so how can we know if the difference in emission factors is not associated with fleet variability?"

Remote sensing emission factor data are sensitive to vehicle age, engine load, and catalytic converter temperature. When sampling a large fleet of vehicles, the impacts of outlier data associated with a single vehicle are reduced. The study was designed to sample the same set of buses, in the same operating conditions, under the same load before and after the switch to B20. A total of number of measurements averaged for each emission factor ranged from 241 to 538 providing very good confidence in the mean (or average) measurements (<8%).

Comment: "The methods used are not the same as the Federal Test Procedures, how can we be sure that the results are meaningful?"

The Federal Test Procedure (FTP) for vehicle emissions is a standardized test originally designed as criteria for certifying new vehicles. The consistency of the testing conditions allows emissions from one vehicle to be compared directly to another. Using results from the FTP to predict emissions in the real world is fraught with problems. The influences of factors such as temperature, driving mode, vehicle maintenance, and fuel quality are usually not addressed with FTP testing. In contrast, field measurements of vehicle exhaust capture emissions in the real world from in-use vehicles. In-Plume and Cross-Plume system measurement also have limitations in that the vehicles are not analyzed over an entire driving cycle and there is generally less control over the fleet measured. To understand the intricacies of fleet emissions, there is a need for both laboratory tests and field measurements.

In this study, two novel measurement methods were used to quantify emissions from the school bus fleet. The results of each method were compared with the other and good agreement was observed for CO, NO, and PM emissions factors (all comparable species). Although these results should not be used to certify the production of a particular type of engine for use on highways, the results provide meaningful and useful information on the effects of using off-specification biodiesel in a vehicle fleet.

Comment: "The vehicle loads were not consistent when passing through the test section, how does this affect the results and conclusions?"

The remote sensing instrumentation was not able to accurately measure the acceleration of the vehicles passing the exhaust sensor, so the quantitative load on the engine is unknown. Measurements did show that school bus speeds were very similar from phase I to phase II (<10% different). Moreover, the configuration of the experimental setup standardized the operating modes of the buses passing the sensors. The presence of the In-Plume inlet caused drivers to slow down to a generally consistent speed passing through the test section. The greatest variability is linked to driver behavior. These factors are unlikely to change from one test phase to the next. Given the large number of data points and the consistency of the experimental setup, vehicle load is not likely to bias the studies conclusions.

Comment: "The report seems more like a method analysis report rather than a emissions evaluation."

Indeed, much of the report is focused on describing the methods and validating the results. This detail was needed since non-standard measurement methods were used. The extra detail in the operation of instrumentation and the validation of the datasets are intended to provide the reader with sufficient information to evaluate the quality of the results.

Comment: "Average behavior is more important that median behavior when making policy decisions."

We agree that for emission inventories, the average emissions factor is most important for calculating total emissions along with accurate activity data. This dataset highlights the difference in emissions distributions as measured from gasoline and diesel vehicles. Gasoline vehicle emission factors from individual vehicles are highly skewed whereas diesel emissions are more normally distributed. Consequently, when averaging a small number of data points (<1000), one high emitting gasoline vehicle can substantially influence the emission factor average. In these cases, the median value tends to be a more stable measurement when compared to the average. The use of the median in the report is to try to account for large differences in the mean that may be associated with a small number of high emitting vehicles. All relative difference in emissions factors between phases I and II are presented in the text as the relative changes in the mean values.

Appendix C. List of Acronyms

The following acronyms are used throughout the report.

Acronym	Definition
ASTM	American Society for Testing and Materials
B100	100% biodiesel
B20	20% biodiesel blended with petroleum diesel
BC	Blackcarbon
CI	Compression ignition
CO	Carbon monoxide
COMPASS	Community Planning Association of Southwest Idaho
CVS	Constant volume system
DOE	Department of Energy
DRI	Desert Research Institute
EC	Elemental carbon
EF	Emission factor
ELPI	Electronic low pressure impactor
FTIR	Fourier transform infra-red
FTP	Federal Test Procedure
GVW	Gross vehicle weight
HC	Hydrocarbon
HDDV	Heavy duty diesel vehicle
HDGB	Heavy duty gasoline bus
HDGV	Heavy duty gasoline vehicle
I/M	Inspection and maintenance
IR	Infra-red
ITD	Idaho Transportation Department
LDDV	Light duty diesel vehicle
LDGT	Light duty gasoline truck
LDGV	Light duty gasoline vehicle
LIDAR	Light detection and ranging
MCT	Mercury-cadmium-tellurium
MIL	Malfunction indicator light
MJSD	Meridian Joint School District
NAAQS	National Ambient Air Quality Standards
NO	Nitric oxide
OBD	On-board diagnostics
OC	Organic carbon
PM_{10}	Particulate matter less than 10 μm aerodynamic diameter
$PM_{2.5}$	Particulate matter less than 2.5 μm aerodynamic diameter
PMT	Photo multiplier tube
QCM	Quartz crystal microbalance
SEM	Scanning electron microscopy
SI	Spark ignition
U.S. EPA	United States Environmental Protection Agency
UV	Ultraviolet
VERSS	Vehicle exhaust remote sensing system
VIN	Vehicle identification number
VMT	Vehicle miles traveled
VOC	Volatile organic compound
VSP	Vehicle specific power